EGE UNIVERSITY

GRADUATE SCHOOL OF NATURAL AND APPLIED SCIENCES

(MASTER OF SCIENCE THESIS)

ENHANCED SURFACE TOPOGRAPHIES IN LIQUID CRYSTAL POLYMER NETWORKS

Burcu SIRMA

Supervisor: Assoc. Prof. Dr. Serap CESUR

Co-supervisor: Prof. Dr. D. J. (Dirk) BROER

Chemical Engineering Department

Date of Presentation: 03.08.2018

Bornova-İZMİR
2018

Burcu SIRMA tarafından yüksek lisans tezi olarak sunulan "Enhanced Surface Topographies in Liquid Crystal Polymer Networks" başlıklı bu çalışma EÜ Lisansüstü Eğitim ve Öğretim Yönetmeliği ile EÜ Fen Bilimleri Enstitüsü Eğitim ve Öğretim Yönergesi'nin ilgili hükümleri uyarınca tarafımızdan değerlendirilerek savunmaya değer bulunmuş ve 03.08.2018 tarihinde yapılan tez savunma sınavında aday oybirliği/~~oyçokluğu~~ ile başarılı bulunmuştur.

Jüri Üyeleri:		**İmza**
Jüri Başkanı	: Assoc. Prof. Dr. Serap CESUR	.....
Raportör Üye	: Prof. Dr. Mustafa DEMİRCİOĞLU	.....
Üye	: Prof. Dr. Mehmet POLAT	.....

EGE ÜNİVERSİTESİ FEN BİLİMLERİ ENSTİTÜSÜ

ETİK KURALLARA UYGUNLUK BEYANI

EÜ Lisansüstü Eğitim ve Öğretim Yönetmeliği'nin ilgili hükümleri uyarınca yüksek lisans tezi olarak sunduğum "Enhanced Surface Topographies in Liquid Crystal Polymer Networks" başlıklı bu tezin kendi çalışmam olduğunu, sunduğum tüm sonuç, doküman, bilgi ve belgeleri bizzat ve bu tez çalışması kapsamında elde ettiğimi, bu tez çalışmasıyla elde edilmeyen bütün bilgi ve yorumlara atıf yaptığımı ve bunları kaynaklar listesinde usulüne uygun olarak verdiğimi, tez çalışması ve yazımı sırasında patent ve telif haklarını ihlal edici bir davranışımın olmadığını, bu tezin herhangi bir bölümünü bu üniversite veya diğer bir üniversitede başka bir tez çalışması içinde sunmadığımı, bu tezin planlanmasından yazımına kadar bütün safhalarda bilimsel etik kurallarına uygun olarak davrandığımı ve aksinin ortaya çıkması durumunda her türlü yasal sonucu kabul edeceğimi beyan ederim.

03.08.2018

Burcu SIRMA

ÖZET

SIVI KRİSTAL POLİMER AĞLARDA GELİŞTİRİLMİŞ YÜZEY TOPOGRAFİLERİ

SIRMA, Burcu

Yüksek Lisans Tezi, Kimya Mühendisliği Anabilim Dalı
Tez Danışmanı: Doç. Dr. Serap CESUR
İkinci Danışmanı: Prof. Dr. D.J. (Dirk) BROER
Ağustos 2018, 122 sayfa

Sıvı kristaller istenilen yönde kolaylıkla hizalanabilir ve moleküler düzenleri ışık gibi dış bir uyarıcı ile değiştirilebilir. Moleküler düzeydeki bu hareket yüzey topografyasında saptanabilir değişiklikler sağlar. Bu çalışmada, akıllı katmanlı sistemler olarak yumuşak polimerik substratlarla desteklenen ışığa duyarlı azobenzen katkılı sıvı kristal polimer ağlar tasarlanmıştır. Akıllı kaplamalarla ilgili yapılan çalışmaların çoğu bir alt tabaka olarak cam levhaların kullanımına odaklandığı için bu çalışmanın ilk amacı, tabakaların uygun kombinasyonlarının sağlanmasıdır. İkinci amaç polarize ışık tetiklemeli osilasyon yapan yüzey topografilerinin geliştirilmesidir. Bu tür sistemlerin geliştirilmesi durumunda, kullanıcılara cevap veren dokunsal ekranların veya kendi kendini temizleyen yüzeylere sahip güneş panellerinin tasarlanması ilginç olabilir. Sıvı kristalleri hizalamak için hem mekanik olarak ovuşturulmuş tabakalar, hem de foto-hizalama tabakaları kullanılmıştır. Uygulanan substratlar oksijen plazma ile muamele edilmiş polidimetilsiloksan (PDMS), farklı ön kürlenme sürelerine sahip akrilat bazlı tetra(etilen glikol) diakrilat (TTEGDA) ve farklı hacim konsantrasyonlarında monomer 2-etilheksil akrilat (2-EHA) içeren TTEGDA'dır. Akrilat bazlı sistemler PDMS destekli substratlardan daha iyi optik anizotropi göstermiştir. Ayrıca, 2-EHA miktarının artırılmasının akrilat bazlı substratların depolama modülünü azalttığı ve böylece malzemelerin yumuşaklığını arttırdığı gözlenmiştir. Her bir hizalama tabakası türü için en iyi salınım sonuçları %95 hacim konsantrasyonlarında 2-EHA ve %5 TTEGDA karışımı kullanılarak elde edilmiştir. Mekanik olarak hizalanmış tek eksenli azo-LCPN için en yüksek yüzey deformasyonu ve salınımın genliği sırasıyla, 102.8 ve 18.8 nm olarak ölçülmüştür. Birbirine dikey olarak yönlendirilmiş sıvı kristal moleküllere sahip olan foto-hizalanmış azo-LCPN (500 μm periyodik alanlar) için salınımın kararlı yüzey deformasyonu ve genliği, sırasıyla 360 ve 86 nm olarak ölçülmüştür.

Anahtar sözcükler: Azobenzen, sıvı kristal, ışığa duyarlı sıvı kristal polimer ağlar, yüzey topografisi, akıllı kaplamalar.

ABSTRACT

ENHANCED SURFACE TOPOGRAPHIES IN LIQUID CRYSTAL POLYMER NETWORKS

SIRMA, Burcu

MSc in Chemical Engineering
Advisor: Assoc. Prof. Dr. Serap CESUR
Co-advisor: Prof. Dr. D.J. (Dirk) BROER
August 2018, 122 pages

Liquid crystals can easily be aligned in the desired direction and their molecular orders can be changed by an external stimulus such as light. This movement in a molecular level provides detectable changes in surface topography. In this study, light-responsive azobenzene doped liquid crystal polymer networks supported by soft polymeric substrates were designed as smart layered systems. Since most studies conducted related to smart coatings have focused on the use of glass plates as a bottom layer, the first aim of the study was providing suitable combination of the layers. The second aim was enhancing polarized light-triggered oscillating surface topographies. In the case of enhancing such systems, it would be interesting to design haptic screens giving responses to users, or solar panels having self-cleaning surfaces. Both mechanically rubbed layers and photoalignment layers were used to align liquid crystals. Implemented substrates were oxygen plasma treated polydimethylsiloxane (PDMS), acrylate-based tetra(ethylene glycol) diacrylate (TTEGDA) having different pre-curing times and TTEGDA including different volume concentrations of monomer 2-ethylhexyl acrylate (2-EHA). Acrylate-based systems showed better optical anisotropy than PDMS supported substrates. Moreover, it was observed that increasing the amount of 2-EHA decreased the storage modulus of the acrylate-based substrates, and thus increased the softness of the materials. For each type of alignment layer, the best oscillation results were achieved using a mixture of 95% 2-EHA and 5% TTEGDA. For mechanically aligned uniaxial azo-LCPN, the highest surface deformation and amplitude of the oscillation were measured as 102.8 and 18.8 nm, respectively. For photo-aligned azo-LCPN which has perpendicularly oriented liquid crystal molecules to each other (500 μm periodic domains), the stable surface deformation and amplitude of the oscillation were measured as 360 and 86 nm, respectively.

Keywords: Azobenzene, liquid crystals, light-responsive liquid crystal polymer networks, surface topography, smart coatings.

ACKNOWLEDGEMENT

I would like to express my sincere gratitude to my supervisor, Assoc. Prof. Dr. Serap Cesur, for her continuous support and guidance. I have been extremely lucky to have such a great supervisor who always keeps me motivated for my goals.

I also would like to give special thanks to my co-supervisor, Prof. Dr. Dirk Broer, who gave me an opportunity to study for one year at the Eindhoven University of Technology, the Netherlands. Without his supervision and advice, I would not have completed the experimental activities of my thesis. There I had the opportunity to work in a stimulating international environment and to develop new skills in polymeric functional materials. I also extend my thanks to all team members who worked in Functional Organic Materials & Devices research group at TU/e, especially my daily coach Ph.D. student Matthew Hendrikx for his support.

I am grateful to my best friends, Gülen Erturun, Tuğçe Nur Kasarcı, Cansu Köroğlu and Onur Uzunkavak, for their constant motivation and unconditional friendship.

Most importantly, this journey would not have been possible without the support of my family. I would like to express my wholehearted thanks to my mother, Fatma Sırma, for her emotional support. This thesis is dedicated to the memory of my father, Yüksel Sırma, who passed away last year. I am happy I could able to complete this thesis as I promised him. Thank you dad for everything that you have done for me. I miss you every day...

TABLE OF CONTENTS

Page

TABLE OF CONTENTS (continued)

Page

TABLE OF CONTENTS (continued)

Page

LIST OF FIGURES

LIST OF FIGURES (continued)

LIST OF FIGURES (continued)

LIST OF FIGURES (continued)

LIST OF FIGURES (continued)

Figure Page

LIST OF FIGURES (continued)

LIST OF FIGURES (continued)

Figure Page

LIST OF FIGURES (continued)

Figure Page

LIST OF TABLES

LIST OF TABLES (continued)

LIST OF ABBREVIATIONS

LC: Liquid Crystal

LCPN: Liquid Crystal Polymer Network

PDMS: Polydimethylsiloxane

TTEGDA: Tetra(ethylene glycol) diacrylate

2-EHA: 2-Ethylhexyl acrylate

PI: Polyimide

BY: Brilliant Yellow

1.0 INTRODUCTION

Thanks to materials science that has gained momentum in recent years, smart polymers, also known as stimuli-responsive polymers, have become an attractive topic for researchers. These special materials are capable of showing visible or measurable (micro- or nano-scale) alterations in one of their features such as volume, shape, surface topography and wettability when they are exposed to a particular outer stimulus. According to the functionality of such materials, light, temperature, electric field, chemicals, humidity, and pH can be used as a trigger effect (Wei et al., 2017). As a general approach, stimulus-sensitive systems are designed as a result of some innovative ideas inspired by nature. Recently, superhydrophobic coatings that inspired by lotus plant (Tang, 2015), actuators, sensors and micropumps that inspired by biological oscillating systems (Kularatne et al. 2017) have been studied in terms of their sensitivity against to stimulus. In this thesis, it is aimed to design light-responsive liquid crystal polymer network coatings which exhibit dynamic surface topographies in an oscillating manner during the light actuation. This dynamic motion, which is inspired by cardiovascular rhythms, can be used in diverse possible applications such as haptic screens, sensors and actuators. Another suggested application is self-cleaning surfaces. The main issue with solar panels which are established in desert environments is that they need to be cleaned manually after sandstorms to ensure high energy conversion. Nonetheless, this cleaning process is time-consuming and requires high labor costs. If these surfaces possess continuously rising and falling domains, dust could be removed easily without the need of labor and solvent.

Liquid crystals (LCs) are promising materials for designing such stimuli-responsive systems owing to having special molecular organizations. They may exhibit a distinct phase of matter entitled as liquid crystalline lying between solid and liquid. According to the way of the phase exchange, LCs are separated into two groups that are named as lyotropic and thermotropic systems. Lyotropic systems are formed by dissolving amphiphilic molecules in a convenient solution and the phase transitions are promoted by mostly altering the amount of the used solvents. On the other hand, thermotropic systems are made off organic molecules that show liquid crystallinity depending on the implemented temperature. Most of

the studies aimed to build up new technologies have concentrated on thermotropic LCs because of their practicability in dry surroundings. They own a wide range of applications from flat-panel televisions that are frequently encountered in daily life to sensors that are used for precise intents (Bisoyi and Li, 2016). This thesis focuses on thermotropic LCs in order to conduct the process efficiently.

As shown in Figure 1.1, the liquid crystalline phase can be established either by heating the crystalline solid or cooling the isotropic liquid (reversible process). In the crystalline phase, the molecules possess a well-ordered lattice construction. Unlike this, in isotropic liquid phase, entire molecules move freely, meaning that the same property is seen from each direction. On the other hand, LCs within their intermediate phase exhibit some ordered structures of crystals in addition to exhibiting high mobility similar to liquids (Bisoyi and Kumar, 2011). Thanks to the combination of those two attitudes, the molecules incline to move into one direction called as director (n); hence, LCs present orientational anisotropy, meaning that their physical features are alterable depending on their long axis. For instance, the refractive index and dielectric constant vary depending on whether the light or electric field is horizontal or vertical to the director (Schadt, 1997).

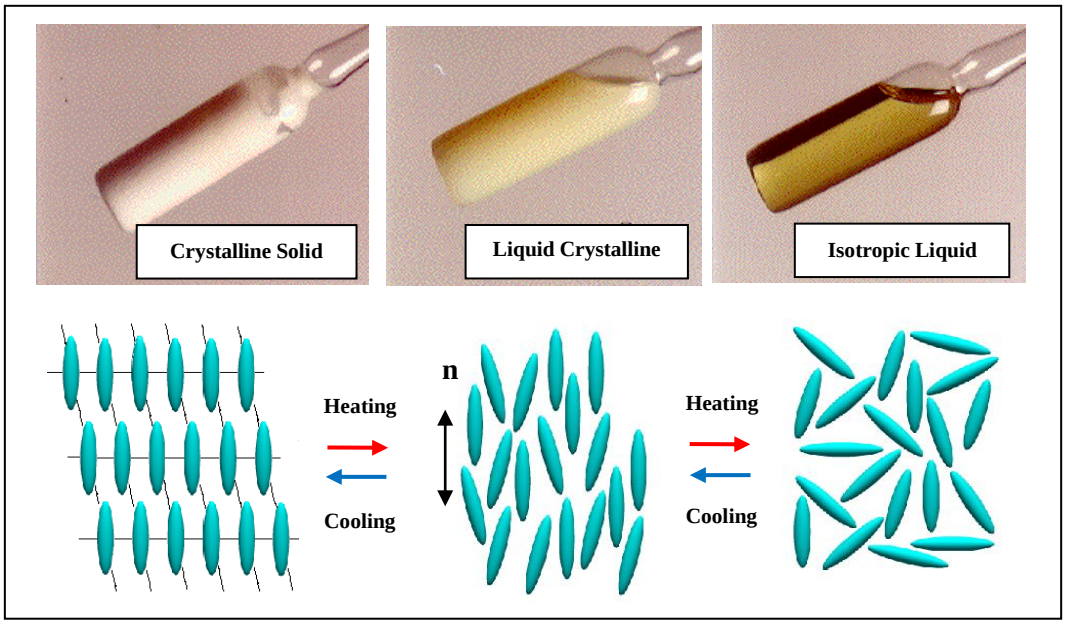

Figure 1.1 Appearance and molecular arrangement of LCs during thermotropic phase transitions.

The director of the molecules points any directions in space, yet LCs can be aligned into a preferred direction on a surface either using external stimuli such as light, electric and magnetic fields or by utilizing alignment surfaces such as mechanically rubbed and photoalignment layers. Practically, achieving the desired alignment has a tremendous effect on the efficiency of all LCs based tools as well as responsive systems. For instance, well-aligned functional LCs based polymers present rapid and large deformations according to the preferred direction of the molecules when exposed to suitable stimuli effect due to their anisotropic features (Liu and Broer, 2014a). Nevertheless, in some cases, the implementation of LCs into the systems might be difficult because they can show liquid crystallinity merely between values of certain temperature. To overcome this limitation, Broer et al. (1989) developed liquid crystal polymer networks (LCPNs) of which their liquid crystalline structures remains to be the same even after heating until high temperatures. LCPNs are designed by photopolymerization of aligned liquid crystal monomers having polymerizable groups, the desired alignments are fixed into highly cross-linked construction as shown in Figure 1.2. With this approach, the characteristics of polymers and LCs are combined in a single system, and therefore, the anisotropic properties of the liquid crystal materials can be exploited even after the film or coating is formed.

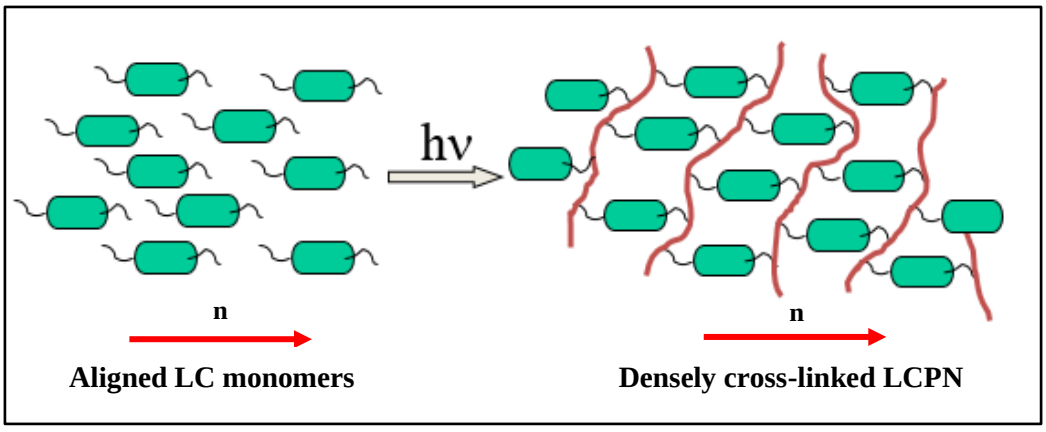

Figure 1.2 Schematic representation for formation of densely cross-linked LCPNs. Vector indicates the preferred direction of molecules.

Light-responsive systems have advantages over electrically or thermally operating systems since they can be operated contactless without requiring

electrodes and heating apparatus (Liu and Onck, 2018). In addition, the light effect can be applied locally at different wavelengths and there is no need to use any solvent to trigger the system like pH- and moisture-operated systems (Liu et al. 2012a). For light-response, a light-sensitive group has to be cross-linked to the polymer skeleton. Although there are a large number of sensitive photochromic groups present such as diarylethenes, spiropyrans, anthracene derivatives, azobenzene is presumably the most commonly used type due to its easy adaptability into LCPNs (Emoto et al., 2012; Hendrikx et al., 2017a).

Light actuation principle is based on reversible photoisomerization of azobenzene molecules. As shown in Figure 1.3, azobenzene can be present as two isomers: trans-state and cis-state. Under ultraviolet (UV) light (~365 nm), azobenzene converts its shape from the trans-isomer having the length of 10 Å to cis-isomer having the length of 5.5 Å (Holland et al., 2003). This geometrical alteration between two isomers pioneers to decline the orientational order of the contiguous aligned molecules in the network. Hence, there occurs a contraction throughout the preferred direction of the molecules, and an expansion perpendicular to it, meaning that an anisotropic deformation is occurred, accompanied by density alterations. On the other hand, the cis form is reverted to trans form by either blocking the light source or keeping the material under visible blue light (~450 nm), and thus the network returns to its first well-ordered construction again (Van Oosten et al., 2008).

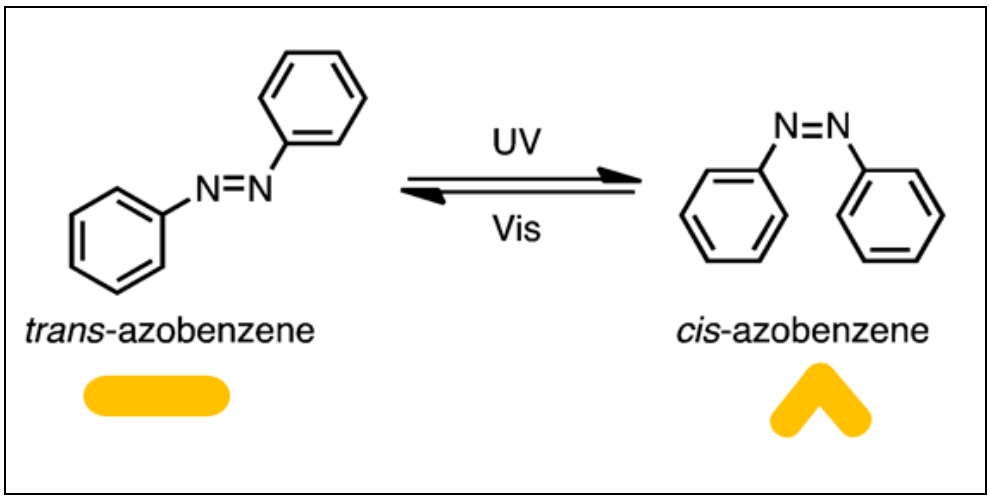

Figure 1.3 Photoisomerization mechanism of azobenzene molecule.

This exceedingly defined photochemistry causes different deformation attitudes in freestanding films (not attached with any surfaces) and substrate-restricted coatings based on azobenzene copolymerized LCPN (azo-LCPN) between on and off states of the light source. As reported by Yu et al. (2003) and Harris et al. (2005), azo-LCPN based freestanding films show bending and curling motions resulting from the contraction and expansion behavior of the aligned LC molecules under UV light. The films reverse to their original flat situations when the light source is switched off. On the other hand, Liu et al. (2012a; 2012b) have made preliminary works in order to investigate the behavior of azo-LCPN coatings on glass plates. In this case, only expansion stress occurs since the contraction is generally manipulated by the glass plate, and therefore switchable surface topographies are achieved between on and off states of UV light (365 nm) as shown in Figure 1.4.

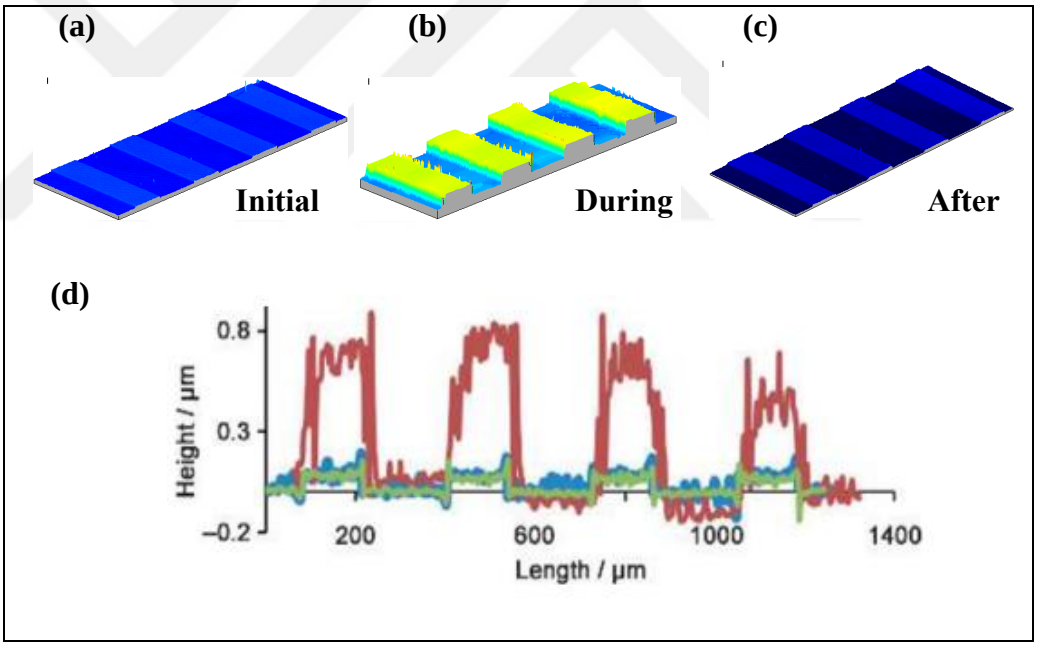

Figure 1.4 3D views of surface topographies (a) before, (b) during and (c) after UV light exposure. (d) Height changes before (blue), during (red) and after (green) light exposure (Liu et al., 2012a).

By taking inspiration from this phenomenon, tribological alternated surfaces which would be a beneficial for motion control and touch-input devices (Liu and Broer, 2014b); switchable surface topographies that allow movement between a mixing and a non-mixing state for microfluidic devices (Liu, 2013); controllable

hydrophobic/hydrophilic surfaces that can be useful for self-cleaning tools (Tang, 2015) have been designed.

All of the studies mentioned above have focused on observing deformations which are obtained only when the light is turned on and off. However, some previous publications have demonstrated that it is possible to design dynamically controlled light-responsive azo-LCPN during light actuation (White, 2018). This controllable movement is related to another substantial character of azobenzene which is called dichroism. Owing to this feature, in the case of using linearly polarized light, the trans-cis isomerization usually takes place in the molecules aligned parallel to the direction of polarized light (White et al., 2009). So, the preferred direction of the network can be changed easily by changing the polarizer direction, resulting in selective deformation. Furthermore, using the light in the range of 440-514 nm (typically blue-green) provokes trans-cis-trans cycle, also known as Weigert effect. Light between these wavelengths can be absorbed by both the trans and cis forms and the dichroism of the azobenzene provides realignment of the molecules perpendicular to the polarization direction of the light source (Lee et al., 2010). White et al. (2008), Serak et al. (2010), Lee et al. (2011) designed azo-LCPN freestanding films that could oscillate with high frequency during polarized blue-green light exposure. Another approach reported by Liu and Broer (2015) represented that using the combinations of polarized UV (365 nm) and visible light (455 nm) notably enhance the oscillatory dynamics.

The first systematic study on oscillating azo-LCPN coatings has been offered by Hendrikx et al. (2017b). For preparation, two neighboring domains (100 μm and 20 μm pitches) were perpendicularly oriented via photoalignment which is an alignment method for providing complex orientations of LCs under the linearly polarized light. Each domain has a planar orientation. By implementing the continuous polarized UV light (365 nm) and blue light (455 nm), continuously rising and falling areas were observed on perpendicularly oriented domains to each other. Figure 1.5 shows the height change and oscillation results of azo-LCPN coatings. With this new phenomenon, there is no need to adjust the frequency of the light source. The oscillation amplitude arises as a result of the ability of the azo-LCPN coatings to respond to the stimulus. The

limitation of this research is that the azo-LCPN coatings were formed on rigid glass substrates, which hinders the lateral stress of the network during light actuation. On the other hand, there is no study in the literature related about designing of oscillating azo-LCPN coatings supported with any substrates different from glass one.

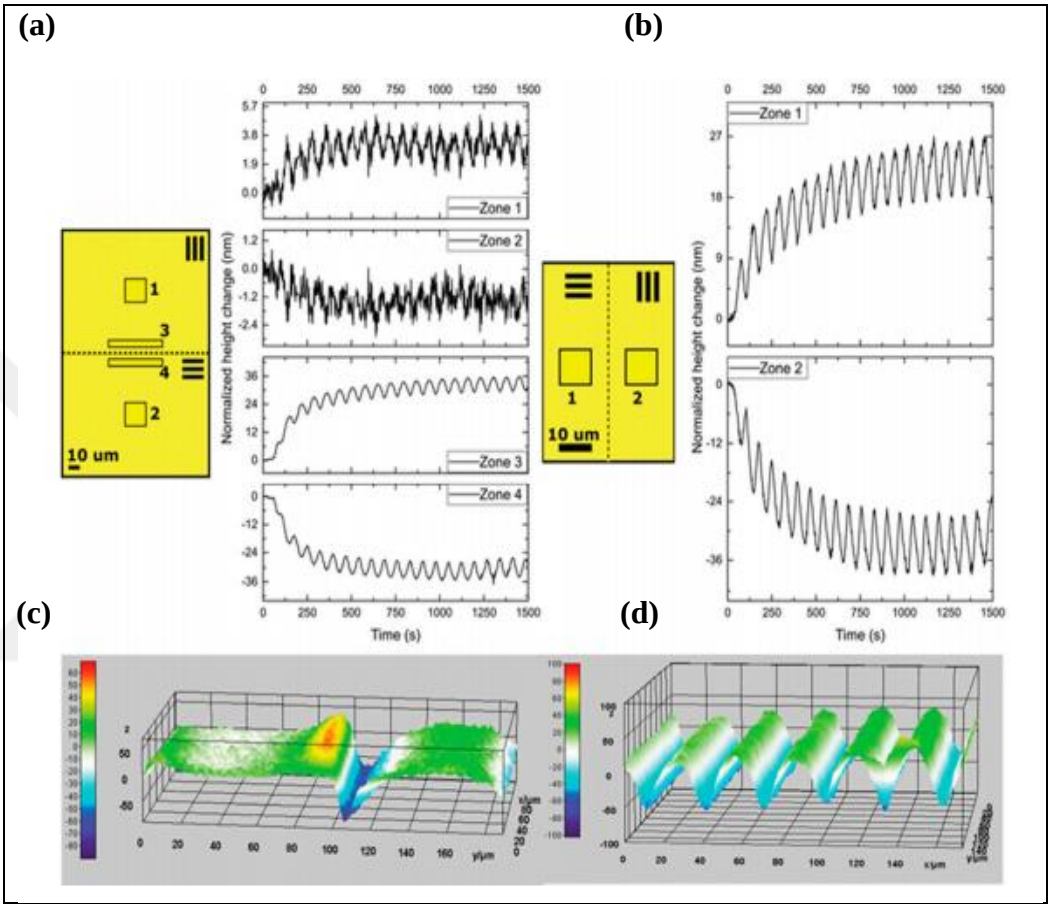

Figure 1.5 Digital holography measurements of azo-LCPN coatings aligned in perpendicular domains with sizes of (a) 100 µm (a) and (b) 20 µm during polarized UV (365 nm) and blue light (455 nm). 3D views of the coatings with (c) 100 µm and (d) 20 µm domains, respectively (Hendrikx et al. 2017b).

The aim of this thesis is to enhance the dynamic surface topographies and oscillation amplitudes of the azo-LCPN coatings supported by soft polymeric layers during light activation. Using soft polymeric substrates ensure both contraction and expansion movement of LCs molecules, and therefore the amplitude of the oscillation and the total height changes between two domains can

be increased. The mechanisms and targets that are expected to be achieved are illustrated schematically in Figure 1.6.

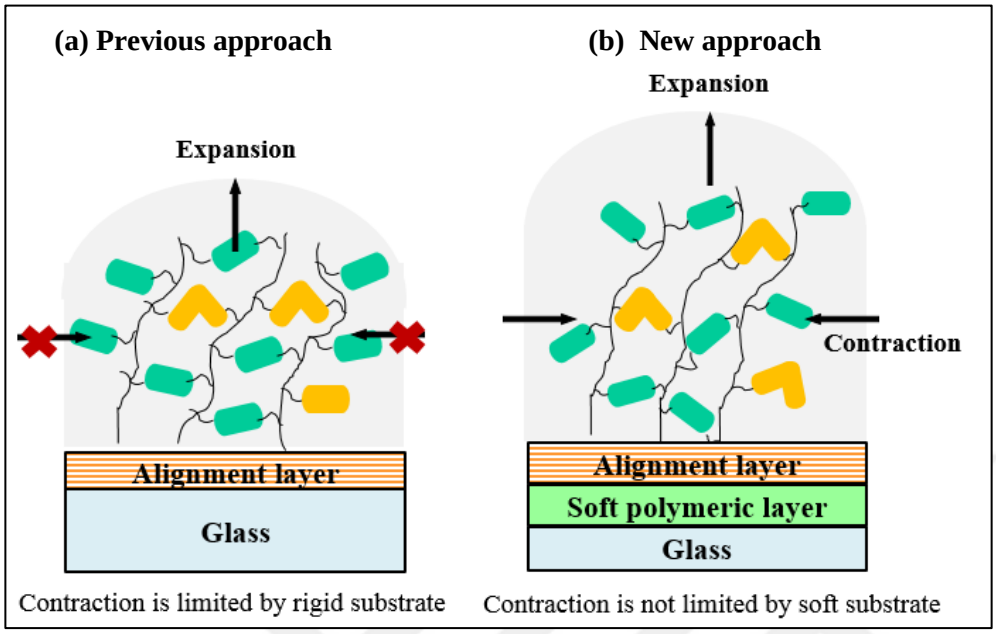

Figure 1.6 Schematic representation for surface deformation with (a) previous and (b) new approaches.

The soft substrates were made from heat curable polydimethylsiloxane (PDMS) or UV curable acrylate-based polymers. To poylmerize acrylate substrates, tetra(ethylene glycol) diacrylate (TTEGDA) or different volume concentrations of TTEGDA and 2-ethylhexyl acrylate (2-EHA) were used. 2-EHA has a glass transition temperature that is well below room temperature and it provides the flexibility and elasticity of the system. Due to the different elasticity of each mixture composition, it was expected to achieve different deformation trends in the azo-LCPN coating. Softer combination was expected to be more deformable. In addition, each type of substrate has different curing times, and therefore different approaches were followed to combine azo-LCPN coating and soft substrates. This study also aims to provide technically suitable LCs orientation and investigate the effects of different alignment layers (mechanical and photo-alignment) on surface deformations. Additionally, light deformation between on and off states was also taken considered for pre-cured TTEGDA to understand the light sensitivity of the system. From this standpoint, this study has gone some way towards enhancing our understanding of light-sensitive

multilayered systems. The aims of the study and the comparison with the previous studies are summarized in Figure 1.17.

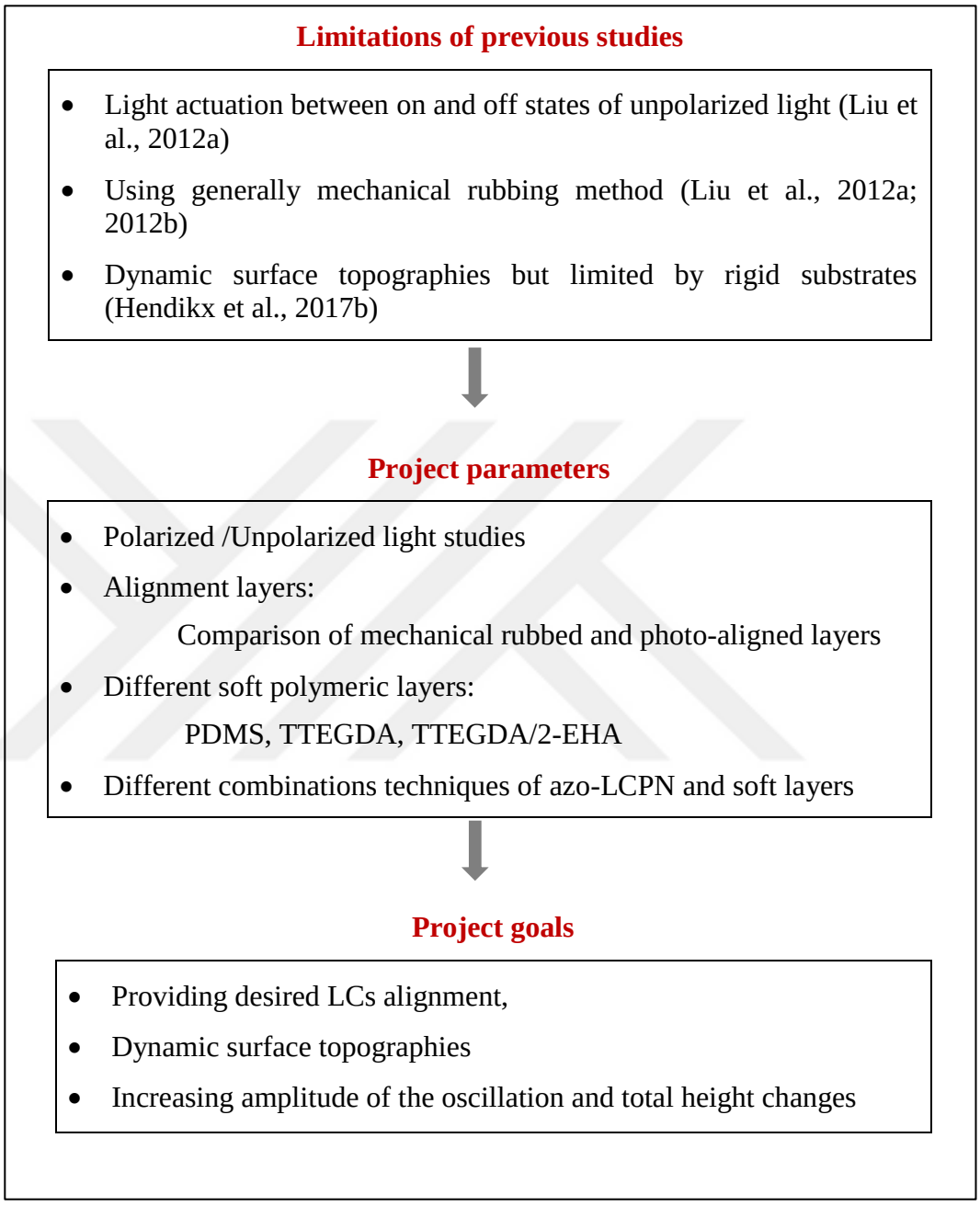

Figure 1.7 Summary of the project parameters and goals.

This thesis is divided into 5 main chapters.

After the introduction, Chapter 2 gives basic general knowledge about the LCs, liquid crystalline polymers, the mechanical rubbing and photoalignment

techniques. Additionally, previously conducted studies on light-sensitive azo-LCPN coatings, which can change the surface topographies, are reported.

Chapter 3 explains the materials used to design azo-LCPN coating, soft substrates (PDMS and acrylate-based) and alignment layers (mechanical and photoalignment). Additionally, different sample preparation approaches for combining the layers are given. The experimental procedures related to the light actuation mechanism of the stimuli-responsive smart layered system are explained.

Chapter 4 includes all alignment and light-actuation results for both PDMS and acrylate-based substrates.

In Chapter 5 and 6, the conclusions depicted from experiments and a few expectations to increase the efficiency of this new approach are given. In addition, the promising applications where these innovative systems can be integrated are given.

2.0 THEORETICAL BACKGROUND AND LITERATURE SURVEY

This section of thesis aims to give general information about the properties of liquid crystalline phase, the formation of light-responsive LCPNs, and the recent studies conducted on improving dynamic surface topographies that are provided with these networks.

2.1 Overview of Liquid Crystalline Phase

Liquid crystalline phase is a technical term used to describe an intermediate phase extending between solid and liquids. Considering its physical appearance, it is regarded as the fourth state of matter. Interestingly, liquid crystallinity emerges spontaneously in many natural systems. DNA, collagen, cellulose, and silk are just a few examples of substances that are capable of showing this unique phase (Rey and Herrera-Valencia, 2012). The first one was explored nearly 130 years ago by botanist Friedrich Reinitzer. While heating a plant-derivative today known as cholesteryl benzoate, he recognized that there took place a blurry fluid at a definite temperature range, meaning that a passing from solid to liquid did not occur immediately. Furthermore, he found that this process is reversible while cooling the material. In 1889, Otto Lehman, was an expert on crystal optic, observed that this blurred fluid altered the direction of polarized light like a crystal, and therefore named this unique substance as Liquid Crystals. In 1922, Friedel reported the effects of electric fields on LCs and classified the liquid crystal phase. By the middle 1950s, George Gray systematically synthesized many of LCs which are recognized within academic communities today. In 1968, the first LC display was designed by benefitting from the electro-optical properties of LCs (Geelhaar et al., 2013). Since then, scientists have been working on synthesizing various LCs and integrating them into various applications such as optical and smart systems.

As a function of temperature, thermotropic LCs change their molecular organization, and therefore different phases called as mesophases are formed. The most commonly used types are smectic and nematic phases. Two terms that are called as positional and orientational order should be explained first to understand

the systems. While the positional order means tidy spaces between molecules, the orientational order indicates the tendency of the molecules in the same direction. In crystalline phase, there exists both long-range positional and orientational order due to the lattice structure of the molecules (Figure 2.1a).

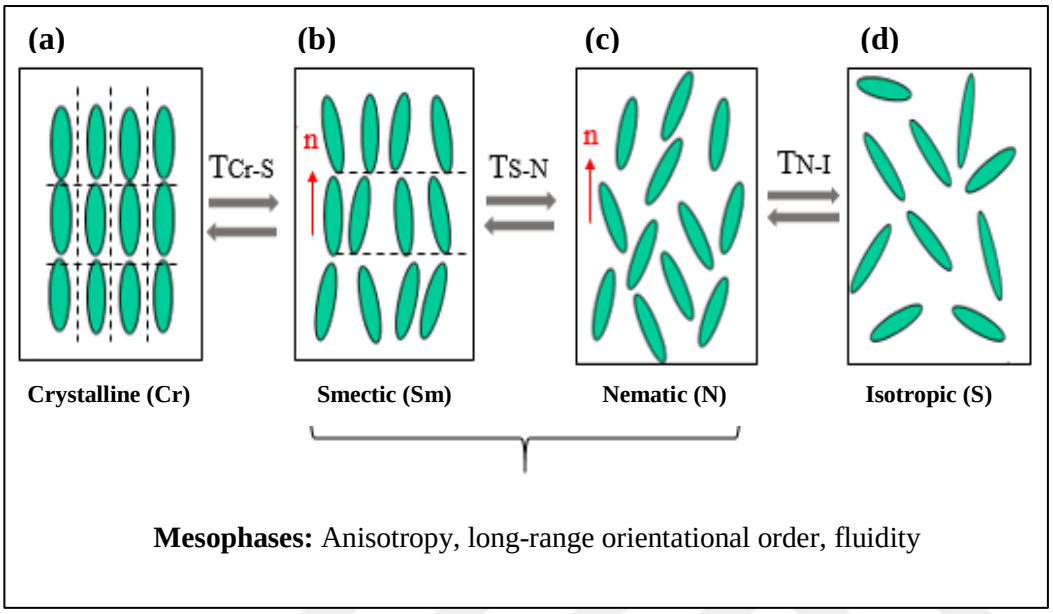

Figure 2.1 Molecular arrangements in (a) crystalline, (b) smectic, (c) nematic and (d) isotropic phase.

Smectic phase: When the material is heated above melting temperature, the smectic phase where the molecules have layered structures (two dimensional) emerges. Here, the molecules lose some of the positional order but keep the long-range orientational order. In this case, the molecules still flow throughout the director n as shown in Figure 2.1b. However, the mobility is limited owing to the unbalanced forces of the molecules located on the sheets (Palffy-Muhoray, 2007).

Nematic phase: At higher temperatures, there occurs nematic mesophase in which the molecules completely lose their positional order, yet still maintain the long-range orientational order (Figure 2.1c). Since the present molecules do not bind to any sheets, they have higher fluidity than the molecules in the smectic phase. Further increasing the temperature causes the formation of the isotropic phase where the molecules move independently (Figure 2.1d). The notations of

T_{Cr-S}, T_{S-N} and T_{N-I} means the crystalline-smectic, the smectic-nematic and the nematic-isotropic transition temperatures, respectively (Palffy-Muhoray, 2007).

It should be noted that the transition temperatures are different for each material which shows liquid crystallinity. Generally, different LCs are blended to provide the temperature range which show liquid crystallinity. Nematic LCs are useful for many applications because of their easy process and high anisotropy. This project concentrates on the nematic phase.

2.2 Structure of Liquid Crystals

From a technical point, the most substantial subject in designing LCs is procuring a proper structure. Mesogen is a technical term to describe individual molecules that form LCs. The form of the mesogenic part has to be in a convenient geometry in order to assure orientational anisotropy. According to the shape of the mesogenic components, thermotropic LCs are subcategorized into two types: calamitic (created by rod-like molecules), and discotic (created by disc-like molecules). The calamitic mesogens like pentyl-cyanobiphenyl (Figure 2.2a) exhibit high anisotropy smoothly because their axial component is much larger than the radial component. Nonetheless, the discotic mesogens such as triphenylene-based structures (Figure 2.2b) represents short-range anisotropy because of their geometry. This structure restrains the linear behavior of the system (Luckhurst, 1993).

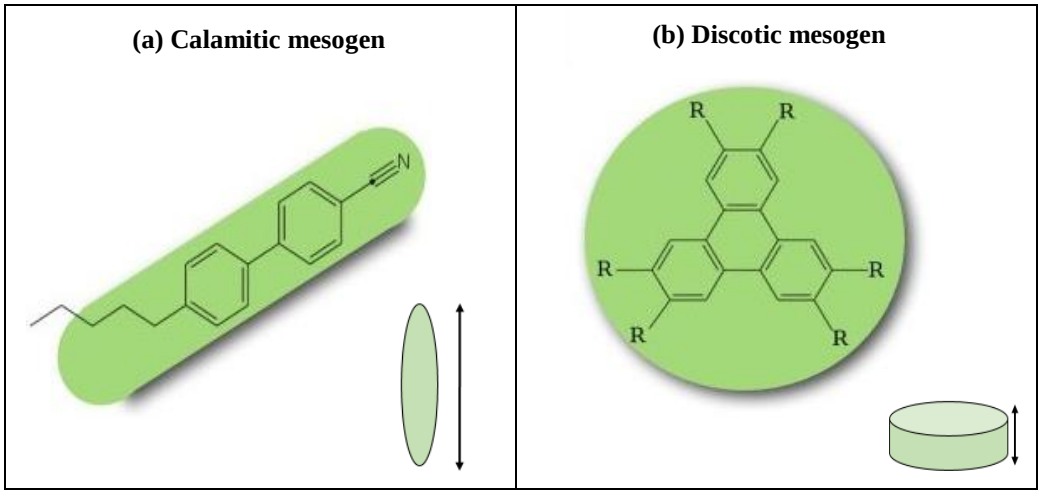

Figure 2.2 Chemical structure of (a) calamitic and (b) discotic mesogens**.**

The materials used in this study are chosen from calamitic in order to utilize the advantage of their elongated structure. Each unit within the mesogen has a different task; hence, it is important to be familiar with the structure existing in the molecules. In general, the calamitics are synthesized by utilizing organic molecules. Even though there present numerous organic compounds, merely some of them exhibit the liquid crystallinity. Such kinds of structures are built-up from a rigid central core (linearly bonded aromatics) that is attached flexible chains (usually aliphatic). The aromatic rigid core is responsible for unidirectionality of the system since the rigidity creates confinements on bond-rotation. There may be more than two aromatic groups that are bonded together by linker groups. Figure 2.3 represents some examples of the molecular structure of calamitics.

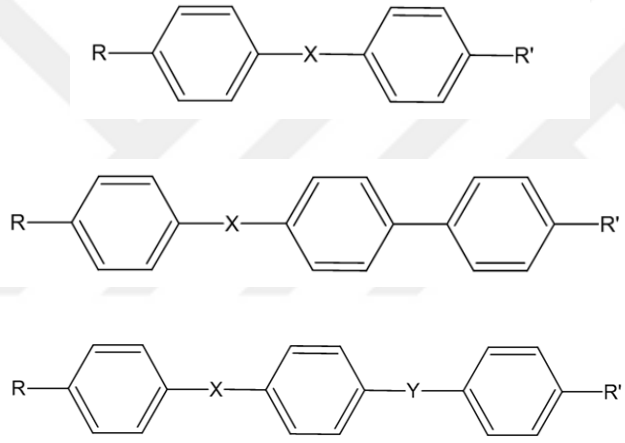

Figure 2.3 Basic molecular structure of calamitic mesogens.

The structure with a longer core of the molecules causes higher melting temperature. Flexibility has to be provided in the structure to lower the melting point and to stabilize the molecular alignments between mesophases. This flexibility is supplied by the flexible chains and terminal groups. Another important point of designing the systems mainly depends on the polarity of the terminal groups. In general, one of the terminal groups is a stiff polar substituent and another one is a non-polar substituent (Qaddoura and Belfield, 2009). Some of the frequently used groups are given in Table 2.1.

Table 2.1 Examples for each unit used to synthesize calamitic mesogens

Linking group: X and Y	**Terminal group R and R'**	
	Non-polar	**Polar**
-N=N- -CH=CH- -CH=N- -COO- -CH_2-CH_2-	Alkyl Alkoxy	-CN -F/Cl/Br -NO_2 -COOH -NCS

2.3 Structure of Liquid Crystal Monomer

Polymeric systems showing liquid crystallinity have been attracted much interest due to its availability in various implementation. A typical LC monomer contains one or two reactive terminal groups which are attached to a mesogenic part; hence, it is regarded as a reactive mesogen (RM).

In terms of ensuring rapid polymerization process, it is very important to choose an appropriate terminal group. Even though many reactive components have been tested, the acrylates are regarded as to be the most convenient groups for this purpose. RMs having two acrylates (diacrylate mesogens) can form densely-crosslinked polymer networks rapidly even if a photoinitiator is implemented at low concentration. However, in most cases, they have higher crystalline to nematic transition temperature (above the room temperature), meaning that they present in their crystalline phase. To overcome this issue, mostly, a blend of low molar mass mono and diacrylate mesogens is selected to depress processing temperatures. Furthermore, they are low molecular weight monomers; hence, they can be easily oriented when the appropriate temperature and alignment methods are applied (Liu and Broer, 2014a).

Table 2.2 gives the example of mono- and diacrylate RMs and their phase exchange temperatures. The numbers between the lines indicate transition temperatures (Celcius). The value between bracket, which is written as Cr-(N-44)-76-I, means that the nematic phase occurs only during the supercooling.

Table 2.2 Example of mono and diacrylate RMs with their transition temperatures

Chemical Structure	Transition temperature
Reactive acrylate group **Calamitic mesogens** 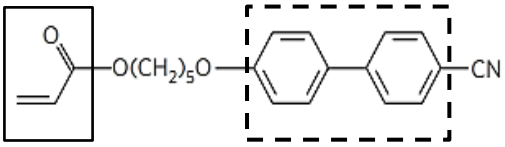	**Cr-(N-44)-76-I**
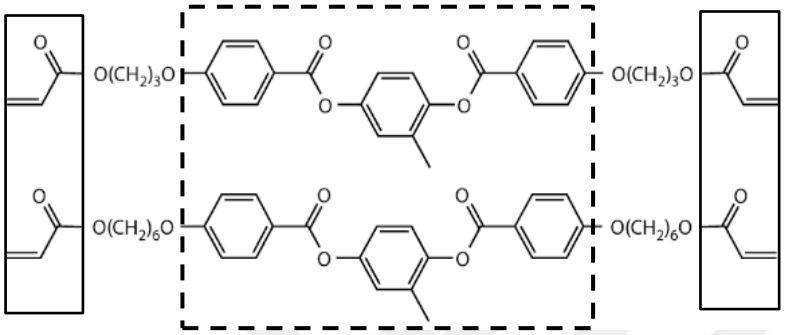	**Cr–73–N–129–I**
	Cr–86–N–116–I

2.4 Optical Properties of Nematic Liquid Crystals

LCs display different colorful textures according to their phase behavior when examined by polarized optical microscopy. The reason for this is that it depends on the light velocity and the polarization direction. Polarizer is a filter that allows the light to be directed only in a certain direction. When the isotropic material is placed between two polarizers that direct the light horizontally and vertically, the light can not pass through the second polarizer. On the other hand, when LC material is placed between crossed polarizing films, it is possible to transmit a certain amount of light depending on the alignment of the sample since it exhibits anisotropic optical properties called as birefringence (Pavlin et al., 2013).

After passing through the first polarizer, the light is split into two beams with different velocities. The refractive index of the material is equal to the ratio of the velocity of the light in the vacuum to the velocity of the material; hence, the beams with different velocities have different refractive indices. The light parallel to the director of LCs has an extraordinary refractive index (n_e) while the light perpendicular to it has an ordinary refractive index (n_o). The difference between

these two refractive indices is described as birefringence ($\Delta n=n_e-n_o$) (Schadt, 1997). For typical nematic LCs, n_o is nearly 1.5 and the maximum value of birefringence may be between 0.05 and 0.5. It is important to produce LCs based devices which have high birefringence for display applications as well as other optical devices.

The light response time throughout the thickness of the material are affected by the birefringence. The anisotropy of the materials mainly depend on the temperature of the system. This dependence disappears after the transition temperature of the nematic-isotropic phase as called as $T_{NI.}$ This feature allows a certain amount of light to pass, depending on the preferred director of the sample. Thus, LCs show bright regions when looked at between crossed polarizers, apart from when the director is positioned either parallel or perpendicular to the polarization direction (Hale et al., 2004). The system is shown in Figure 2.4. In this study, this property is the first accepted parameter to check the alignment quality of the samples.

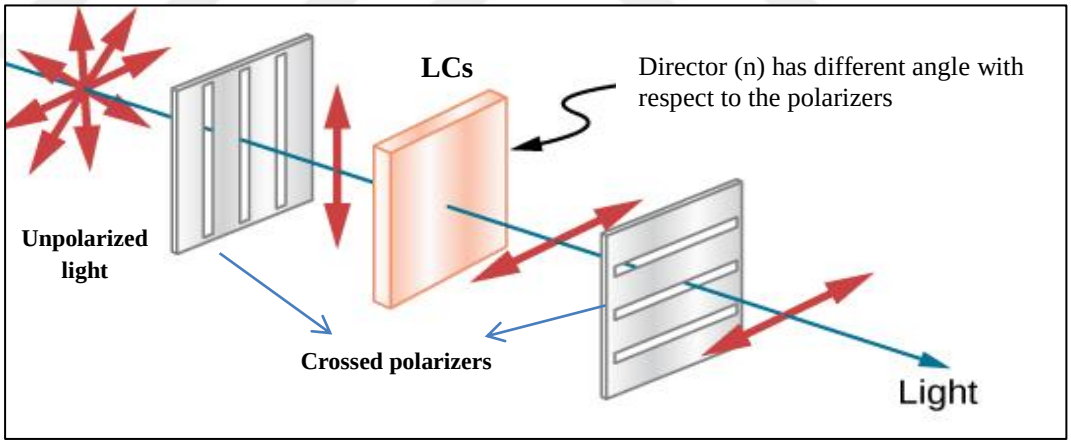

Figure 2.4 The transmission of light throughout the LCs located between crossed polarizers.

2.5 Types of Liquid Crystal Alignment

Alignment is necessary for benefiting from the properties of LCs. Especially in the nematic phase, the director of the molecules can be forced to align into the preferred direction on a surface utilizing an alignment surface in order to be used practically. This is a technically based on Pauli's theory which is known as steric

forces. The provided steric forces prevent distinct molecules (molecules in alignment surface and LCs) from interacting to each other, resulting in a specific orientation. Essentially, liquid crystal / solid surface interactions are also affected by complex interplays such as van der Waals forces, dipole-dipole interactions and chemical restriction (Kim et al., 2014). This subsection only focuses on the general alignment methods and materials to design such alignments.

Commonly utilized nematic alignments are homeotropic where n is vertical to the surface (Figure 2.5a), uniaxial planar where n is parallel to the surface (Figure 2.5b), tilted where n is located with a certain angle relative to the surface (Figure 2.5c), and twisted where n has a planar turn of 90 degrees (Figure 2.5d). There is also one pervasive kind used that is called as chiral-nematic cholesteric (Figure 2.5e). The generation of such alignment is made by implementing a chiral dopant to nematic LCs. The molecules collocate within the sheets to give helix construction and thus the vector n varies along the sheets (Bisoyi and Li, 2016).

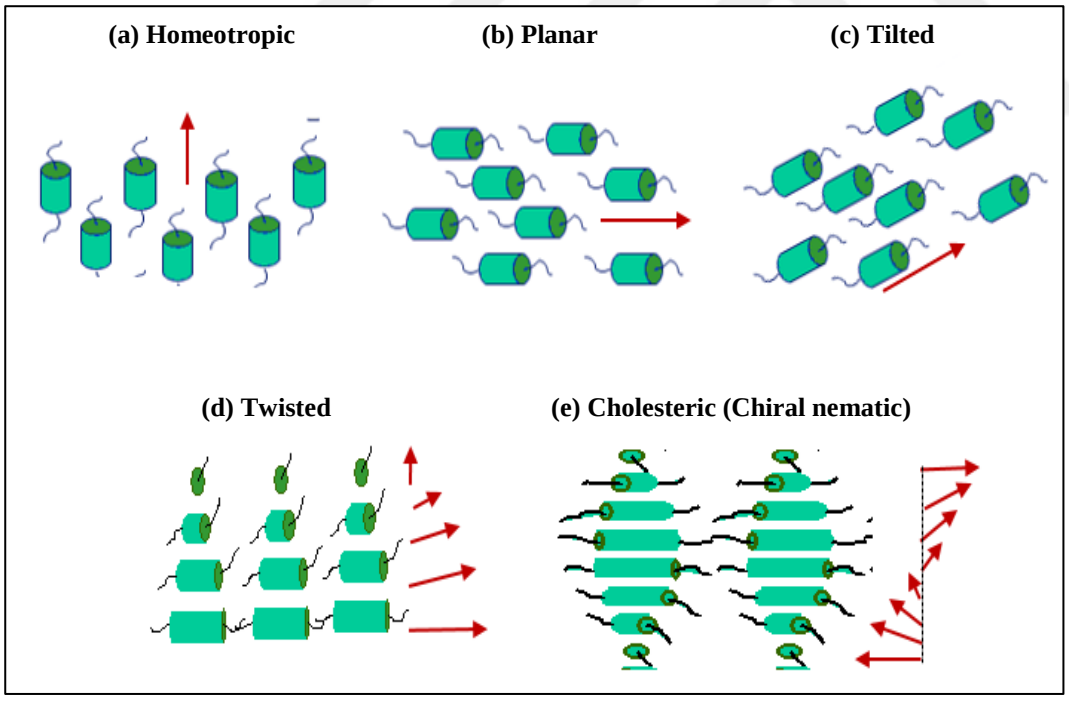

Figure 2.5 Basic illustration of (a) homeotropic (b) planar, (c) tilted, (d) twisted, (e) cholesteric alignment. Green rods indicate the calamitic molecules. Red arrows indicate the preferred director (n) of the molecules.

2.6 Alignment Techniques

Several surface alignment techniques have been developed to be used in both practical and technological enforcements. Table 2.3 lists some techniques implemented by researchers. First part in this table summarizes the mechanical alignment methods such as rubbing, air rubbing and friction transmission. Among them, mechanical rubbing has been widely used as a conventional technique for the fabrication of LC displays as well as other LCs based tools (Nemoto et al., 2012). The second part in Table 2.3 reports the photoalignment process, which is an approach to align LCs implementing linearly polarized light, for different sorts of film forms. This study concentrates on designing uniaxial planar alignment by mechanical rubbing and multidomain planar alignment by implementing photoalignment techniques which include the spin coating of photosensitive materials.

Table 2.3 Literature survey for different surface alignment techniques

Alignment method		**Reference**
Mechanical alignment techniques	Mechanical rubbing	Conventional approach
	Air-rubbing	(Hwang and Chien, 2009)
	Strecthing porous polymer film	(Fujikake et al., 2003)
	UV irraditaed friction transmission	(Tanigaki et al., 2006)
Photoalignment techniques (different types of film forms)	Spin coating of photosensitive film	(Hendrikx et al., 2017a)
	Langmiur-Blodget film	(Seki et al., 1994)
	Polyelectrolyte layered film	(Park and Advincula, 2002)
	Functionalization of photosensitive film	(Sasaki et al., 2012)
Physical patterning	Wrinkling	(Ohzono et al., 2009)
	Nanoimprinting	(Chiou et al., 2006)

Mechanical rubbing: This procedure relies on uniaxially rubbing of a thin alignment material coated substrates to form nano-grooves. When the LCs are filled into these grooves, the material is aligned in the same direction as the friction. Therefore, uniaxially aligned LCs are obtained (Figure 2.6a). Until now, polyvinyl alcohol, acrylic polymers, vinyl polymers and polyimides have been tested as alignment materials. Among them, polyimides are commonly used because of their thermal durability, low cost, processability and chemical stability against LCs. However, the rubbing method has some drawbacks resulting from the interaction type during the implementation. The friction action on the polymer surface causes accumulation of static charges and formation of fine dust particles which adversely affect the working capacity of the tools (Bisoyi and Li, 2016). For this reason, alternative methods are being improved to overcome these limitations.

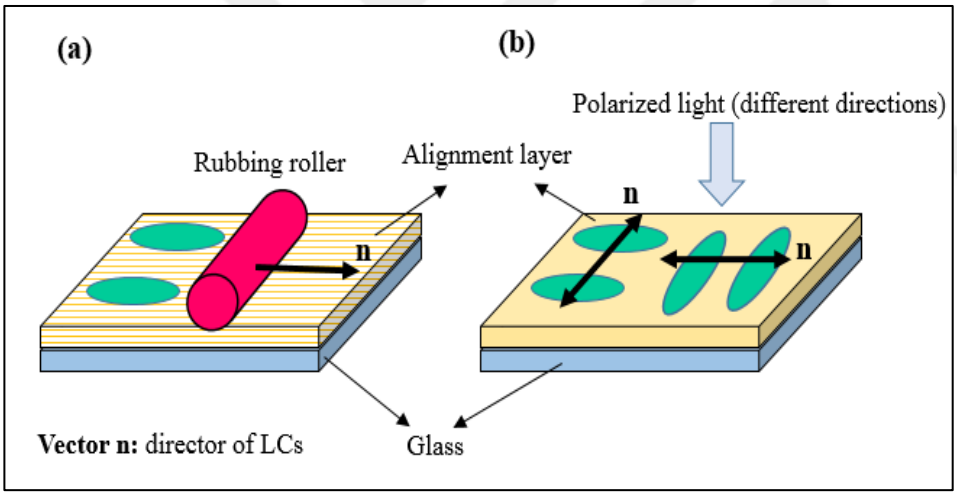

Figure 2.6 General mechanism of preparing (a) rubbed and (b) photo-aligned surfaces.

Photoalignment: This is an untouched approach that is completely conducted with light and it can be used as an ideal approach to avoid the problems that are come across with mechanical alignment techniques. Furthermore, a high-quality uniform LC orientation which has adjustable anchoring energy, and pretilt angle can be designed. For spin coating approach, the glass plates are covered by the photosensitive material such as coumarins, cinnamates and azo-dye compounds. The coated substrates are exposed to high energy linearly polarized UV light thoroughout a mask and the light-sensitive molecules are oriented

parallel or perpendicular to the direction of polarization of the light due to the selective photoreactions of the materials. It is possible to design multi-domain alignments such as molecular alignment with vertically aligned structures or different angles by changing the polarization direction (Figure 2.6b). LCs adapt to these alignment directions due to anisotropic interfacial interaction (Bisoyi and Li, 2016).

In general, photoalignment materials are categorized into three main groups depending on their photochemical reactions during linearly polarized light actuation (Seki et al., 2013). Some studies are given in Table 2.4 classified by the photoreactions and polymer types employed, which are used to design photoalignment layers. In this study, the azo group based alignment material is used.

Table 2.4 Materials used to design photoalignment layers (Seki et al., 2013)

Photoreaction	Polymer type
Irreversible photo-destruction	Polyimides, polysilanes, polystyrene, polyesters and some other aromatic polymers
Photo-crosslinking such as [2 + 2] cycloaddition	Cinnamate, courmarin, tetrahydrophthalimide
Trans-cis isomerization	Azobenzene, stilbene, cinnamate

2.7 Formation of Light Responsive Liquid Crystal Polymer Networks

Low molar mass LC monomers possess the fundamental features of LCs such as controlled-directionality; hence, prior to photopolymerization, a mixture of them can be easily aligned by utilizing the same procedures (such as rubbing and photo-alignment) that are implemented to the LCs (as described in Section 2.5). Subsequently, all obtained alignments can be frozen by photopolymerization as shown in Figure 2.7. Thanks to this freezing ability, the final product have all

properties that the starting materials have. The main point is adjusting the polymerization temperature at their nematic temperature range.

The reason for the fixation attitude can be explained by two properties of the system. The first one is due to their highly cross-linked construction (quite often 3 GPa) the transition from the nematic to the isotropic phase cannot be seen. Another one is related to the nature of the photopolymerization. Thus the phase transition throughout the process is kinetically prevented (White and Broer, 2015). Depending on the enforcement, LCPNs can be produced in the form of a film (without any substrates) or a coating. On the other hand, they can even be integrated into the systems as pigments and additives.

Generally, a small amount of azobenzene-based monomer that possesses two functional groups is implemented into a LC monomer mixture to design light-responsive coating with improved functionalities. In the existence of photoinitiator, UV light starts the polymerization process and forms the azo-LCPN. Figure 2.7 represents the chemical structures of a diacrylate LC monomer and an azobenzene monomer that are widely used in the design of smart systems.

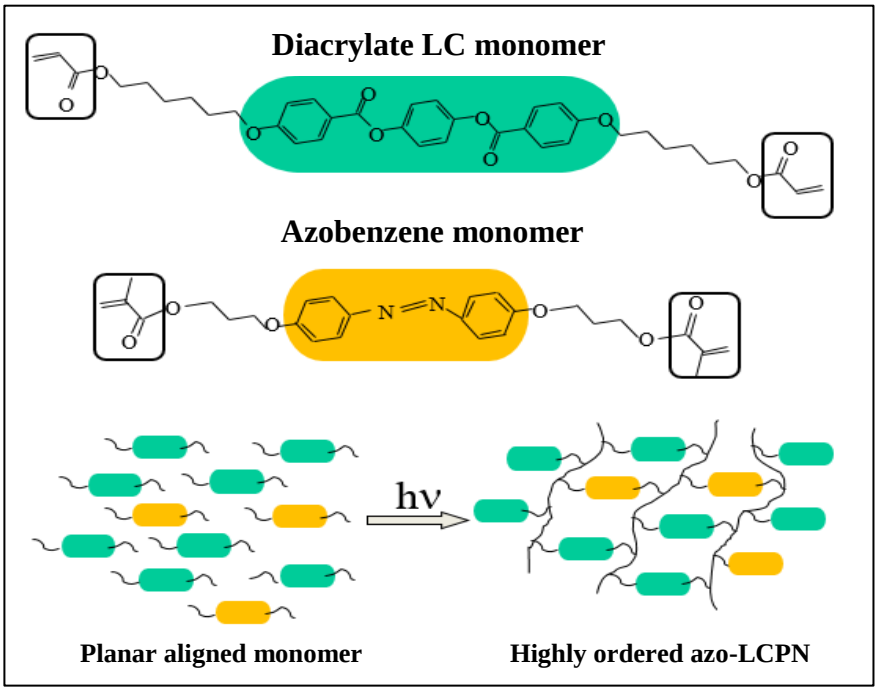

Figure 2.7 Chemical structure of typical diacrylate monomer and azobenzene-based monomer. Schematic representation of azo-LCPN formation.

2.8 Surface Topographies in Light Responsive Azo-LCPN

This subsection of the thesis gives a summary of recent studies on the light-activated surface topographies in azo-LCPN coatings. The general approach to designing such coatings begins with the preparation of monomer mixtures consisting of mono and diacrylate LC monomers, azobenzene and the appropriate photoinitiator. Subsequently, various alignment structures are achieved on the substrates using alignment techniques. Finally, the azo-LCPN coated systems are exposed to light effect (using a suitable light wavelength).

According to the conducted studies, the types of changes in surface topographies can be separated into two groups as indicated by Type A and Type B in Table 2.5. Type A indicates the switchable surface topographies between on and off states of the light source while Type B represents the study that focuses on the designing dynamic surface topographies during the polarized light actuation. As can be seen in Type A1 in the table, the photoisomerization of azobenzene compound and its interaction with LCPN structure can lead to considerable changes in height, friction coefficient, wettability and roughness of the coating. Type A2 shows the study where the azo-LCPN is coated on the soft layers instead of the rigid glass.

Table 2.5 Some studies conducted on light-switchable surface topographies

Type of surface topography change	**Substrate type**	**Movement in the coating with light**	**Reference**
Type A: Switchable surface topographies **On state:** UV light (365 nm)	**Type A1:** Glass	Height change	(Liu et al., 2012a; 2012b) (Liu, 2013)
		Friction coefficient change	(Liu and Broer, 2014b)
		Wettability change	(Tang, 2015)
		Roughness change	(Liu et al., 2015)
	Type A2: Soft layer	Height change	(Zhou, 2016)
Type B: Dynamic surface topographies (365 nm and 455 nm)	Glass plate	Oscillation behavior and height change	(Hendrikx et al., 2017b)

Although this thesis concentrates on the mechanism of Type B, type A will also be explained to give the general knowledge of the light actuation mechanism. Table 2.6 shows the conducted studies related to light-triggered height changes in the azo-LCPN coating (Type A). For orienting LCs, basically, the mechanically rubbed surfaces were used in each study. Different LC alignments such as cholesteric, periodically oriented cholesteric-homeotropic, cholesteric-isotropic, vertically aligned cholesteric and planar areas were used. Then, azo-LCPN coatings were exposed to UV light (365 nm) to see alterations in surface topographies.

Table 2.6 Some studies related to height changes in azo-LCPN coating for Type A

Substrate type	Type of alignment	Alignment technique	Height change	Reference
Type A1: Glass	Cholesteric	Mechanically rubbed PI	1 μm	(Liu et al., 2012b)
	Cholesteric and isotropic	Mechanically rubbed PI	0.9 μm	(Liu, 2013)
	Cholesteric and homeotopic	Mechanically rubbed PI Additional external: electric field	0.8 μm	(Liu et al., 2012a)
	Perpendicularly oriented cholesteric	Mechanically rubbed PI Additional external: surfactants	0.6 μm	(Liu and Broer, 2014b)
Type A2: Soft PDMS	Cholesteric	Mechanically rubbed PI	1.264.μm	(Zhou, 2016)
Type A2: Soft Acrylate	Cholesteric	Mechanically rubbed PI	0.116.μm	(Zhou, 2016)

Even though the measured height change under the light actuation points to promising results, the followed preparation technique is complex. For instance, an

electric field has to be applied to produce homeotropic oriented domains. On the other hand, the cholesteric consist of helical axes and LC molecules rotates along their helix axis. Pitch is the space where LCs traveled along the helical axis for a complete turn. The prominent point in designing is adjusting the amount of chiral dopant in the mixtures to ensure the length of pitch; hence, this requires too much effort and many calculations for design. To eliminate this workload, the planar aligned azo-LCPN coating is selected in this study.

Type A2: All conducted studies mentioned above have only focused on designing azo-LCPN coatings on rigid glass substrates. In this case, the expansion that is perpendicular to the common direction occurs and contraction movement in the lateral aspect is limited by the rigid substrate. Zhou (2016) put forward a new approach to provide this lateral stress as well as increasing the surface deformation during the light-actuation. In this study, the azo-LCPN coatings were supported with soft polymeric substrates: polydimethylsiloxane (PDMS) and acrylate based polymers including mostly 2-Ethylhexyl acrylate (2-EHA) with a small amount of tri(propylene glycol) diacrylate. Monomer 2-EHA has glass transition temperature nearly -50 ℃, thus the final product becomes soft and elastic at room temperature. On the other hand, PDMS has a silicon atom bonded with two oxygen atoms as can be seen in Figure 2.8.

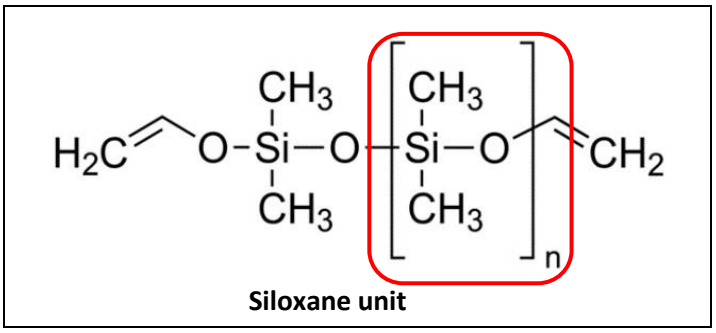

Figure 2.8 Chemical structure of PDMS.

This siloxane unit has the ability to broaden within the polymer in two directions. Compared to many traditional polymers which are composed of carbon backbones, PDMS possesses a lower glass transition temperature (Tg is around -125 °C). This is very beneficial to obtain chain flexibility (Lötters et.al., 1997). Therefore, soft combinations can be achieved even at room temperature.

Due to lack of polar groups in the polymer, untreated PDMS surfaces become hydrophobic at this step and it should be modified to make it hydrophilic before being covered with LC blend. Otherwise, the LCPN cannot be spread over the PDMS surfaces completely. The surface interactions have substantial effects on the formation of each type of coating as well as LCPN coating. The common methods are illuminating the surfaces with plasma or ultraviolet (UV), making graft photopolymerization, and sol-gel treatment of the surfaces (Trantidou et al., 2017). For spin coating approach, Zhou (2016) tried to modify the surface of PDMS substrate performing UV ozone and oxygen plasma treatment for different times. Then, the surfaces were covered with LC monomer mixtures. With this approach, the optical quality of the samples shows poor quality. It was found that the maximum modulation was increased from 0.411 μm (rigid substrate) to 1.264 μm (at 1000 μm pitch) using PDMS substrate instead of using glass one. On the other hand, the azo-LCPN coating on acrylate polymer exhibits 0.116 μm maximum deformation which was relatively smaller than the height changes in a rigid one.

Recently, the effect of wavelength and intensity of the light that used to activate azo-LCPN on volume increase on the coatings was investigated by Liu and Broer (2015). Unlike previous studies, two light sources with the wavelengths 365 nm (UV light) and 455 nm (blue light) with various intensity (I) were implemented. Firstly, the well-oriented azo-LCPN coating was illuminated with single wavelength (UV light, 365 nm) at 300 mW cm^{-2} intensity through a mask and the regional volume enhancement were found around 3%. On the other hand, using the combination of UV and blue light as a dual wavelength was improved the volume increase of the coating reaching about 12%. Maximum height changes were reached when the $I_{455\ nm}$ / $I_{365\ nm}$ ratio is around 0.1

Type B: The literature shows that it is possible to design azo-LCPN which is sensitive to the polarized UV light due to the dichroism of the azobenzene molecules. For improvement, a considerable insight has been gained by Hendrikx et al. (2017b). They designed oscillating smart azo-LCPN coatings that can alter their topographies between on and off states of the polarized UV light. This method represents an innovative alternative to design dynamic surface

topographies in azo-LCPN coatings since the oscillation frequency is provided by the unique properties of light-sensitive smart material. Mechanically rubbed PI and photoaligned LPP alignment layers were used to design such coatings. UV (365 nm) and blue light (455 nm) combinations were used to oscillate the coatings in this study. The detailed information related to this study and the height changes during the oscillation behavior (at room temperature) are given in Table 2.7.

Table 2.7 Parameters for the study related to Type B (Hendrikx et al., 2017b)

Substrate type	Alignment layer	Alignment type of azo-LCPN
Glass	Mechanically rubbed PI	Uniaxial planar
	Photoalignment of linearly photopolymerizable polymer	Perpendicularly aligned domains (0°/90° oriented director)

As reviewing the literature, there is no study related to Type B except from the conducted by Hendrikx et al.(2017b). On the other hand, there is no study in the literature related about designing of oscillating azo-LCPN coatings supported with any substrates different from glass one. Using glass substrate limits the bending behavior of the coating since there occurs no contracton in the lateral side of the coating.

2.9 The Aim of the Study

The motivation of this thesis is to ensure both contraction and expansion movement of the molecules in the smart azo-LCPN coating supported with soft polymeric substrates such as PDMS and acrylate-based substrate (TTEGDA/2-EHA) because soft substrates allow the coating shrinkage (Figure 2.9). This movement can provide higher deformations and oscillations than the values found using the vertical movements of the molecules. The finished products manufactured by laminating the substrates with nematic azo-LCPN coatings resemble a sandwich appearance when viewed in micron sizes. For this reason, it

is proposed that these systems are called "smart layered systems". In addition, the alignment layers that allow the LC molecules to be arranged in a fixed orientation (nematic uniaxial planar or photo-aligned) exist between those two polymeric layers. Two alignment approaches that are mechanically rubbed polyimide and photo-aligned brilliant yellow layers were used for enhancement.

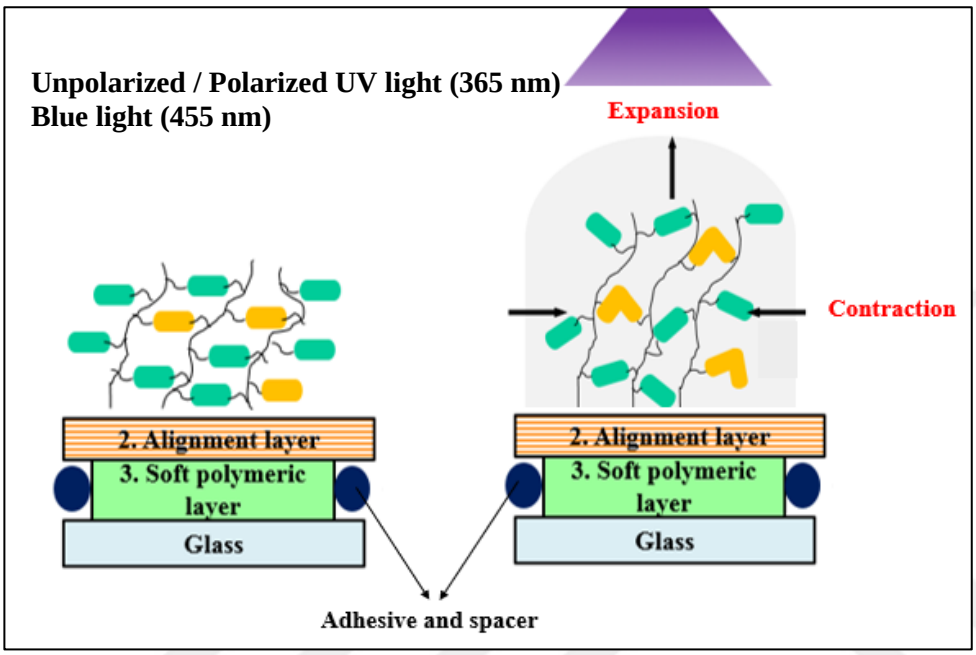

Figure 2.9 Basic respresentation of the light actuated smart layered systems.

Although Zhou (2016) worked on the design of uniaxial planar aligned azo-LCPN/PDMS layered system, this study only focused on the designing of switchable surface topographies. Here, oxygen plasma treatment was implemented to change the surface property of the PDMS substrates. Compared to the other common methods, the plasma treatment does not require heavy labor task and the results can be obtained quickly.

Also, the literature shows no consensus on azo-LCPN coated TTEGDA and TTEGDA/2-EHA combinations. Therefore, the UV-curing behaviour of the mentioned systems is optimized in this study. The effect of the softness of the substrates on both alignment and oscillation behavior is investigated by increasing the 2-EHA concentration in the substrate compositions.

3.0 EXPERIMENTAL

This part of the thesis contains the necessary information about the starting materials and sample preparation methods used to fabricate light-sensitive coatings on the soft substrates. The instruments having different setups which were used to characterize the samples are also mentioned in detail.

3.1 Materials

The product name and basic properties of used materials for each layer are given in Table 3.1.

Table 3.1 Materials used to design smart layered systems

Layers	Materials	Product name	Purpose
Azo-LCPN coating	Mono and diacrylate LC monomers	RM 82, RM 105, RM 23	Providing skeleton of LC polymer network
	Azobenzene	A3MA	Photomechanical effect
	Photoinitiator	IRGACURE 819	Starting photopolymerization reaction
Alignment layers (2 types)	Type 1: Polyimide solution	A1051	Mechanical alignment
	Type 2: Diazo dye solution	Brilliant yellow	Photoalignment
Soft substrates (2 types)	Type 1: PDMS	Slygard 184 base and curing agent	Heat curable silicon polymer
	Type 2: Acrylate-based polymer	TTEGDA	UV curable acrylate polymer
		2-EHA	Increasing softness of substrate (Used with different concentration)
		IRGACURE 819	Starting UV curing reaction

3.1.1 LC monomer blend for azo-LCPN coating

For light-sensitive nematic layer, the blend including 32.5 wt% of a diacrylate LC monomer (RM 82) and 61.5 wt% of monoacrylate LC monomers (consisting of 46.04 wt% RM 105 and 15.46 wt% of RM 23) with 5.2 wt% of azobenzene-based molecule A3MA as an additive was used. For crosslinking, 1.05 wt% of photoinitiator IRGACURE 819 (Ciba Specialty Chemicals, Switzerland) was also added to this blend. Reactive LC monomers RM 82, RM 105 and RM 23 were bought from Merck (UK) and the azobenzene molecule was synthesized by Syncom (Groningen, the Netherlands). Firstly, all monomers were completely dissolved in dichloromethane (DCM, Sigma Aldrich) to mix them uniformly and then DCM was evaporated. Table 3.2 shows the chemical structures of the materials used for light-sensitive nematic coating.

Table 3.2 Chemical structures of monomers used for LC blend.

Materials	Chemical Structure
RM 82 (diacrylate)	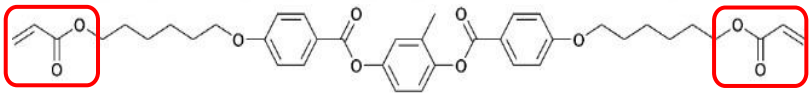
RM 105 (monoacrylate)	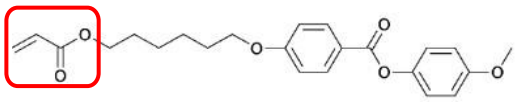
RM 23 (monoacrylate)	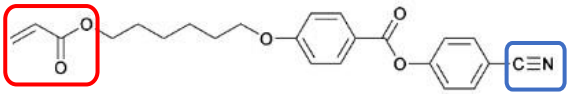
A3MA (azobenzene)	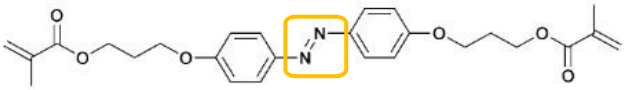
IRGACURE 819 (photoinitiator)	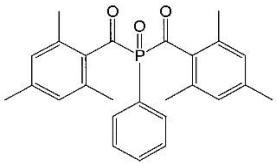

All LC monomers used in this study are composed of calamitic mesogenic central units and acrylate terminal groups (indicated with red circles in Table 3.2)

that can be polymerized. They exhibit high polymerization speed because the acrylate groups can be reacted quickly with other double bonds with the existence of photoinitiator under the UV irradiation (White and Broer, 2015). Diacrylate RM 82: In addition to their general properties, RM 82 is responsible for crosslinking of the system due to having two functional acrylates on both sides. The length of the aliphatic spacer (6C) of it is relatively higher than the spacer length in other used monomers. This chain provides the elasticity of the network and has a positive effect on the light-response behavior of the system. If RM 82 is not used in this mixture, the bending behavior of the final product would be restricted by the nature of rigid films (Hikmet and Broer, 1991).

Monoacrylate RM 105 and RM 23 are used to enhance the mechanical properties and viscosity of the final product. RM 23 possesses a benzonitrile group on one side of the chain (indicated with blue circle). Having this group makes this monomer more polar than the monomer RM 105. For dissolving of monomer blend in any solvent, the ratio of RM 105 to RM 23 had to be adjusted properly (Jin, 2013). It is worth repeating that the desired planar nematic order of LC monomers can be locked into the polymer network by keeping the polymerization temperature of the system in their nematic phase range. However, considering the phase transition values of RM 82, the nematic phase occurs at very high temperature between 86-116 °C. In this case, it is very difficult to maintain the process with this temperature range. For this reason, the combination of RM 82/RM 105/RM 23 is used in this study for the adjustment of the appropriate process temperature which improves the thermal quality of the system. The selected ratio of LC monomers in this study provided a technically suitable solubility in DCM and an extensive nematic phase temperature range extending from 35 °C to 80 °C.

IRGACURE 819 and A3MA: If the properties of the additives used are examined, photoinitiator IRGACURE 819 have an extensive UV absorption between 300-450 nm with even small concentrations as reported by the manufacturer. This means that the fixation of the alignment in LCPN can be achieved with this range of light wavelength for photopolymerization. A3MA monomer has azo groups (indicated with an orange circle in Table 3.2) that can

photoisomerize when exposed to UV light. The absorption peaks for the trans- and cis-states of A3MA are at 356 nm and 400 nm, respectively (Van Oosten et al. 2008).

3.1.2 Materials for alignment layer

For mechanical rubbing, Polyimide A1051 (PI, Sunever, Nissan Chemical) solution was used. Brilliant Yellow (BY, ChemCruz) was used as photoalignment material. BY dye was dissolved in N, N-dimethylformamide (DMF, 99.8%, Sigma-Aldrich) with a concentration of 1.5% by weight. As indicated with orange circles in Table 3.3, BY dye contains dichroic-azo groups. This structure provides an advanced molecular orientation of the LC film under the linear polarized light. The underlying reason for this action is that azo molecules tend to align in the polarized light direction.

Table 3.3 Chemical structure of alignment materials

Alignment type	Material	Chemical Structure
Type 1: Mechanical alignment layer	A1051 polyimide (PI)	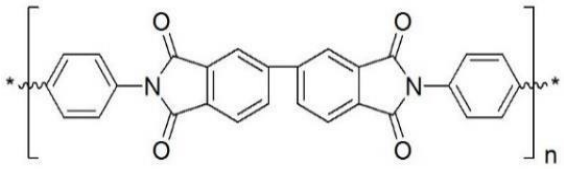
Type 2: Photoalignment layer	Brilliant Yellow (BY)	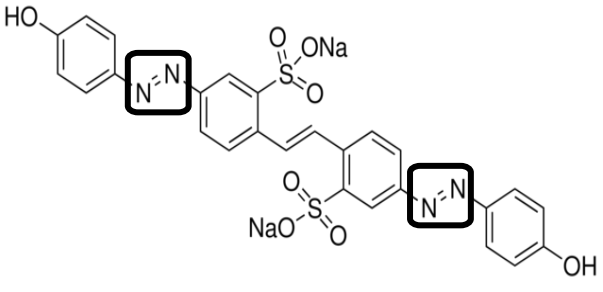

3.1.3 Materials for soft layers

For heat curable PDMS substrate, Sylgard 184 containing prepolymer and curing agent (supplied from Dow Corning, USA) in a weight ratio of about 10/1

were used as recommended by the manufacturer. Sylgard 184 elastomer prepared with this ratio has the elastic modulus value from 1.32 MPa to 2.97 MPa depending on the selected curing temperature (Johnston et al., 2014). Considering the elastic modulus of typical LCPN is around a few GPa (Liu and Broer, 2014a), this value allows us to accept PDMS as a soft material in every situation.

For UV curable acrylate-based substrate, TTEGDA (Sigma-Aldrich) and IRGACURE 819 as a photoinitiator were used. Monomer 2-EHA (Sigma-Aldrich) was added into the mixture as a more flexible additive to make softer acrylate polymer. The chemical structures of the monomers used to design soft layers are shown in Table 3.4.

Table 3.4 Chemical structure of monomers for acrylate-based monomer mixture

Soft polymeric layer	Material	Chemical Structure
Type 1: Heat curable silicon-based polymer	PDMS	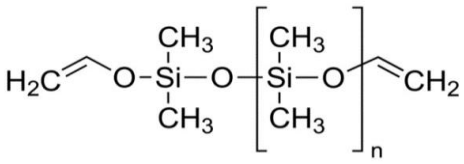
Type 2: Acrylate-based polymer	TTEGDA	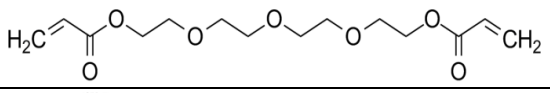
	2-EHA	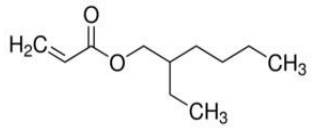
	IRGACURE 819	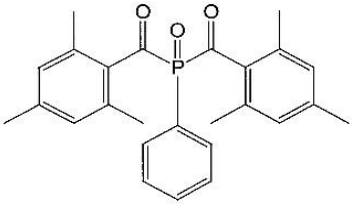

3.1.4 Adhesive and spacer for assembling layers

Ultraviolet Sealant 91 (UVS91) obtained from Norland Products Inc. (USA) was performed as an adhesive to combine the layers. This adhesive is a single

component and solvent-free design that can be cured rapidly at room temperature under UV light. They do not react chemically with any types of LCs.

Each layer used to design the smart layered systems has a certain thickness and the layers must be uniformly distributed over the applied surface. For this aim, micro pearl spacer SP220 (Sekisui Chemical Company) having different particle diameter was mixed with UVS91 sealant. Cell gaps with 6 and 70 μm thickness were used for azo-LCPN and acrylate, respectively. PDMS thickness was controlled just by using silicon holder during the curing step (1 mm).

3.2 Sample Preparation

The sample preparation steps and parameters for each substrate are given in Figure 3.1. There are three main steps involved in obtaining a good alignment quality. The steps can be explained as follows: (1) preparing polyimide (PI) or brilliant yellow (BY) alignment layers, (2) formation of well-oriented azo-LCPN and (3) manufacturing of smart layered systems by assembling the layers.

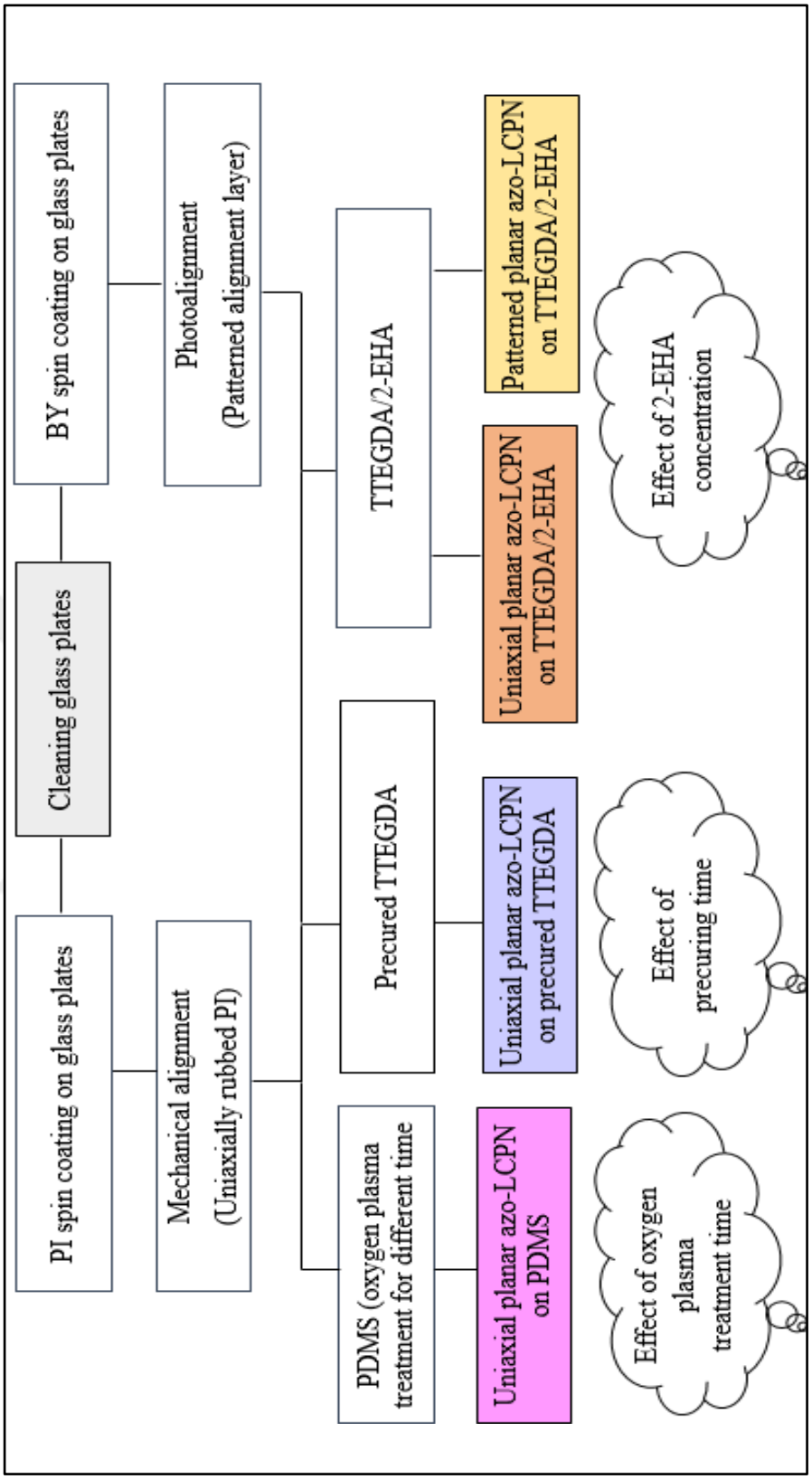

Figure 3.1 Flowchart for the steps associated with preparation of smart layered systems.

3.2.1 Preparation of alignment layers

Cleaning step: Prior to any alignment layer deposition, glass cleaning must be done properly. Glass plates as 3 cm x 3 cm were treated with acetone and then isopropanol for about 10 minutes each in an ultrasonic bath followed by blowing with N_2 gases (Figure 3.2a-b). The cleaning step was finished with treating the glasses with UV ozone for 20 minutes. UV ozone cleaning technique works with the light of two wavelengths, 185 nm, and 254 nm. Firstly, oxygen molecules in the air decompose with UV light at 185 nm to synthesize ozone O_3. The produced O_3 reacts with UV light at 253.7 nm and produces radical oxygen (O*). Secondly, O* can easily interact with surface organic substances and carbon-oxygen based molecules are formed (Figure 3.2c). Thus, the clean surfaces without any organic contaminants are achieved and they are ready for being coated with the alignment layers.

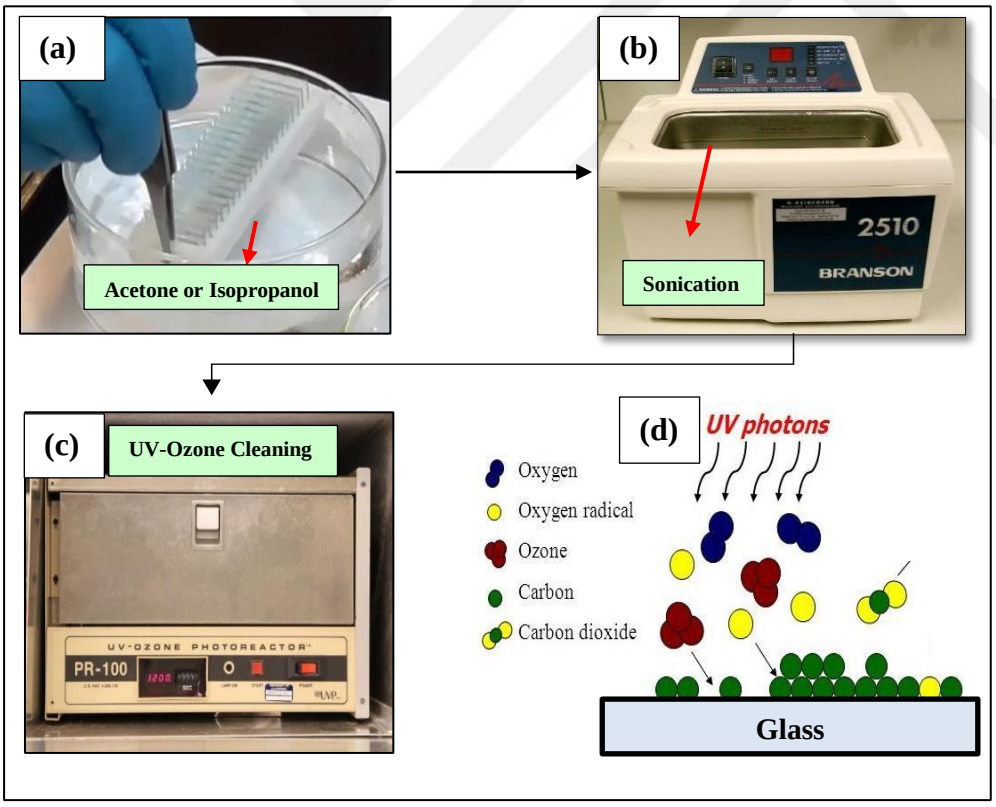

Figure 3.2 (a) Putting the glasses in acetone/isopropanol solution. (b) Sonication using Branson 2510 Ultrasonic Bath. (c) UV Ozone Photoreactor PR-100 UV and (d) UV Ozone mechanism.

Deposition step: Depending on the preferred alignment layer, cleaned glasses were laminated with polyimide (PI) or brilliant yellow (BY) solutions by spin coating technique which is a widely used coating method for uniform thin film production (a few nm to μm). The mechanism includes settling the selected solution onto the center of the glass plate and then rotating the substrate with high speed by a spin coater. The solution flows radial direction outwardly of the surface because of the centripetal force. At the end of the rotation, the surplus liquid runs over the surface and thin films are formed (Sahu et al., 2009). After thermal curing process, the films were left to cool down to the room temperature. The fabrication parameters for each alignment layer are given in Table 3.5.

Table 3.5 Spin coating process parameters for each alignment layers

Alignment type	Deposition material	Spin-up parameter	After spin-off	Parameters
Type 1: Mechanical alignment layer	PI	1000 rpm, 30 sec	Step1: Evaporation of organic solvents on a hot plate	110 °C for 10 min
			Step 2: Crosslinking reactions of polymer backbone in an oven	180 °C for 90 min
Type 2: Photoalignment layer	BY	3000 rpm, 30 sec	Evaporation of organic solvents on a hot plate	90°C for 30 min

Figure 3.3 represents the tools that were used during the deposition of both alignment layers.

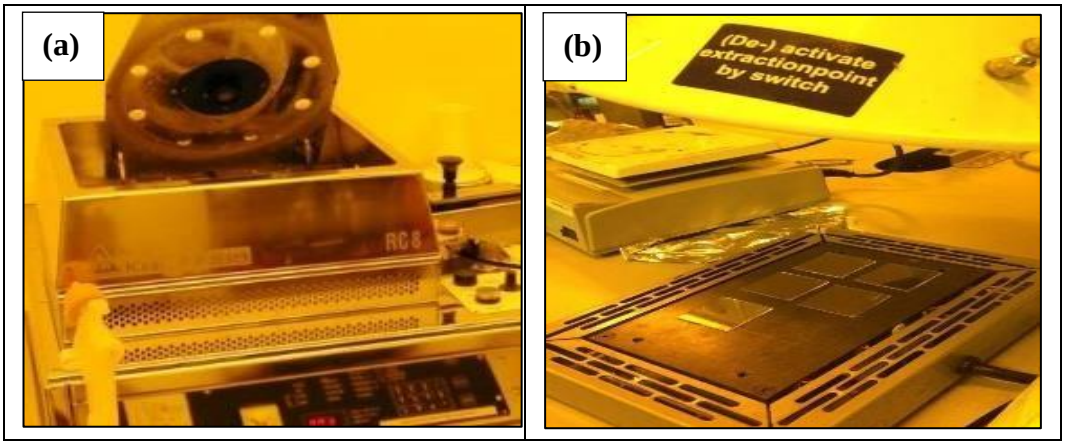

Figure 3.3 (a) Karl Suss RC8 spin-coater and (b) PI/BY films on the hot plate.

Mechanically rubbed PI film: Upon cooling down the room temperature, PI film surfaces were mechanically rubbed using a velvet-cloth to generate a corrugated surface. This action was repeated in the same direction for 5 times. The rubbing direction was shown on the glass plate in Figure 3.4.

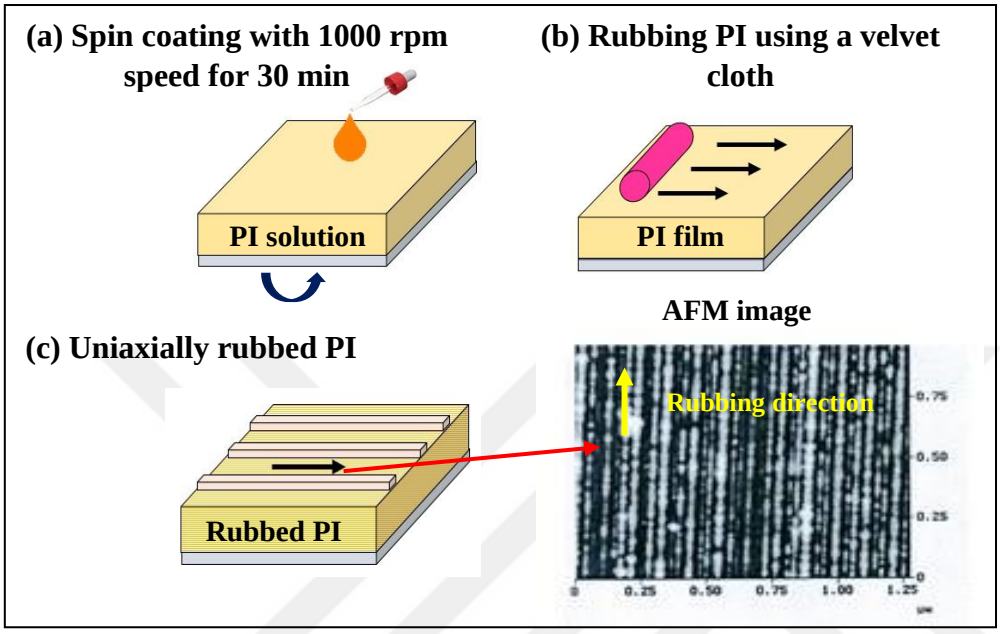

Figure 3.4 (a) PI solutions were deposited on the cleaned glasses and thin films were cured at 110 °C (10 min) and then at 180 °C (90 min). (b) PI films were rubbed in one direction. (c) Mechanically obtained alignment layers were ready. The arrows on the samples indicate the rubbing direction.

Photo-aligned BY film: The most important feature of this technique is that the BY coated layers are rewritable performing different direction of polarized light. The light intensity was kept around 30 mW/cm^2.

For the sample preparations randomly oriented BY molecules (Figure 3.5a) were illuminated applying two steps: masked and flat (Figure 3.5b-c). The first illumination is performed using mask containing periodic lines of 500, 100, 50, 25, 0.75, 0.25 and 0 μm, respectively (Figure 3.5d). The second illumination is done by removing the mask under the polarized light oriented at 90° with respect to the first illumination. The areas remained under the mask that cannot be aligned (indicated by the black line) in the first step are aligned in the second step. It can be said that the areas in periodic lines have 0°/90° orientation relative to each other in the final patterned layer (Figure 3.5e)

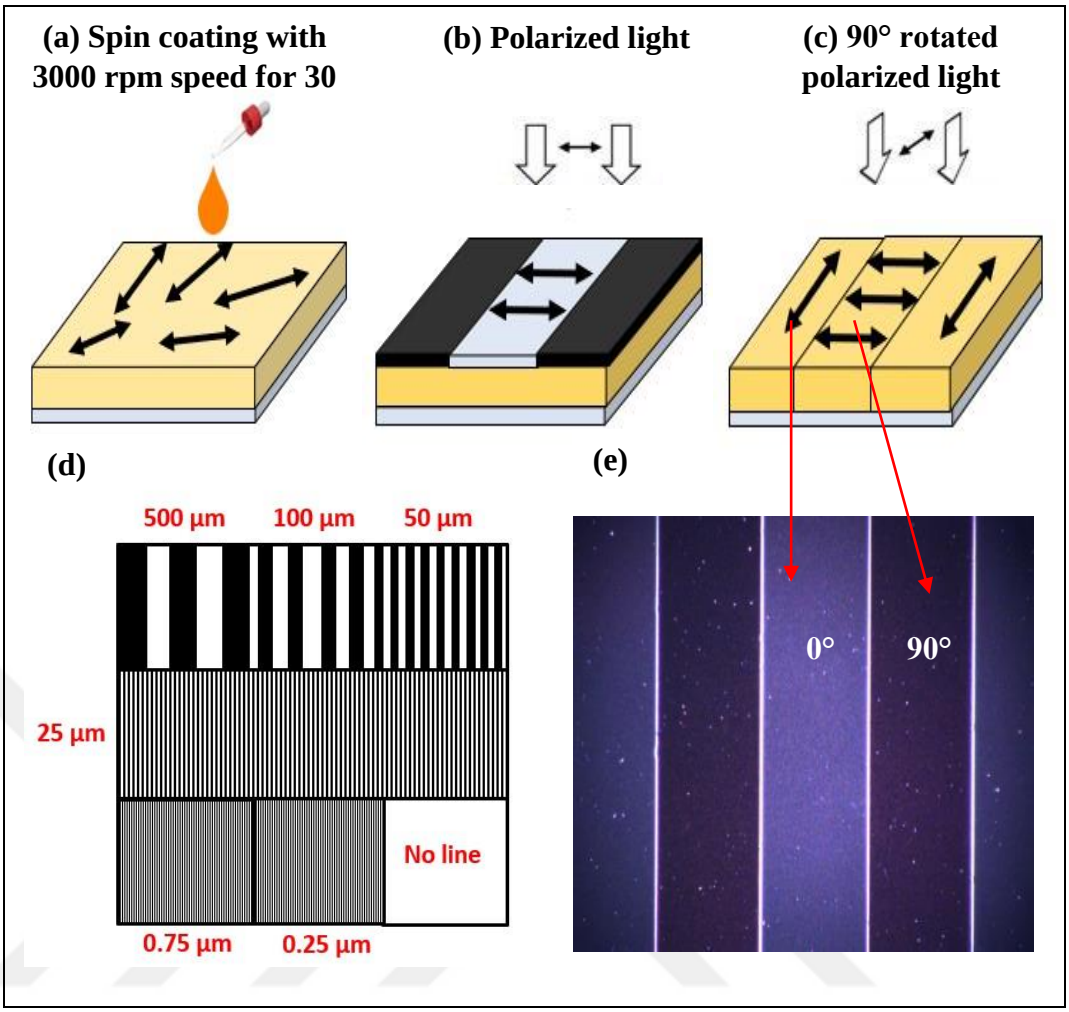

Figure 3.5 Schematic representation of preparing patterned alignment. (a) Spin coating, (b) masked and (c) flat illumination, (d) mask with periodic lines and (e) polarizing optical microscope image of patterned domains.

The photo-patterning exposure times were changed to obtain the appropriate time required for masked (M) and flat (F) illumination. For instance, PAT_8M2F indicates the sample which was first illuminated with the mask for 8 min and then illuminated with 2 min by removing the mask by changing the light direction. The sample codes are given in Table 3.6.

Table 3.6 Notations for the patterned alignment layers

Patterned cell name	MF (First masked, second flat)	
	M exposure time (min)	F exposure time (min)
PAT_6M7F	6	7
PAT_6M6F	6	6
PAT_6M5F	6	5
PAT_6M4F	6	4
PAT_6M3F	6	3
PAT_6M2F	6	2
PAT_5M4F	5	4
PAT_5M3F	5	3
PAT_5M2F	5	2

3.2.2 General approach for formation of azo-LCPN

Well-oriented azo-LCPN coatings were fabricated on the aligned substrate by photopolymerization process. LC blend was exposed by UV light for 10 minutes using a mercury lamp (EXPR Omnicure S2000) with a cut-off filter ($\lambda >$ 400 nm, Newport FSQ-GG400 filter). Undesired activation of the azobenzene molecules prior to light actuation was prevented using this cut-off filter. Because the absorption peaks for the trans to cis states of azobenzene A3MA is at 360 nm (Van Oosten, 2009). Therefore, the main task is only making the azo-LCPN without activation of azobenzene compound in this step. Additionally, photoinitiator IRGACURE 819, which is also used in the LC blend, has an extensive absorbance wavelength distribution as indicated by the manufacturer. Thus, it does not cause any problem to start the photopolymerization with the light

source having the wavelength higher than 400 nm. The photo-polymerization setup is shown in Figure 3.6a-d.

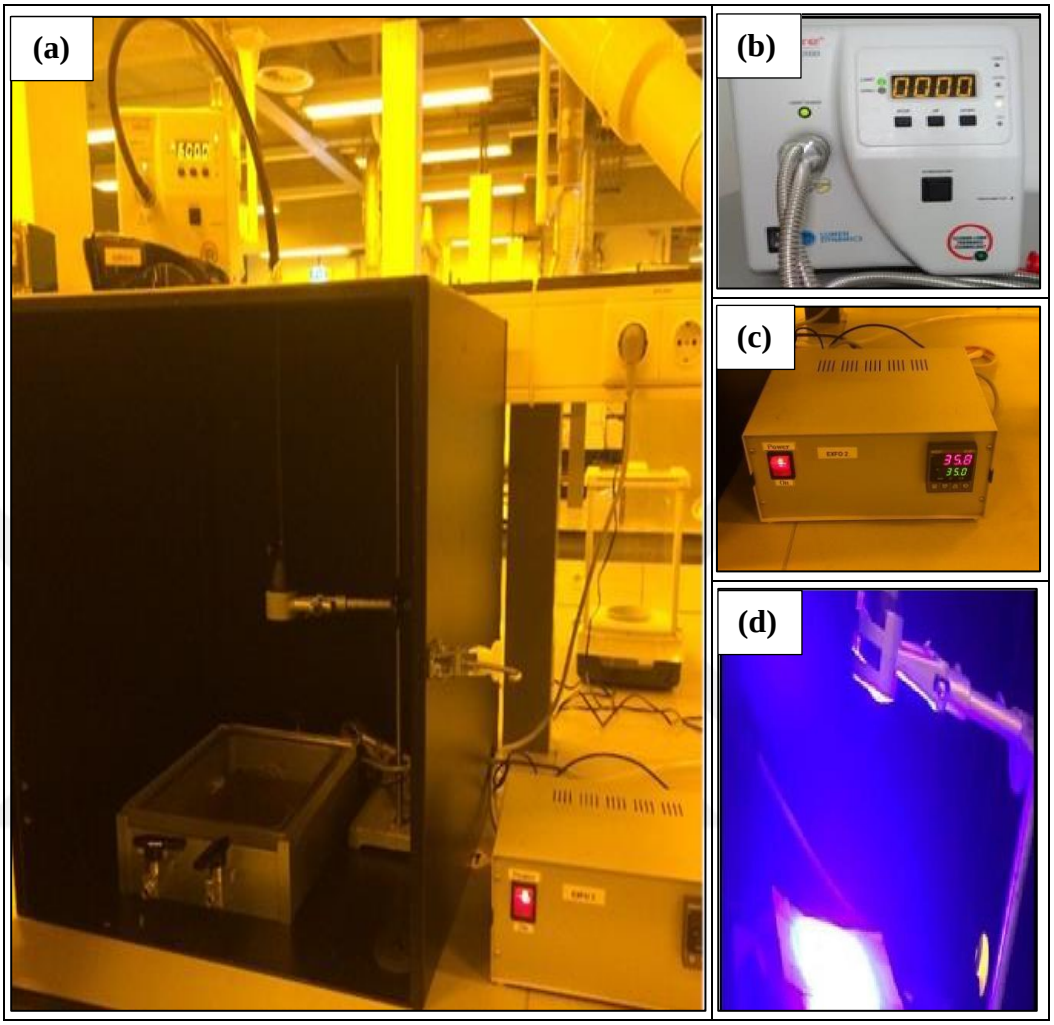

Figure 3.6 Photograph of the photopolymerization apparatus. (a) General appearance of the system with protective box. (b) Mercury lamp (Omnicure S2000). (c) Temperature controller which was connected to N_2 box. (d) UV light bulb.

The light source was kept at equal distance (approximately 30 cm) above each sample to control the intensity. All process was carried out in a protective container because of the harmful effects of UV rays on the human body. The setup also contains a nitrogen box connected to the temperature controller. Azo-LCPN coated samples were polymerized in inert atmosphere (N_2) filled box. Especially, it is important that the spin-coated LC molecules are retained in this box in order to achieve uniform temperature distribution.

3.2.3 Combinations of azo-LCPN and soft layer

In this thesis, the smart layered systems containing azo-LCPN coating were obtained by testing different alignment-substrate combinations and production methods. Here, different combinations of uniaxially aligned and patterned azo-LCPN on different substrates such as modified PDMS, pre-treated acrylate and acrylate are explained in detail.

3.2.3.1 Uniaxial planar aligned azo-LCPN on PDMS

Replication: PDMS mixture containing pre-polymer/curing agent (10/1) was poured into the bottle. The mixture was placed into the vacuum chamber and kept there under 0.5-1 atm pressure until all bubbles removed (approximately 15 min). This step plays an important role in the production because the presence of air bubbles notably decreases the durability of the azo-LCPN/PDMS system obtained as final product.

Afterwards, the mixture was poured into the silicon wafer with a depth of 1 mm and then one PI aligned glass layer put on it. This combination was then cured in an oven at 60 °C for 1 hour to replicate uniaxial planar orientation into the PDMS substrate. The glass plate was removed from the aligned PDMS surface. Each step performed from preparation of the mixture to the end of the replication is shown in Figure 3.7a-i.

Adjusting hydrophilicity: The surfaces were treated with Emitech K1050X oxygen plasma reactor, under 50 W for 0, 15, 30, 45, 60 and 75 s, respectively. Then, aligned PDMS substrates were ready for being covered with the smart material. The steps for the modification are shown in Figure 3.7f-i.

Azo-LCPN formation: LC blend was first dissolved in DCM (25wt% solid) and then directly spin-coated on aligned PDMS substrate in 2500 rpm for 30 sec. It was assumed that this method aligns the LC molecules along the field of rubbing direction. Subsequently, photo-polymerization was started under the UV light (as mentioned in Section 3.2.2).

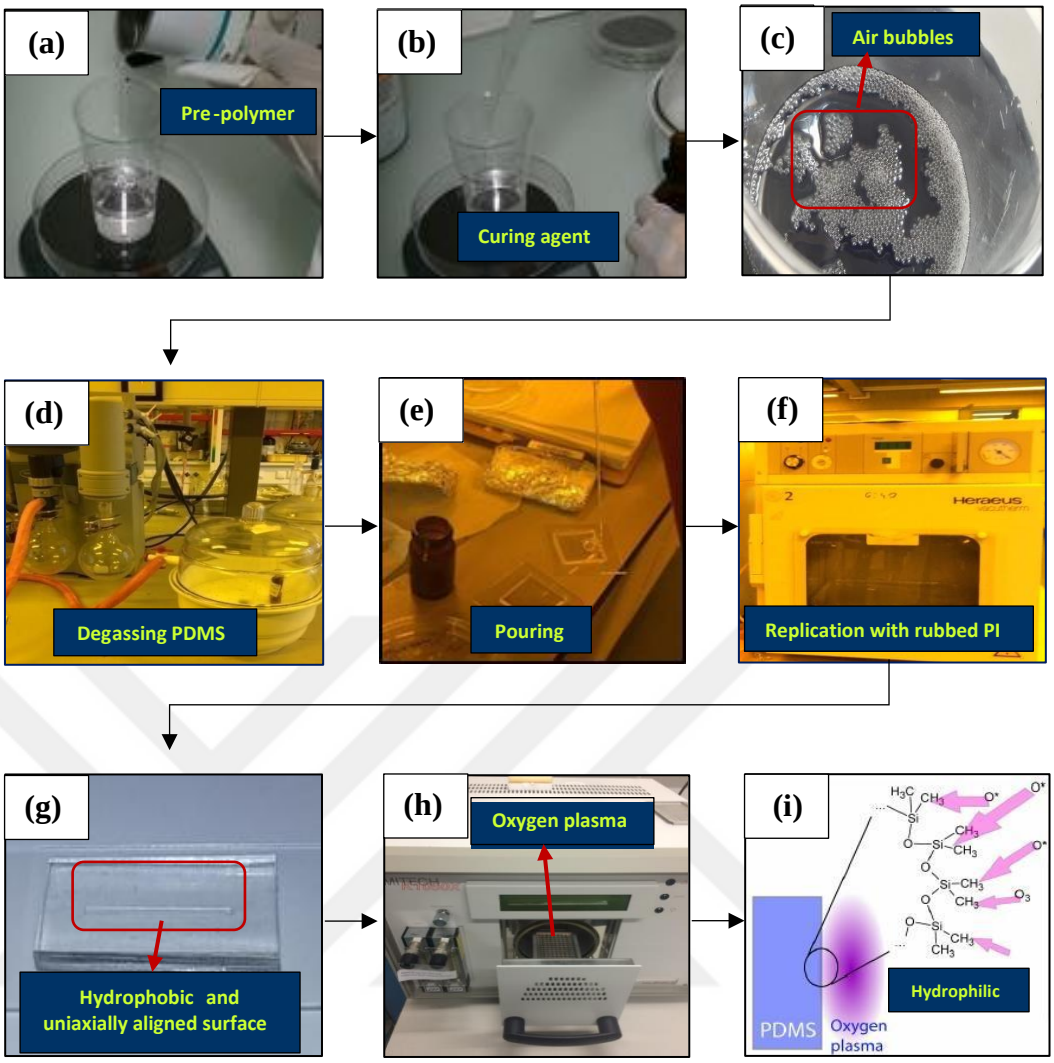

Figure 3.7 Steps for designing modified and aligned PDMS surface: (a-c) mixing Sylgard 184 pre-polymer and curing agent, (d) degassing of PDMS mixture using vacuum controller CVC 3000, (e) pouring the mixture into the holder, (f) curing PDMS mixture against to uniaxially rubbed PI alignment layer in Heraeus-vacuum drying oven, (g) obtaining hydrophobic, aligned surface after removing of PI alignment layer, (h) modifying the surface in an oxygen plasma reactor (Emitech K1050X) and (i) obtaining modified uniaxial aligned hydrophilic PDMS surface.

This layered system can be coded as UA_PDMS_X. UA is used for uniaxially aligned azo-LCPN. X indicates the applying time for plasma treatment. It is one of the process parameters in the investigation of the samples. Figure 3.8 illustrates the schematics of UA_PDMS_X sample preparation steps.

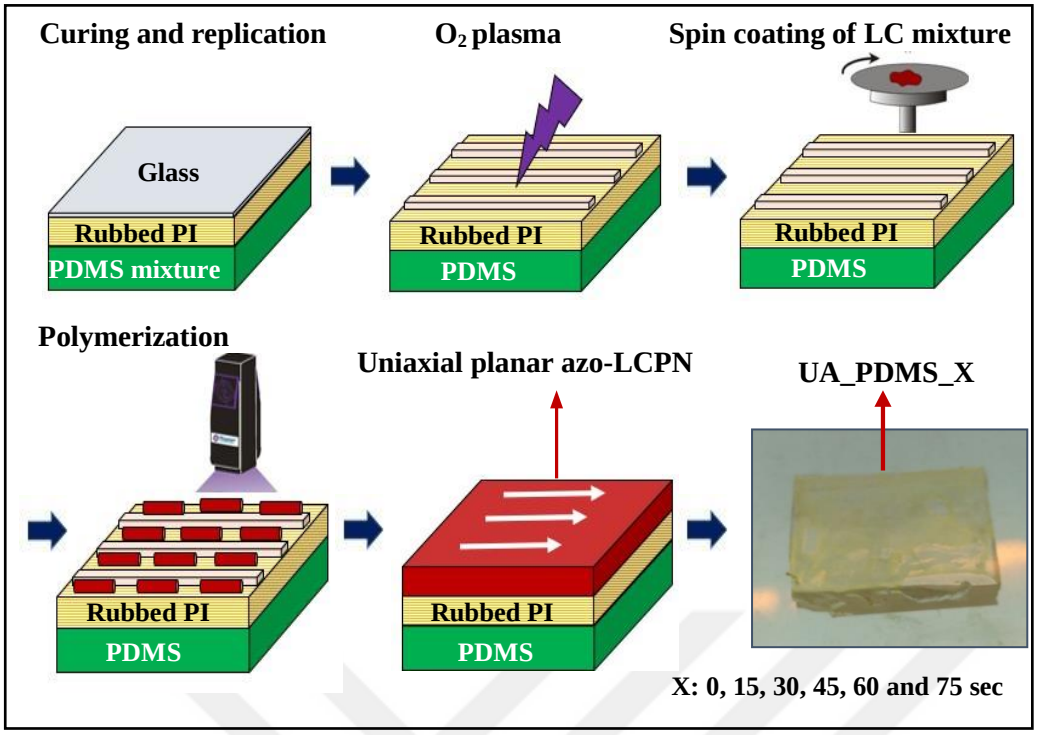

Figure 3.8 Schematic illustration for sample preparation of uniaxially aligned azo-LCPN formation on modified PDMS.

3.2.3.2 Uniaxial planar aligned azo-LCPN on pre-treated acrylate

Replication: The cell consisting of rubbed PI and Silane A174 treated (ST) glasses is glued together with 70 μm cell gaps and then filled with TTEGDA mixtures. The reason for using ST glass is to enhance the distribution of acrylate monomers onto the glass plates (Zhou, 2016). Subsequently, TTEGDA substrates were cured against to rubbed PI under the low intensity UV light (4.5 Joules/cm^2 of light energy) for 30, 45, 60, 75, 90, 120, 150, 180, 210, 240, 270 and 300 secs. It means that substrates were aligned prior to covering with azo-LCPN coating. The thickness of the acrylate substrate was kept as 70 μm for each substrate.

Azo-LCPN formation: After applying the pre-treatment on TTEGDA films, the aligned substrates and rubbed PI layer were bonded together with uniform thickness (6 μm), and then capillary filling the cell at 75 °C with the LC blend in its isotropic state and cooling down to nematic state (35 °C). Then, the cells were polymerized as mentioned in Section 3.2.2. For the light actuation, all cell structures were opened. The layered system including uniaxially aligned azo-

LCPN on pre-aligned TTEGDA can be coded as PCUA_X. Here, X shows the time for treatment with low intensity UV light. It is one of the process parameters in the investigation of those samples. Figure 3.9 represents the schematics of PCUA_X production.

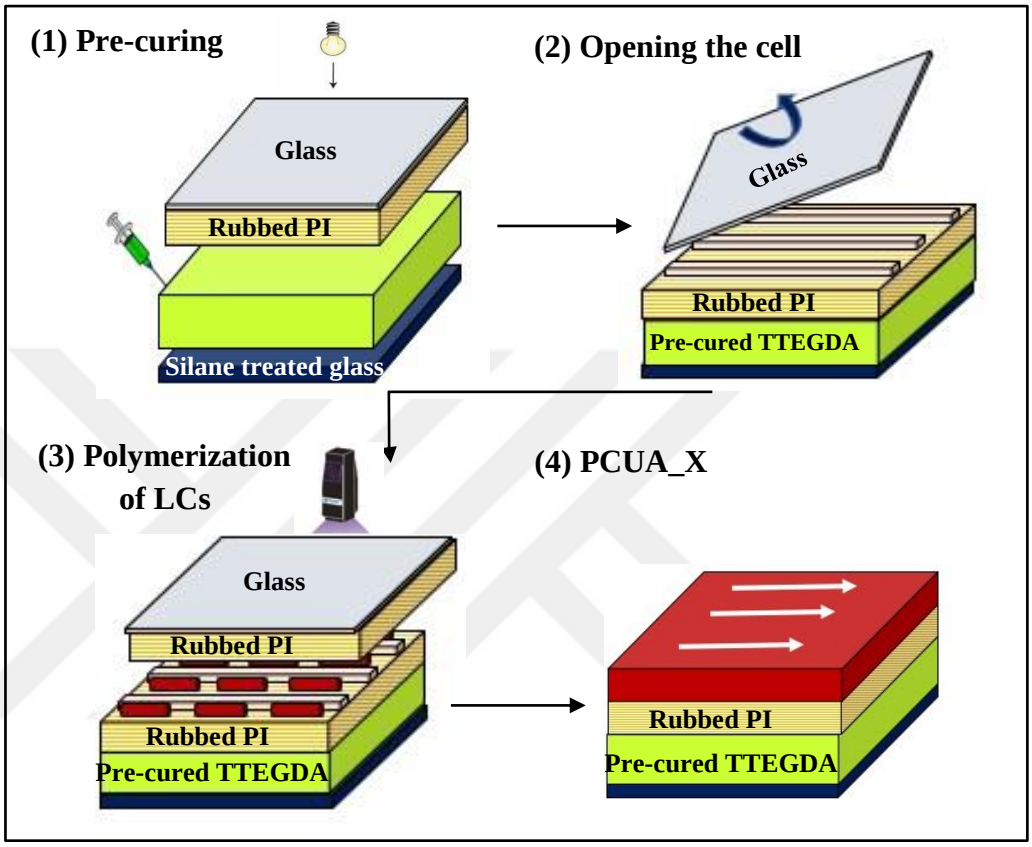

Figure 3.9 Schematic representations of preparing pre-cured layered system.

3.2.3.3 Uniaxial planar / patterned aligned LCN on acrylate substrates

This method consists of two steps. In the first step, the LC blend was filled between the cell containing alignment layers (uniaxial planar rubbed PI or patterned BY cells with the thickness of 6 μm). Subsequently, the cell is filled with LCs at 75 °C and cooled down to 35 °C. The photopolymerization was started implementing the same equipment and the procedure as stated in Section 3.2.2. Thus, well-oriented azo-LCPN coatings were achieved. To design the desired smart layered system with the soft layer, the cell was opened using a razor blade. Upon opening the cell, the film is retained on one of the glass plates.

The second step of the procedure includes curing an acrylate polymer mixture against to this flat well-oriented azo-LCPN coating. With this method, both curing and alignment of the acrylate substrates were obtained at the same time compared to previous pre-treatment method. The cell gap was again controlled with 70 μm spacers for acrylate substrate. A schematic representation of this preparation method is shown in Figure 3.10.

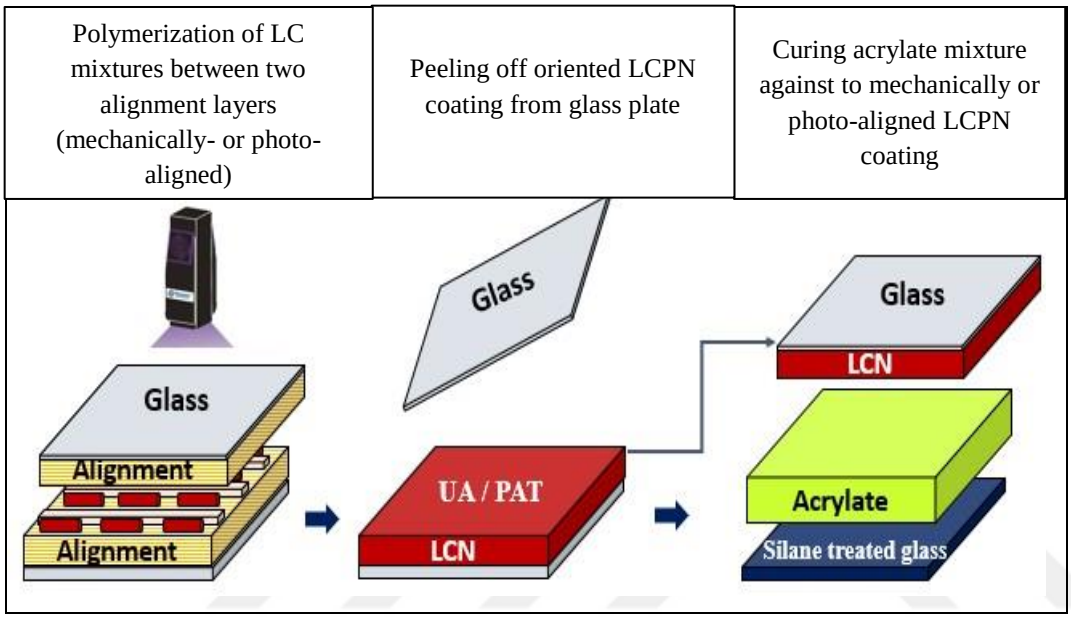

Figure 3.10 Schematic representation of fabrication of directly cured samples.

In this set of experiments, addition to those preparation methods, the acrylate soft substrates (70 μm thickness) were produced by mixing different concentrations of TTEGDA and 2-EHA (vol.%) to investigate the effect of substrates mechanical properties on the oscillatory actuation.

TTEGDA and 2-EHA are notated as T and E, respectively. For instance, T100 substrate means that there is no 2-EHA monomer in the formulation and the substrate contains only TTEGDA. T80E20 indicates the substrate which has 80 vol.% of TTEGDA and 20 vol.% of 2-EHA in the mixture. The uniaxial planar aligned and patterned aligned azo-LCPN can be named as UA and PAT_MF (depending on the selected exposure time), respectively. Table 3.7 exhibits the notation system is used for all samples.

Table 3.7 Notations for all samples characterized in this study

Alignment	Substrate	Parameter X	Sample code
Uniaxial planar	PDMS	Effect of O_2 plasma time (sec)	UA_PDMS_0
			UA_PDMS_15
			UA_PDMS_30
			UA_PDMS_45
			UA_PDMS_60
			UA_PDMS_75
	Pre-cured TTEGDA	Effect of pre-curing time (sec)	PCUA_15
			PCUA_30
			PCUA_45
			PCUA_60
			PCUA_75
			PCUA_90
			PCUA_120
			PCUA_150
			PCUA_180
			PCUA_210
			PCUA_240
			PCUA_270
			PCUA_300
Uniaxial planar	Directly cured TTEGDA/2-EHA	Effect of 2-EHA concentration (vol. %)	UA_T100
			UA_T80E20
			UA_T60E40
			UA_T40E60
			UA_T20E80
			UA_T5E95
Photo-aligned	Directly cured TTEGDA/2-EHA	Effect of 2-EHA concentration (vol. %)	PAT_MF_T100
			PAT_MF_T80E20
			PA_MF_T60E40
			PAT_MF_T40E60
			PAT_MF_T20E80
			PAT_MF_T5E95

3.3 Sample Characterization

In this study, the azo-LCPN coating, acrylate-based substrates and final products were characterized by different characterization tools as given in Table 3.8. This section includes the detailed explanation for each technique.

Table 3.8 Characterization tools and tasks used in this study

Characterization tool	Model	Target	Samples
UV-Vis Spectrophotometry	Shimadzu UV-3102PC	Measuring dichroic ratio	Azo-LCPN coating
Crossed Polarizers	Thorlab	Alignment quality of azo-LCPN coating	All samples
Polarized Optical Microscopy (POM)	Leica DM 2700	Alignment quality of patterned azo-LCPN coating	All samples
Digital Holographic Microscopy (DHM) • **365 nm UV light** • **455 nm blue light**	DHM® R210, Lyncée Tec	Measurement of dynamic surface topographies	Samples which have suitable alignments
Dynamic Mechanical Analyzer (DMA)	TA Instruments, Q800	Storage modulus of acrylate-based substrates	T100, T80E20, T60E40, T40E60, T20E80
Differential Scanning Calorimetry (DSC)	TA Instruments, Q800	Thermal properties of acrylate-based substrates	T80E20, T60E40, T40E60, T20E80, T5E95

3.3.1 UV-Vis spectroscopy

UV-Vis spectroscopy is a special instrument to measure the absorption or reflectance of the samples performing light in the UV spectral range. In this study, the azo-LCPN coating which has 2 um thickness was prepared and the light absorption capacity of the coating was characterized under the linearly polarized light that was both parallel and perpendicular to the preferred direction of the LCs.

Moreover, dichroic ratio which is a term to define the ratio between the light absorption of azobenzene throughout the molecular alignment of LCs and perpendicular to it was measured for 365 nm and 455 nm light. This characterization was done to figure out the performance of the selective light actuation.

3.3.2 Crossed polarizers and POM

The alignment quality of azo-LCPN coated samples was macroscopically checked according to the light transmittances between two polarizers arranged perpendicular to each other. Additionally, POM was used to investigate the microstructure of the patterned azo-LCPN samples by taking advantages of the optically anisotropic character of LCs. The general appearance of characterization tools are shown in Figure 3.11.

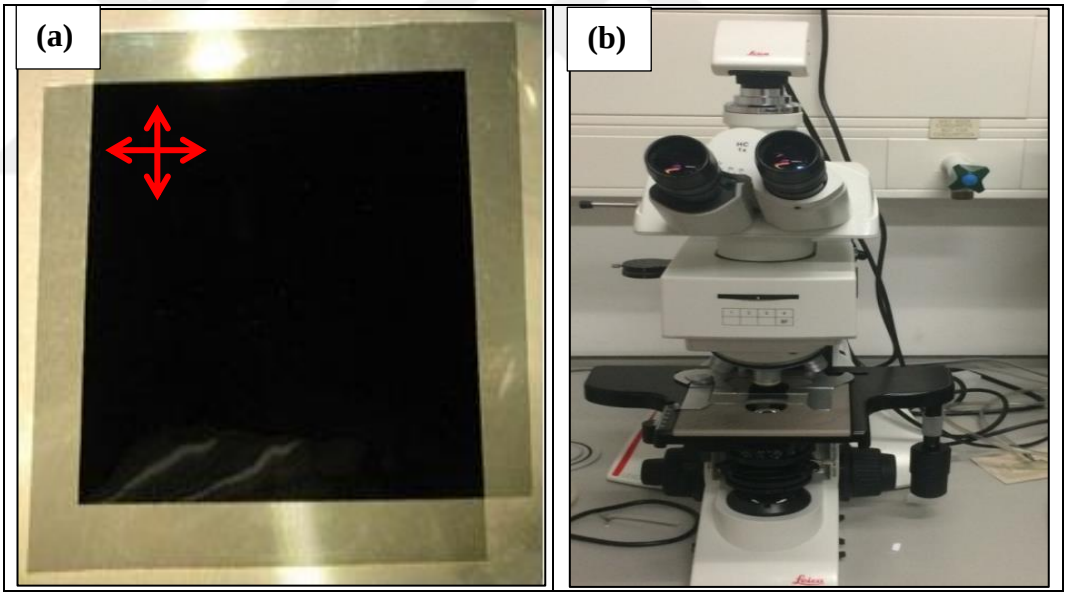

Figure 3.11 (a) Crossed polarizing films, (b) POM Leica DM 2700.

Procedure: When the angle between the light polarization plane and the preferred director of planar LCs is 45°, the highest light transmission is achieved; hence, the bright regions appear. On the other hand, when the sample is placed parallel to one of the preferred polarizers, the dark regions should be seen. This is a commonly used approach to check the samples before the light actuation and the followed technique in this study is given in Table 3.9.

Table 3.9 Procedure for checking LC alignment quality

Position of the preferred direction (n)	**0°**	**45°**
Representation of the directions of the polarizer (P)	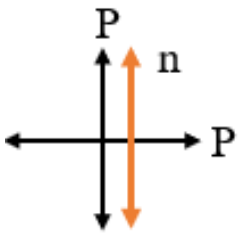	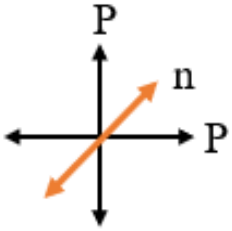
Color	Dark	Bright

3.3.3 Digital holographic measurement

The surface topographies of the samples were characterized in detail using a DHM during light actuation. Different from traditional microscopes, DHM is a type of microscopy that combines digital holography with microscopy. Recently, the use of DHM has become popular because of its advantages of full field, non-destructive, high-resolution and 3D imaging, which captures the quantitative phase information of microscopic samples.

In general, holograms are produced with an optical set-up including a laser light source, mirrors and lenses for beam guiding and then they are collected by a recording device. Figure 3.12a shows a general configuration of the set-up. Light wave from a laser is split into two beams by a beam splitter (BS). One of the first beams is used to illuminate the object and then it is scattered at the object surface. This beam is called objective beam. The other beam, called reference beam, is used to illuminate the light sensitive medium directly after reflected by the mirror. The object and reference light beams are collected by the camera and then the interference pattern is constructed. This recorded interference pattern is called hologram. In reconstruction, the original object is recreated by illuminating the hologram with the reference beam (Figure 3.12b). A virtual image can be observed by the users and this image is indiscernible from the original object (Yepes, I. S. and Gesualdi, 2017).

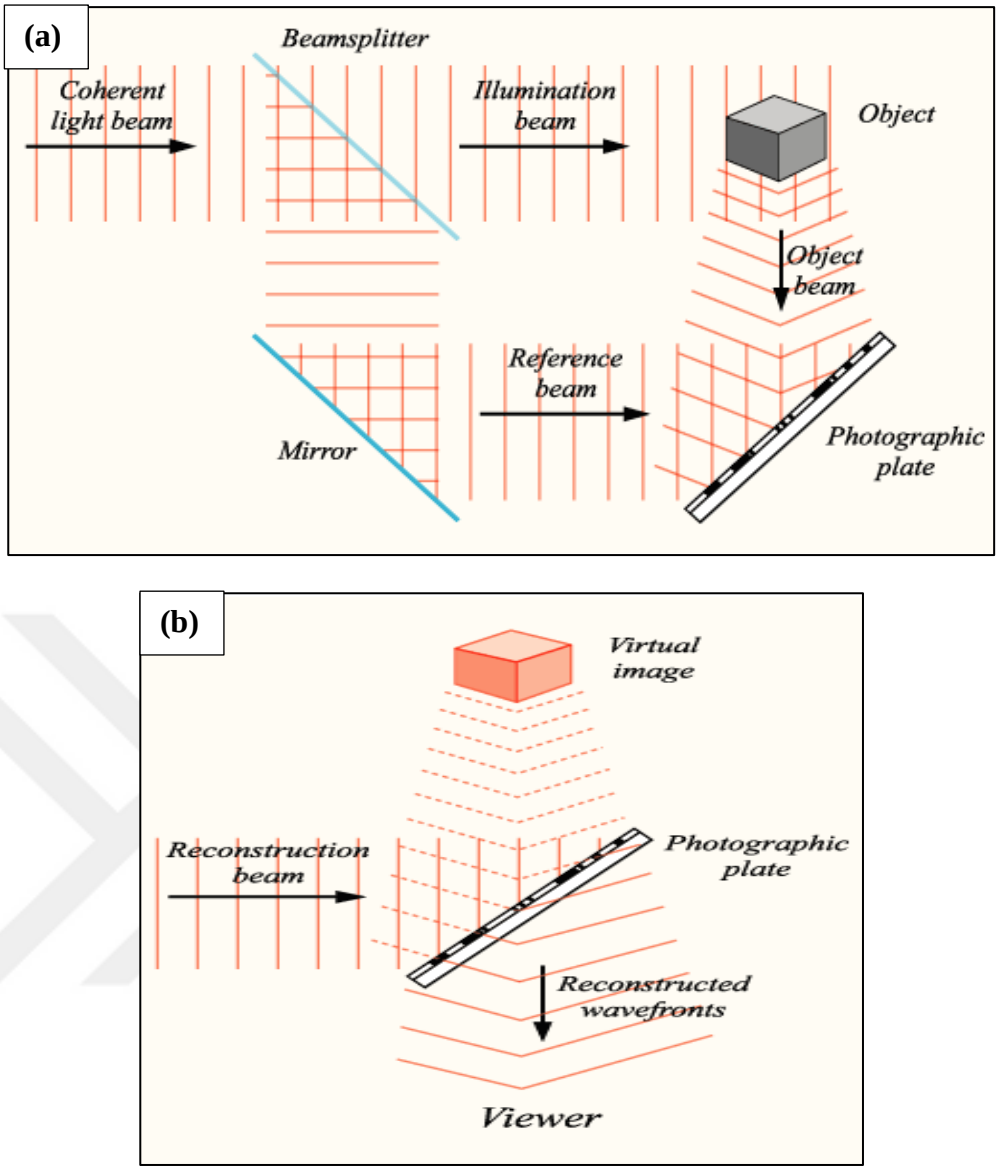

Figure 3.12 Basic principle of (a) hologram recording and (b) hologram reconstruction.

In digital holography, the holographic interference pattern is digitally recorded by a charge-coupled device (CCD) camera and transferred to a computer as an array of numbers. This method lets recording and reconstruction of three-dimensional (3D) images of real objects because a hologram gives both the intensity and phase information about the object. With this technology, the experimental enforcement of digital holographic systems for recording, as well as for numerical and optical reconstruction of 3D objects became possible. The holograms of the transparent materials at different depths can be recorded at the same time and an auto digital focus is possible. 3D images of a sample can be recorded hundreds of times in a second.

Procedure: For the light-actuation experiments, DHM was equipped with UV (λ = 365 nm, M365L2, Thorlabs) that illuminates the sample from the bottom and blue light LEDs (λ = 455 nm, M455L3, Thorlabs) that comes from the upper side of the sample (Figure 3.13a-b). The reflected light from the sample is collected by the microscope objective and combined with the reference beam for recording digital images. The holograms are then digitally interpreted by means of the Koala Acquisition & Analysis (Lyncée Tec SA, Switzerland) to reconstruct an image of intensity and phase profiles (Figure 3.13c-d). Numerical reconstruction of the sample is done to provide real time monitoring of phase mean values on different defined areas on the coating. The real-time analysis of the dynamic surface topographies of the samples is performed in detailed and 3D images are produced (Figure 3.13e).

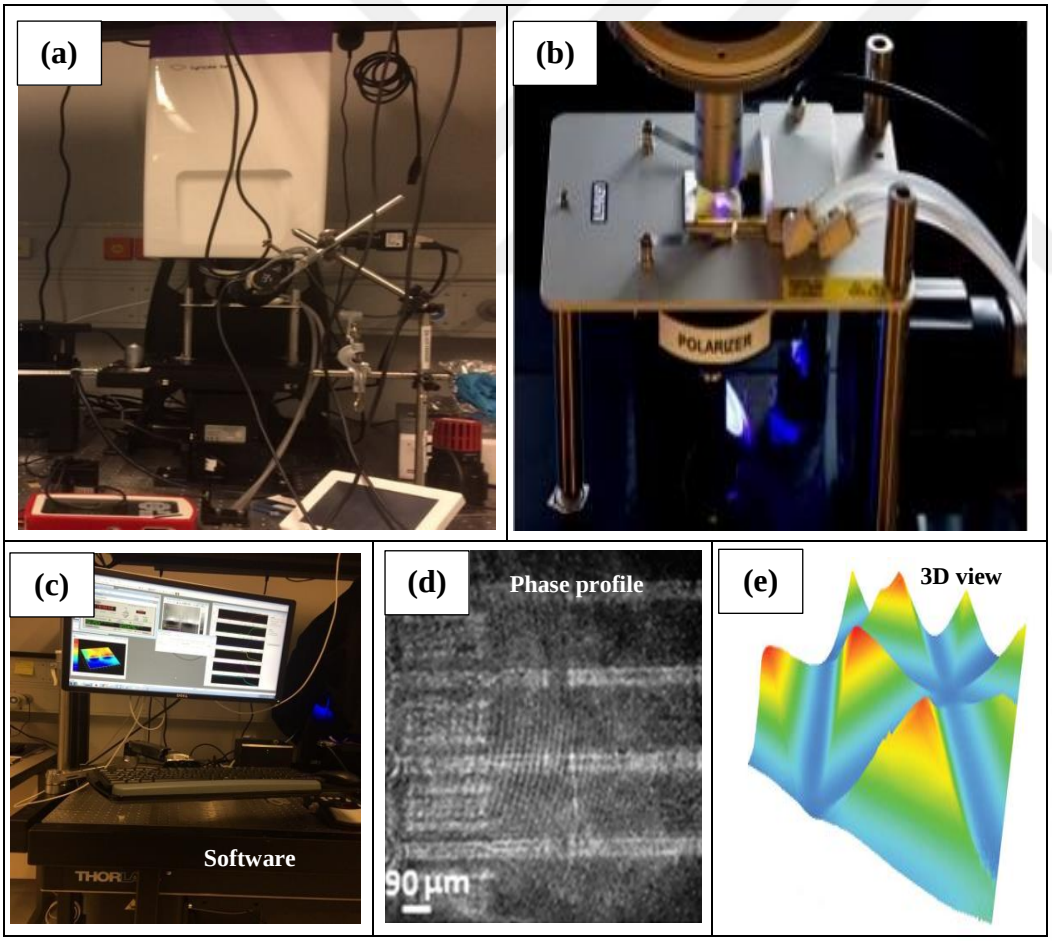

Figure 3.13 (a) DHM R210 Lyncee Tec SA), (b) The setup for illuminating the samples while monitoring with DHM. It is equipped with thermo controlled stage (Linkam). (c) Software: Koala. (d) Produced hologram. (e) 3D appearance.

For oscillating surface topographies, DHM was combined with a polarizer (10LP-UV, Newport) mounted in a rotating stage (Thorlabs). The existent smart coated surfaces were recorded for 30 sec without illumination to record the initial flat thickness of the substrates. After 30 sec, the LC films were illuminated by switching both UV and blue light at the same time with the UV polarizer set to rotate at a speed of 2.5° s^{-1}. Depending on the sample, UV light can be polarized. The measurement of the height changes was monitored by recording the holograms for 10 full rotations of the polarizer. Then, the LCPN coating was exposed with blue light until obtaining stable surface (typically 20-30 min). All produced graphs were normalized with respect to the initial flat surface thickness. Creation of videos and image analysis was performed with an image processing program called as ImageJ.

3.3.4 DMA and DSC

The storage modulus of each acrylate-based substrate was tested by DMA which is an analytical tool that determines the mechanical properties of a broad range of materials such as polymer solutions and composites. DMA records temperature-dependent viscoelastic properties and determines the modulus of elasticity by applying a force to the sample. The thermal properties of the samples were analyzed by DSC at a heating rate 5°C/min, under continuous nitrogen flow. Figure 3.14 represents the DMA and DSC characterization tools.

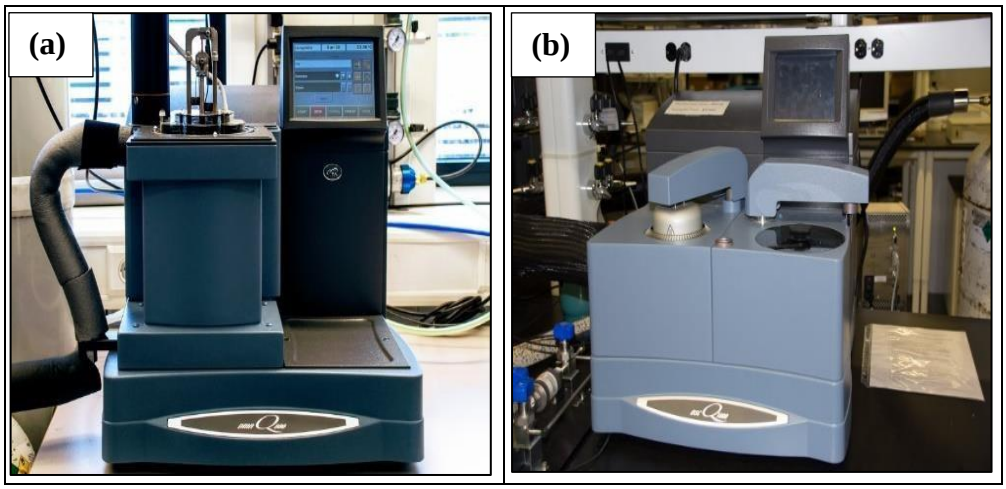

Figure 3.14 Photographs of (a) DMA Q800 and (b) DSC Q1000.

4.0 RESULTS AND DISCUSSIONS

Under this title, the characterizations results and interpretations of the smart layered systems manufactured are given in four subsections. In the first subsection, the anisotropic light absorption capacity of the used azo-LCPN coating is reported in order to figure out its light sensitivity. In the second and third subsections, the alignment results of uniaxial planar aligned azo-LCPN implemented PDMS and both pre-cured and directly cured acrylate substrates are reported, respectively. The suitable method for combining the layers is detected. In the fourth subsection, the results obtained from the experiments which were carried out with polarized light to detect the oscillation behavior of the uniaxial planar and photo-aligned azo-LCPN based systems are reported. In the final subsection, the effect of 2-EHA concentrations used in acrylate substrates on the samples is investigated using the graphical results and 3D representations of dynamic surface topographies.

4.1 UV-VIS Characterization

The absorption capacity of the coating measured by UV-VIS spectroscopy is represented in Figure 4.1.

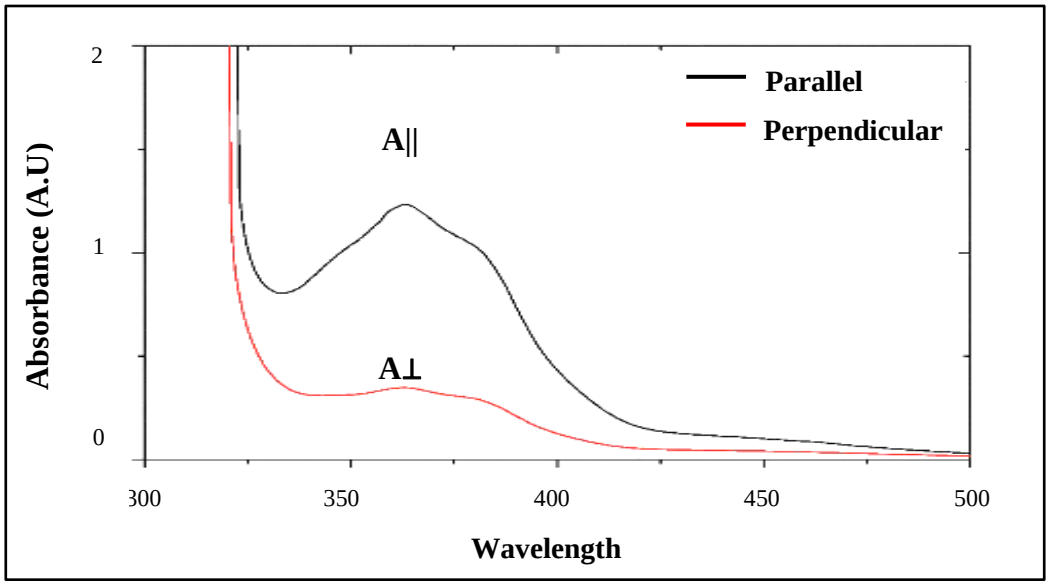

Figure 4. 1 UV/VIS absorption spectra for azo-LCPN coating.

There are two absorbance spectra measured for both parallel (A||) and perpendicular (A⊥) to the polarized light. The ratio of A|| to A⊥ represents the dichroic ratio (A||/A⊥) which is an important term for designing smart light responsive systems as well as optical devices. Due to trans-cis isomerization of azobenzene, the maximum absorption was observed around 365 nm wavelength (UV) as expected. According to the angular dependence of absorption, a significant difference was observed between the curves of A|| and A⊥ at 365 nm wavelength. The reason is that the azo-LCPN coating is more sensitive to linearly polarized UV light which has a parallel polarization direction with respect to the orientation of LCs. On the other hand, the presence of light with a wavelength of 455 nm (blue light) caused a decrease in light adsorption capacity as shown in Figure 4.1. Both parallel and perpendicular absorbance curves have similar trends that are closed to each other since under the wavelength of 455 nm azo-LCPN is less sensitive to the polarized light.

In the literature, Van Oosten (2009) measured the dichroic ratio (A||/A⊥) of azobenzene units limited to about 3 for 365 nm light. Since the dichroic ratio of the azo-LCPN is affected by many factors such as thickness of the coating, concentrations of azobenzene and temperature, it cannot be generalized with a certain value. For this study, the dichroic ratios (A||/A⊥) were found around 3.1 and 1.7 at 365 nm and 455 nm, respectively. These results embody two properties of the used coating. The first one is that used azobenzene has more tendency to interact with UV light than blue light; hence static surface topographies can be designed between on and off states of UV light as well as the utilization of blue light as a side effect to support the surface movements. The second one is that the combination of polarized UV and blue light can be performed in order to accomplish dynamic surface movements.

It is important to ensure both alignment quality and uniformity of the azo-LCPN smart coating prior to light activation. Nevertheless, the multi-layered systems showing light sensitivity have been a new approach. For this reason, the alignment of LCs between pure glass plates with a thickness of 6 um was first examined in order to gain a better understanding of the alignment expectation

associated with the used material. Figure 4.2 represents the macroscopic images of the LC cell structure between crossed polarizers.

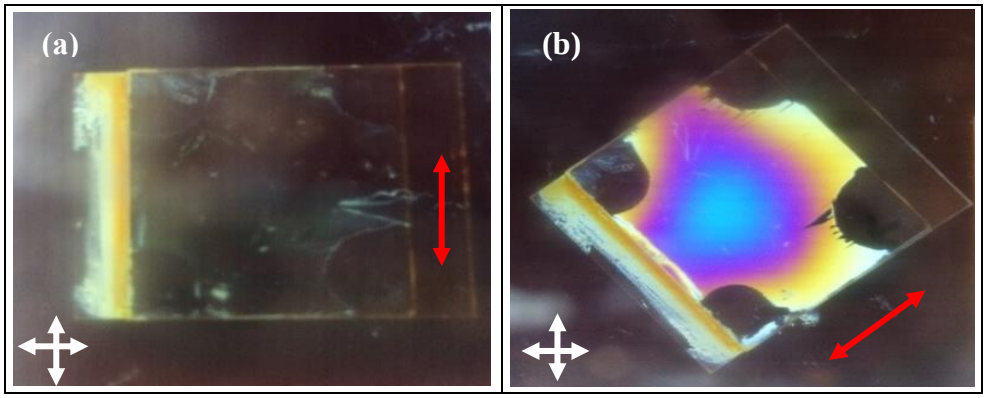

Figure 4.2 Optical images of a uniaxial planar azo-LCPN in a cell structure between crossed polarizers with the director (a) 0° and (b) 45° shifted from the one of the polarizers. The white crossed arrows demonstrate the directions of the polarizers and the red arrow indicates the rubbing direction.

A considerable color change was achieved when rotating the coating at 45° relative to one of the crossed polarizers. At initial position, when the preferred direction of LCs was oriented at 0° related to one of the polarizers, the cell structure showed completely dark regions because the molecules restricted the movement of the polarized light. On the other hand, completely bright regions were observed on the coating at 45° position since the alignment of the LCs allowed the polarized light to pass through**.** Hence, it can be said that the material exhibited high optical anisotropy. The findings from this subsection were then compared with the produced smart layered systems for detecting ideal alignment textures. The samples having an appropriate optical anisotropy were then characterized under the irradiation of both UV and blue light.

4.2 PDMS Substrate

Here, the effect of O_2 plasma treatment time on the wettability and alignment property of uniaxial planar aligned azo-LCPN coated PDMS substrates were examined. Different modification times were applied with a plasma power of 50 W to turns the surface of PDMS from being hydrophobic to hydrophilic. As expected, the PDMS sample without plasma effect (UA_PDMS_0) showed non-

wetting behavior owing to having hydrophobic character. Only some regions of the surface were randomly covered with LC material (Figure 4.3a) and the wettability of the PDMS surfaces enhanced after the plasma oxidation. Until 30 sec, a positive correlation was found between the covered regions of the surfaces and durations (Figure 4.3a-c).

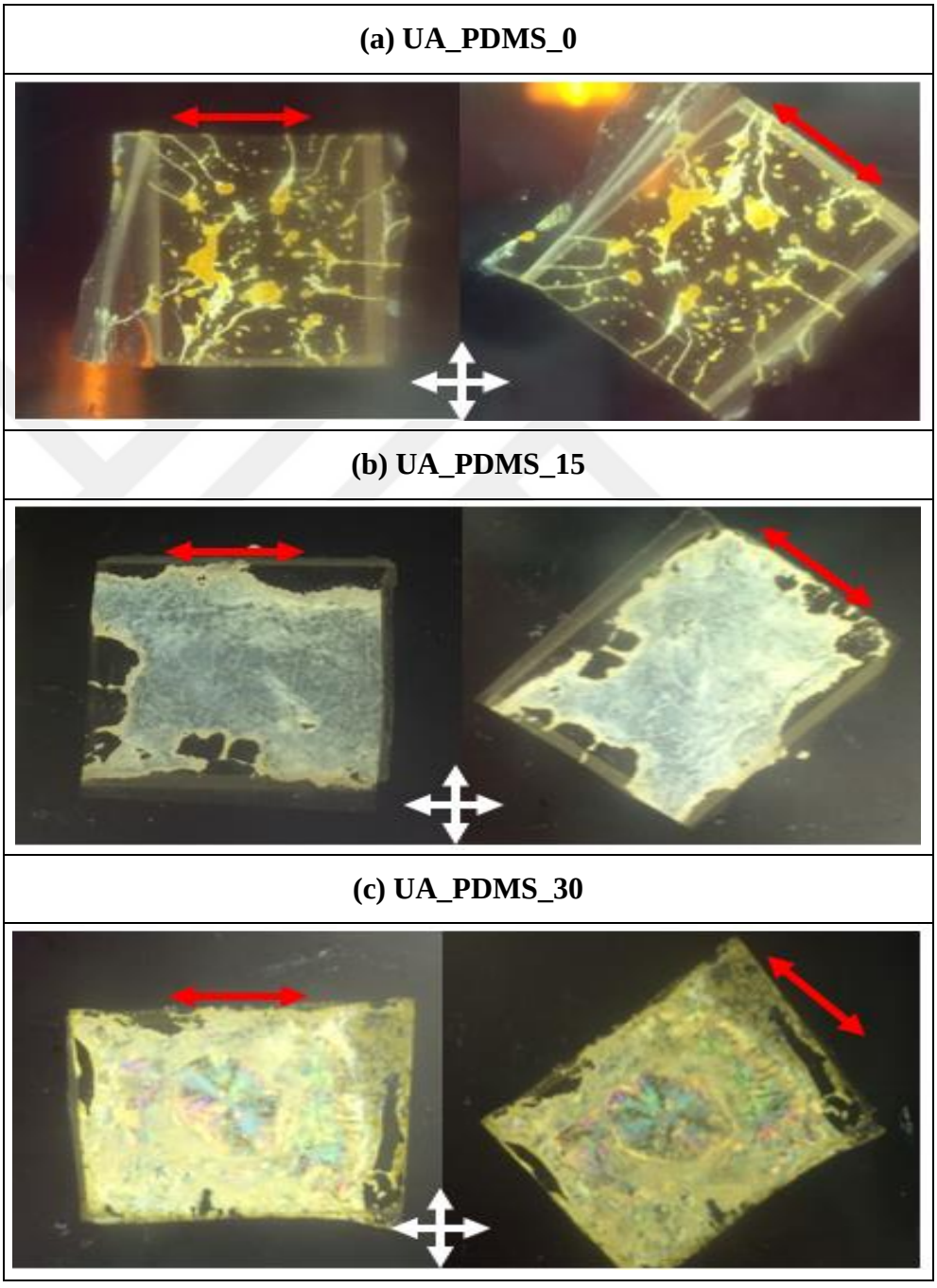

Figure 4.3 Macroscopic images of (a) UA_PDMS_0, (b) UA_PDMS_15 and (c) UA_PDMS_30 between crossed polarizers. Left row: rubbing direction of the coating was parallel to one of the polarizers; right row: the coatings were rotated at 45˚.

There were no significant differences observed between UA_PDMS_45 and UA_PDMS_60 in terms of their wetting behavior (Figure 4.4a-b.). After 60 sec, the interaction between the smart coating and substrate started to decrease (Figure 4.4c).

(a) UA_PDMS_45

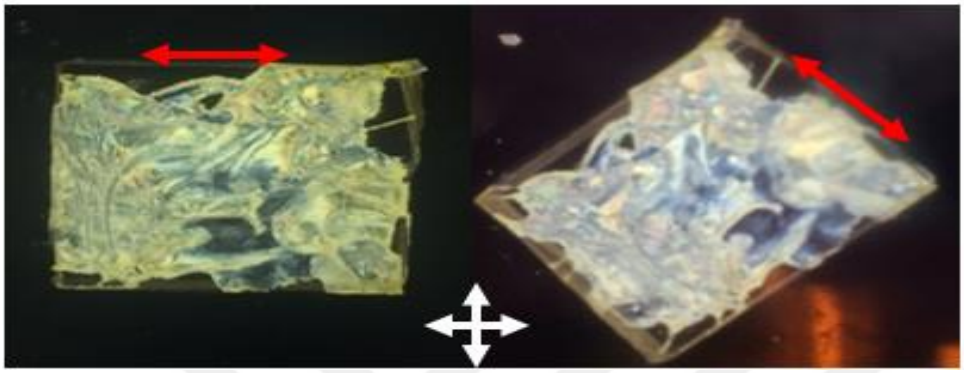

(b) UA_PDMS_60

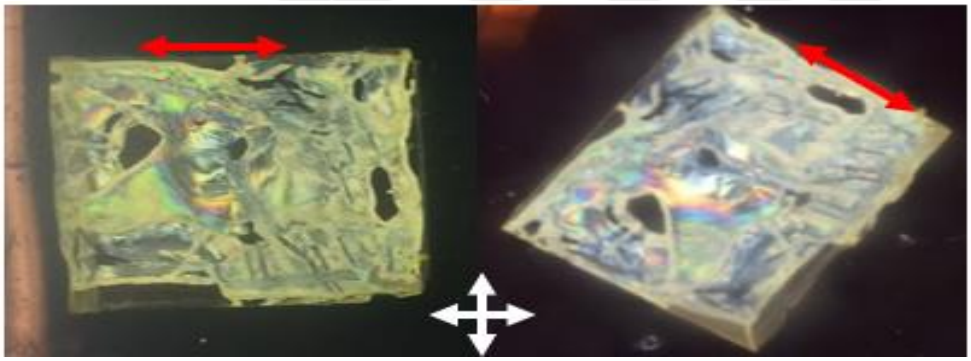

(c) UA_PDMS_75

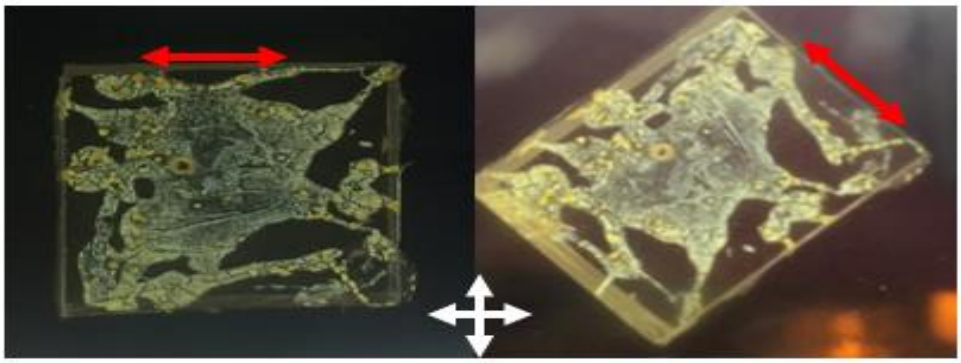

Figure 4.4 Macroscopic images of (a) UA_PDMS_45, (b) UA_PDMS_60 and (c) UA_PDMS_75 between crossed polarizers. Left row: rubbing direction of the coating was parallel to one of the polarizers; right row: the coatings were rotated at 45˚.

It can be concluded that the maximum required oxidation time was between 30 and 45 sec to provide hydrophilicity in the PDMS substrates used for being interacted with LCs

When compared with the alignment results on the glass plates (in Subsection 4.2), the expected optical anisotropy was not achieved for prepared PDMS-based samples while shifting the rubbing direction of the coatings at 45˚ with respect to one of the polarizers. Only UA_PDMS_30 and UA_PDMS_45 showed randomly scattered bright regions which were not uniform (Figure 4.3c and 4.4a).

These observations cannot be generalized to explain all types of azo-LCPN/PDMS combinations but the experiments can be carried out conducting different combination techniques to support the expectations related to the optical quality. Moreover, the alignment quality can be influenced by internal and external experimental conditions such as curing temperature, treatment time and plasma power that alter the structure of the material. In this study, a major source of limitation was due to the high energy ions of the plasma effect. These ions destroyed part of the substrates, and thus had a disruptive effect on the orientation of UA_PDMS_X samples.

From another side of view, Johnston et al. (2014) reported that implementing a higher curing temperature (above room temperature) and longer treatment time lead to make the PDMS harder, more brittle, and much more tending to crack. Based on this approach, the combinations could be carried out using a lower curing temperature (below 60 ˚C) with longer time. It might help to make softer and uniform substrates. However, there is a serious drawback of using this conditions for the layered systems produced. With this approach, the coating of LCs on the substrates has to be done directly after curing step because PDMS shows temporarily rendered hydrophilicity by implementing O_2 plasma treatment. Some studies were performed to keep hydrophilic structures of PDMS for longer times such as one week (Tan et al., 2010; Bodas, D. and Khan-Malek, C., 2007), yet the actual characterization of the surfaces can be time-consuming due to the requirement for analysis.

Owing to the limitations of the material, PDMS is not selected as a suitable material to be used as a substrate. Therefore, the characterization conducted with the combination of azo-LCPN and PDMS is limited at this stage.

4.3 Pre-cured Acrylate Substrates

In this subsection, the influence of pre-curing time of TTEGDA substrates on the alignment properties of uniaxial planar aligned azo-LCPN coated TTEGDA substrates was investigated and the light sensitivity of the selected sample was measured. For pre-curing, each glass supported TTEGDA substrates were kept under low intensity 365 nm UV light prior to covering with LCs. This means that the applied polymerization to form azo-LCPN was carried out in the final section. The samples are indicated by PCUA_X, where X refers to the time spent for the treatment.

4.3.1 Alignment improvement

Figure 4.5a-f shows the captured macroscopic textures of PCUA_X samples which were pre-cured for 30, 45, 60, 75, 90 and 120 sec, respectively. The results demonstrate that the samples treated below 120 sec did not have optical anisotropy. However, using a pre-curing time of 120 sec also damaged the alignment of LCs and unexpected cracks were observed on the substrate (Figure 4.5f). One probable explanation of the result is that there might be an undesired chemical interaction between the LCs blend and pre-cured TTEGDA substrates during the photopolymerization reaction. Since the pre-curing was carried out within a short time, there occurred incomplete polymerization of TTEGDA. The LC mixture dissolved in the substrate composition.

For further investigation, the pre-curing process was performed for longer times such as 150, 180, 240, 270 and 300 sec. The optical images captured between crossed polarizers are given in Figure 4.6a-f.

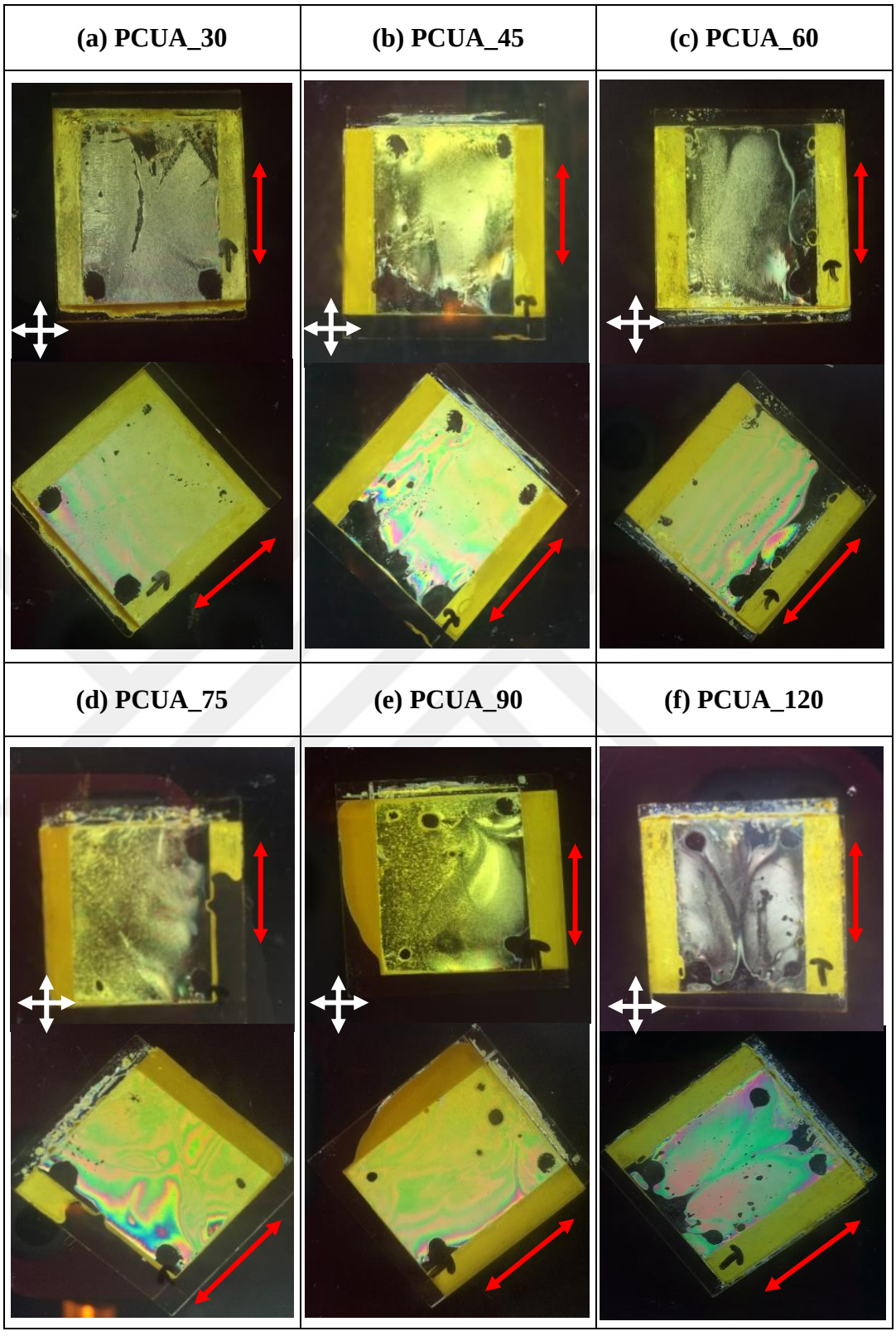

Figure 4.5 Macroscopic images of (a) PCUA_30, (b) PCUA_45, (c) PCUA_60, (d) PCUA_75 (e) PCUA_90 and (f) PCUA_120 between crossed polarizers. The red arrows demonstrate the rubbing direction of the coating.

It was seen that increasing the treatment time had a positive impact on the alignment quality and uniformity. The optical anisotropy of the azo-LCPN coatings were improved by extending the implementation time from 150 to 300 sec due to increasing the cross-linking of TTEGDA monomers (Figure 4.6a-f).

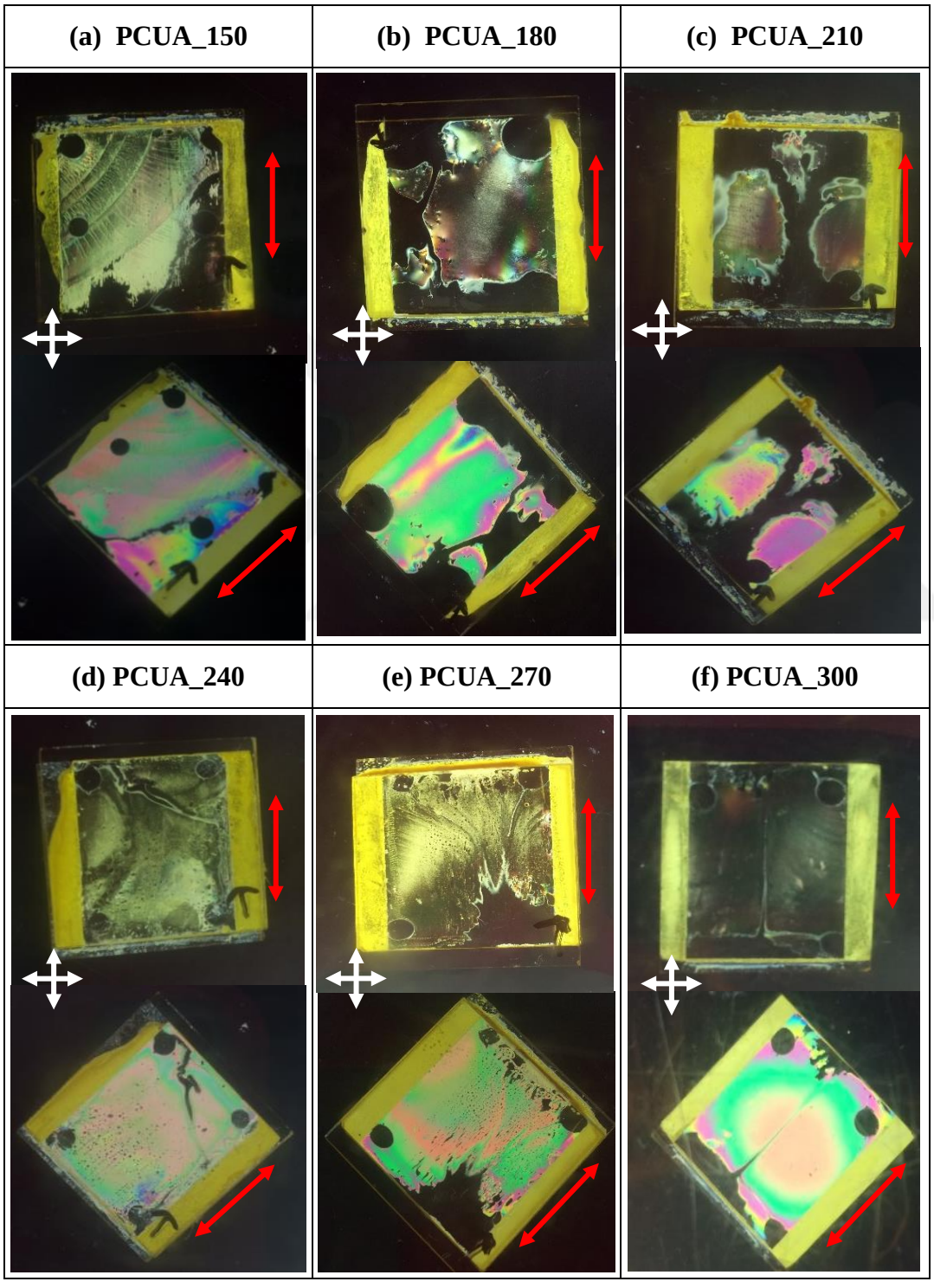

Figure 4.6 Macroscopic images of (a) PCUA_150, (b) PCUA_180, (c) PCUA_210, (d) PCUA_240 (e) PCUA_270 and (f) PCUA_300 between crossed polarizers.

4.3.2 Light actuation result

The surface topography in the coating of PCUA_300 sample (as shown in Figure 4.6f) was investigated in according to its ability to interact with unpolarized light. In order to do analysis, the constructed LC cell was opened and the azo-LCPN coating was exposed to both unpolarized UV (365 nm) and blue (455 nm) LED lights (200 mW cm^{-2} and 20 mW cm^{-2} intensities, respectively). DHM was used to characterize the surface profiles of the coating.

Expectation: Implemented azobenzene converts its molecular shape from elongated trans- to bent cis- state under UV light supported with a small amount of blue light; hence, the molecular order of uniaxial planar aligned azo-LCPN is reduced. Expansion in one direction (up) perpendicular to the orientation of the molecules and contraction in two directions (lateral) that are parallel to the long axis are seen. Mostly, this results in changes in height and volume on the sample. After finding the maximum height on the surface, the polarized UV light is turned off and the sample illuminated with visible blue light (455 nm). By taking advantages of reverse photoisomerization reaction of azobenzene, it is assumed that the twisted film will return to its initial position. The expected mechanism of the light actuation in PCUA_300 is present in Figure 4.7. This analysis was accepted as a baseline for comparison of the measurement of static surface topographies between on and off states of the UV and blue light combinations.

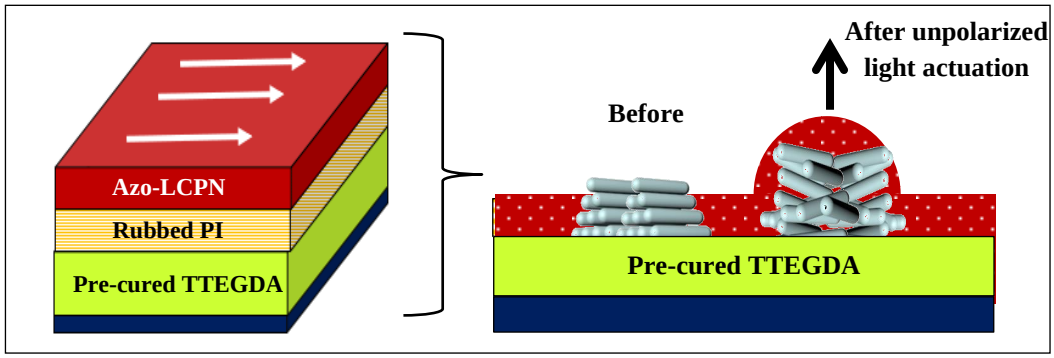

Figure 4.7 General mechanism of switchable surface deformation in PCUA_300 samples.

Figure 4.8 shows the associated phase and surface deformation behavior of randomly selected three domains in PCUA_300. The maximum height change

was measured as 3.3, 3.4 and 3.1 nm for zones 1, 2 and 3, respectively (Figure 4.8b). From this standpoint, it is clear that copolymerized azobenzene into the LC network skeleton was able to be activated, yet the general tendency of the surface deformation was limited to a few nanometres. The observations of the sample were supported with the 3D images recorded before and during the light interaction (Figure 4.8c-d).

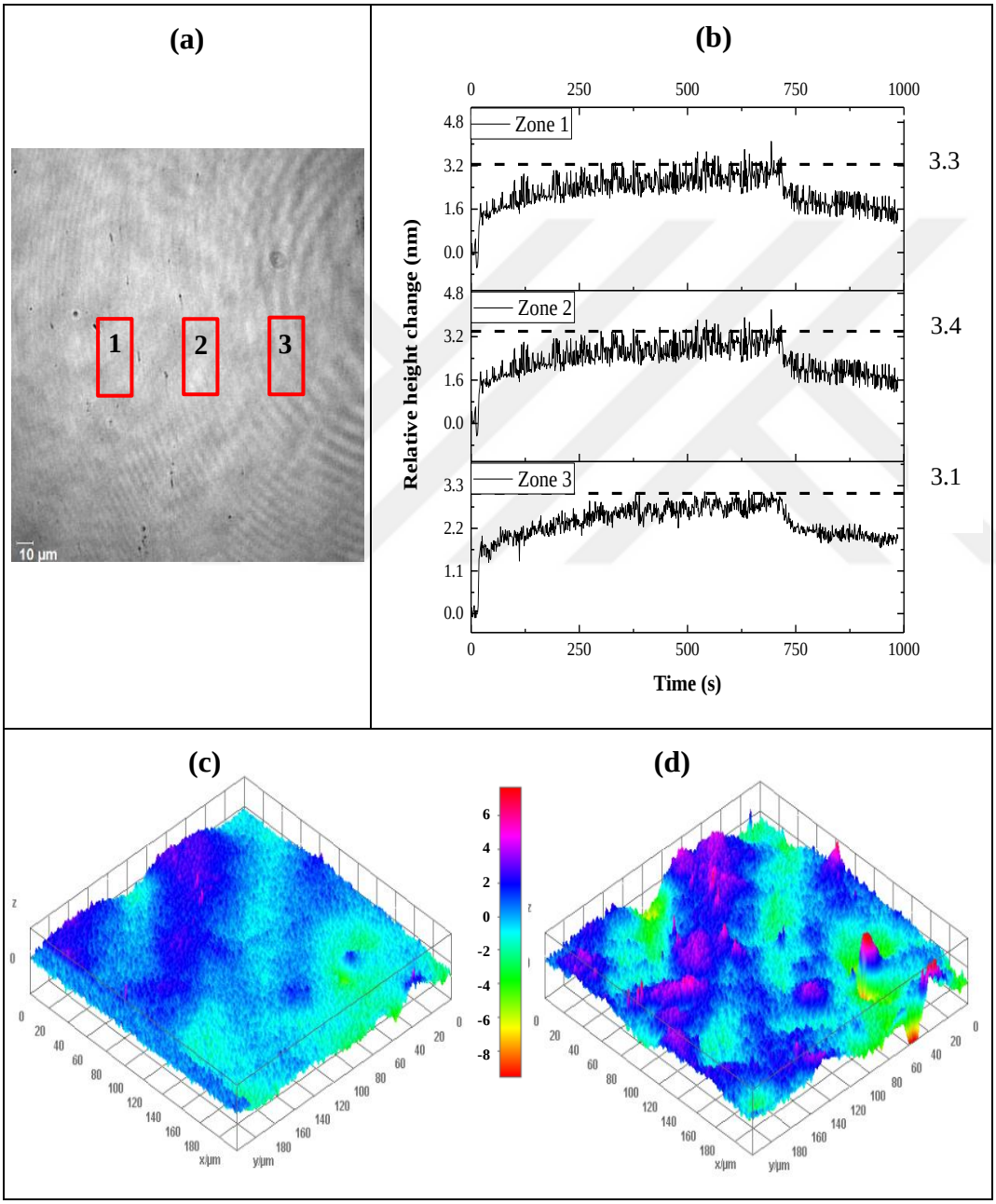

Figure 4.8 DHM measurements of PCUA_300 sample. (a) Phase patterns of the hologram. (b) Relative height change of the selected domains on the coating. 3D images of surface profiles (c) before and (d) after unpolarised light actuation.

After turning off the UV light (at around 750 s), the zones (1, 2 and 3) showed contractive forces to come back to its initial position due to the reverse photoisomerization of azobenzene molecule. However, a fully reversible movement in the surface profile was not accomplished. The results might be associated with the technique selected for the sample preparation since the pre-curing step of acrylate substrate produced some defects that would prevent surface movement (Figure 4.8a).

4.4 Directly Cured Acrylate Substrates

Here, UA_T100 sample which was prepared by directly curing of the uncured acrylate TTEGDA substrate against to the well aligned and polymerized azo-LCPN coating was examined. The effects of the preparation methods on the alignment and light actuation behavior of the azo-LCPN /acrylate based substrates were detected by comprising the results discussed in the previous subsection.

4.4.1 Alignment improvement

Figure 4.9 represents optical images of UA_T00 coating. Comparison of two results (Figure 4.6f and 4.9) reveals that UA_T100 sample indicates better uniformity than the pre-cured sample of (PCUA_300). The optical anisotropy of the samples showed similar propensities.

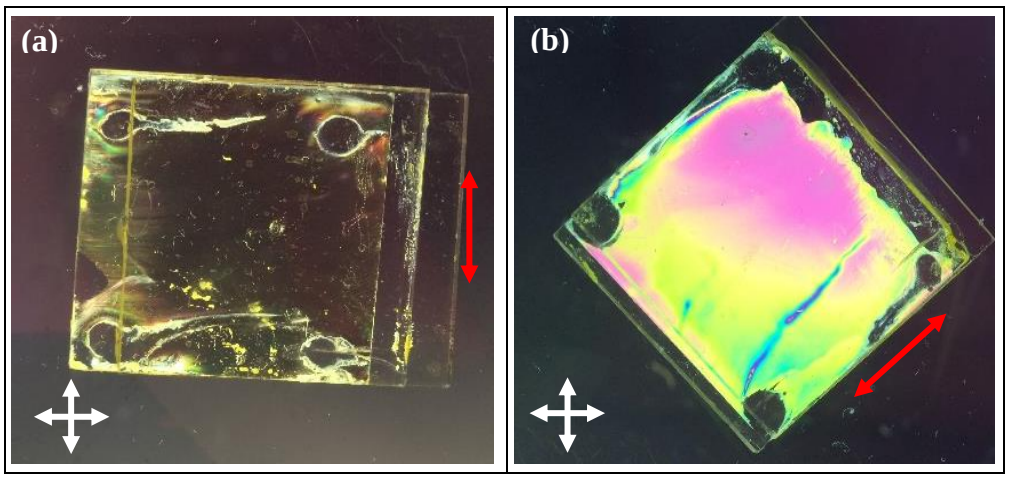

Figure 4.9 Macroscopic optical images of UA_T100 sample between crossed polarizers. Captured images were taken at (a) 0° and (b) 45° position with respect to one of the polarizers.

4.4.2 Light actuation result

UA_T100 coating was exposed to both unpolarized 365 nm UV and 455 nm blue light throughout a mask having lines with 100 μm pitch. The mask was used in order to get an observable deformation. Moreover, the effect of the light intensity on the measurement on UA_T100 sample was investigated for the combinations of different intensities of UV/blue light. For the first one (200 mW cm^{-2} UV and 20 mW cm^{-2} blue lights), the total height change was measured as 36 nm. For the second light combination (150 mW cm^{-2} UV and 15 mW cm^{-2} blue lights), the measured height change was between 11.7 and 14.4 nm (Figure 4.10). The surfaces came back to their initial flat positions after turning off the UV light (around 875 sec).

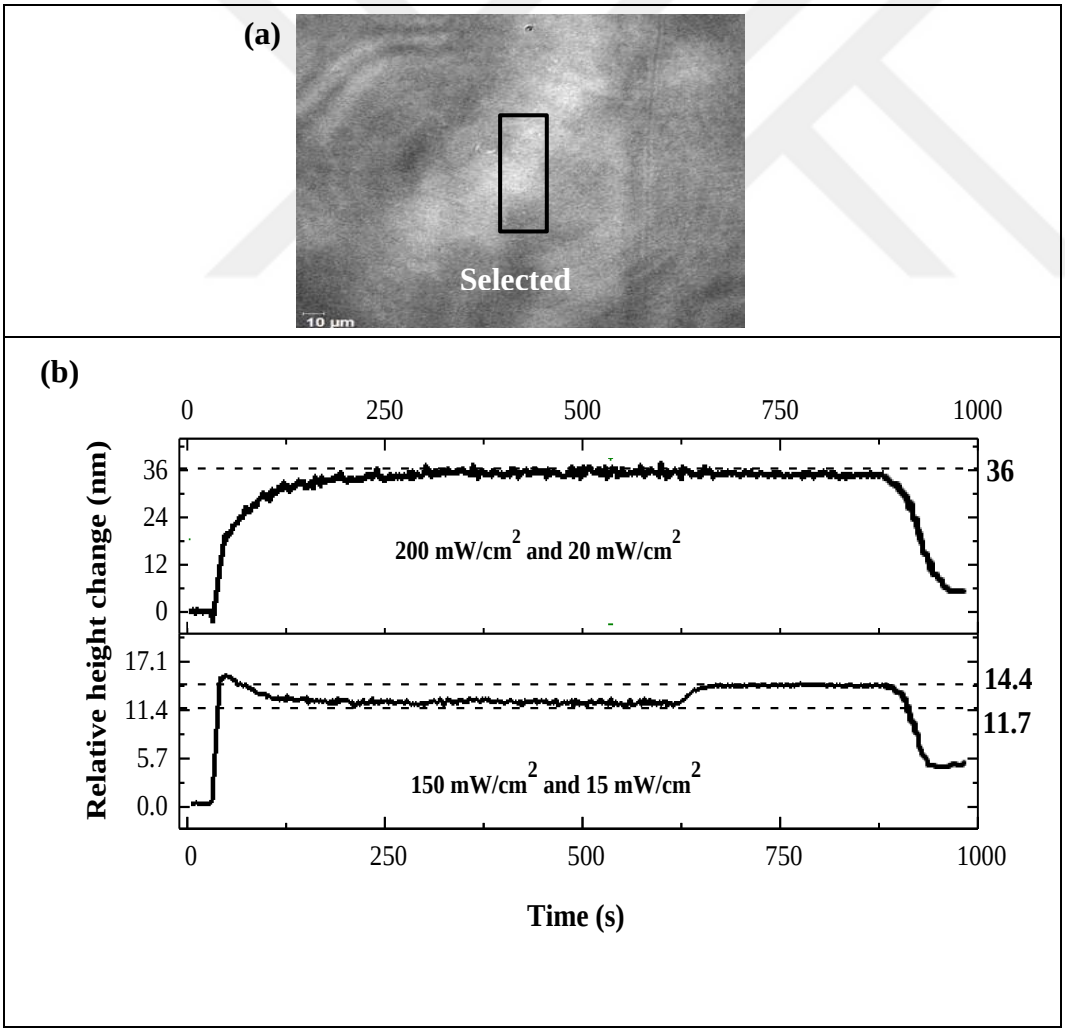

Figure 4.10 DHM measurement of UA_T00 sample (a) Phase patterns of the hologram. (b) Relative height change of the coating during unpolarized light actuation.

The actuation results were supported also by the 3D visualization images (Figure 4.11).

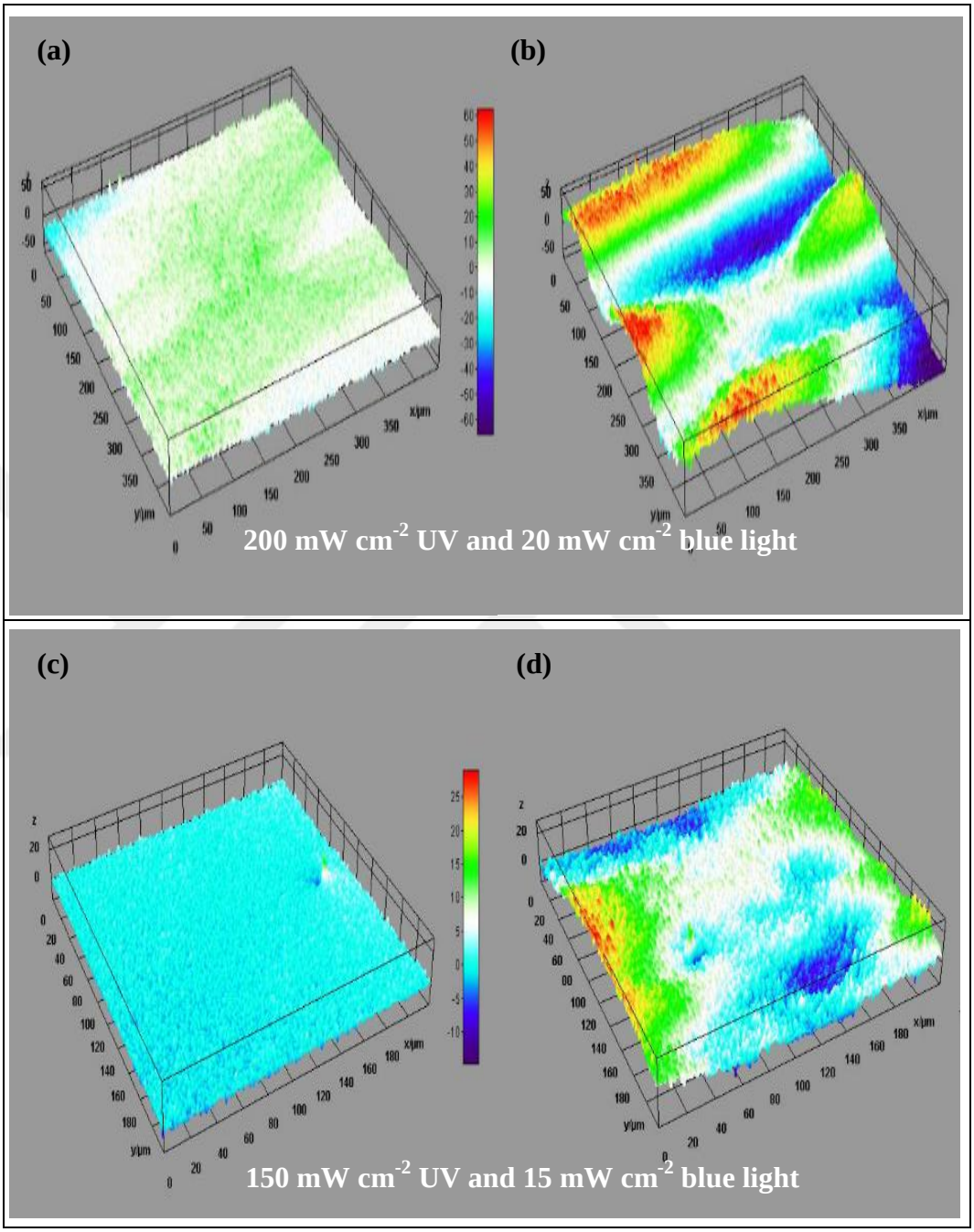

Figure 4.11 3D images of surface topography of UA_T100 sample (a, b) and comparatively higher light intensity (c, d). The captured images show the surfaces (a, c) before and (b, d) during the activation.

The differences between the measured surface deformations demonstrate that increasing the light intensity increased the height changes. Therefore, the

suitable values for the UV and blue lights were selected to be 200 mW cm^{-2} and 20 mW cm^{-2}, respectively. From another side of view, UA_T100 sample exhibited a higher surface deformation than the value measured for PCUA_300 sample (3.4 nm, see in Figure 4.8b) during the light actuation with 200 mW cm^{-2} UV and 20 mW cm^{-2} blue lights. This comparison highlights that the directly curing method improved the light sensitivity of the smart layered systems. The reason can be explained by the lack of the interaction between the LCs and acrylate substrates due to forming of the azo-LCPN prior to curing of the substrate.

These results suggested that UA_T100 sample was a good candidate for the next parametric experiments. One limitation of the sample was that the substrates were prone to cracking because the TTEGDA monomer is not a very soft material at room temperature due to its chemical structure. When the smart azo-LCPN coating is bonded to the substrate, the contraction-expansion behavior of the coating might be limited. On the other hand, the changes in the surface topography can be increased by doping the materials with low Tg into the acrylate composition. Furthermore, polarized UV and blue light system can improve the photomechanical response of azobenzene molecules and provide the oscillation behavior of the system.

4.5 Oscillation of TTEGDA/2-EHA Substrates

In this subsection, the impact of using different concentrations of TTEGDA/2-EHA monomers into TTEGDA substrates in the directly cured substrates was investigated. First of all, the mechanical analysis of the substrates was interpreted. Secondly, both uniaxial planar and photo-aligned azo-LCPN coated substrates were analyzed according to their alignment and oscillation deformation.

4.5.1 DMA results for substrates

The results of DMA measurements of the substrates containing 0, 20, 40 and 60 vol.% of 2-EHA are given as plots in Figure 4.12a-b and 4.13a-b, respectively. The plots represent storage modulus of substrates (70 μm thickness)

against temperature. The storage modulus is a term to define the stored energy which is illustrating the elastic deformation. A decrease in the storage modulus indicates that a material becomes softer. It should be noted that the temperature range was kept at room temperature during the analysis.

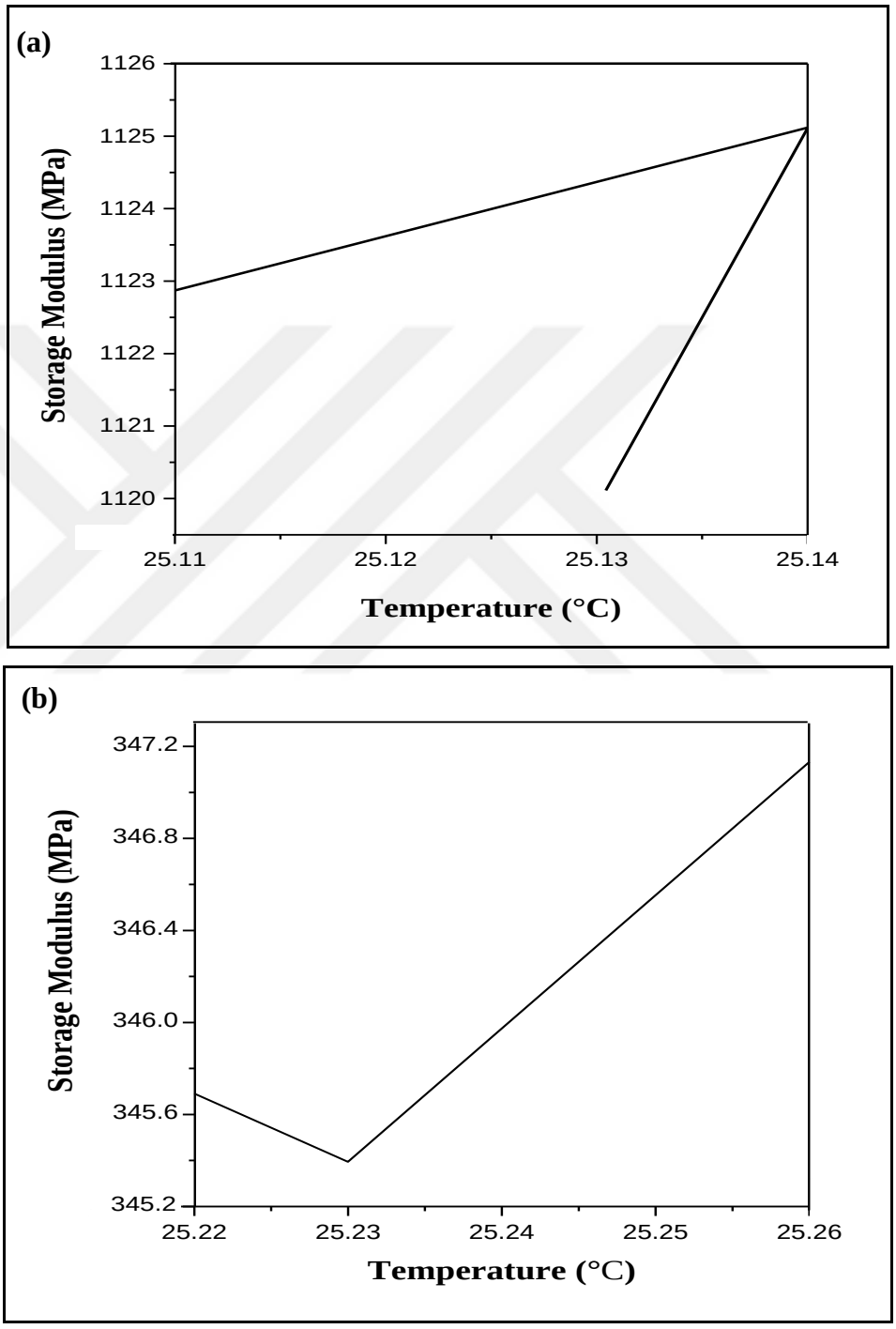

Figure 4.12 Plots of storage modulus versus temperature for (a) 0 and (b) 20 vol.% of 2-EHA doped TTEGDA substrates.

Comparison of the results indicates that the substrate including only TTEGDA (0 vol.% of 2-EHA) in the formulation showed a higher storage modulus (between 1120-1125 MPa) than the other TTEGDA/2-EHA based compositions. The exact value for the storage modulus cannot be said because of the following trends of the curves (Figure 4.12a).

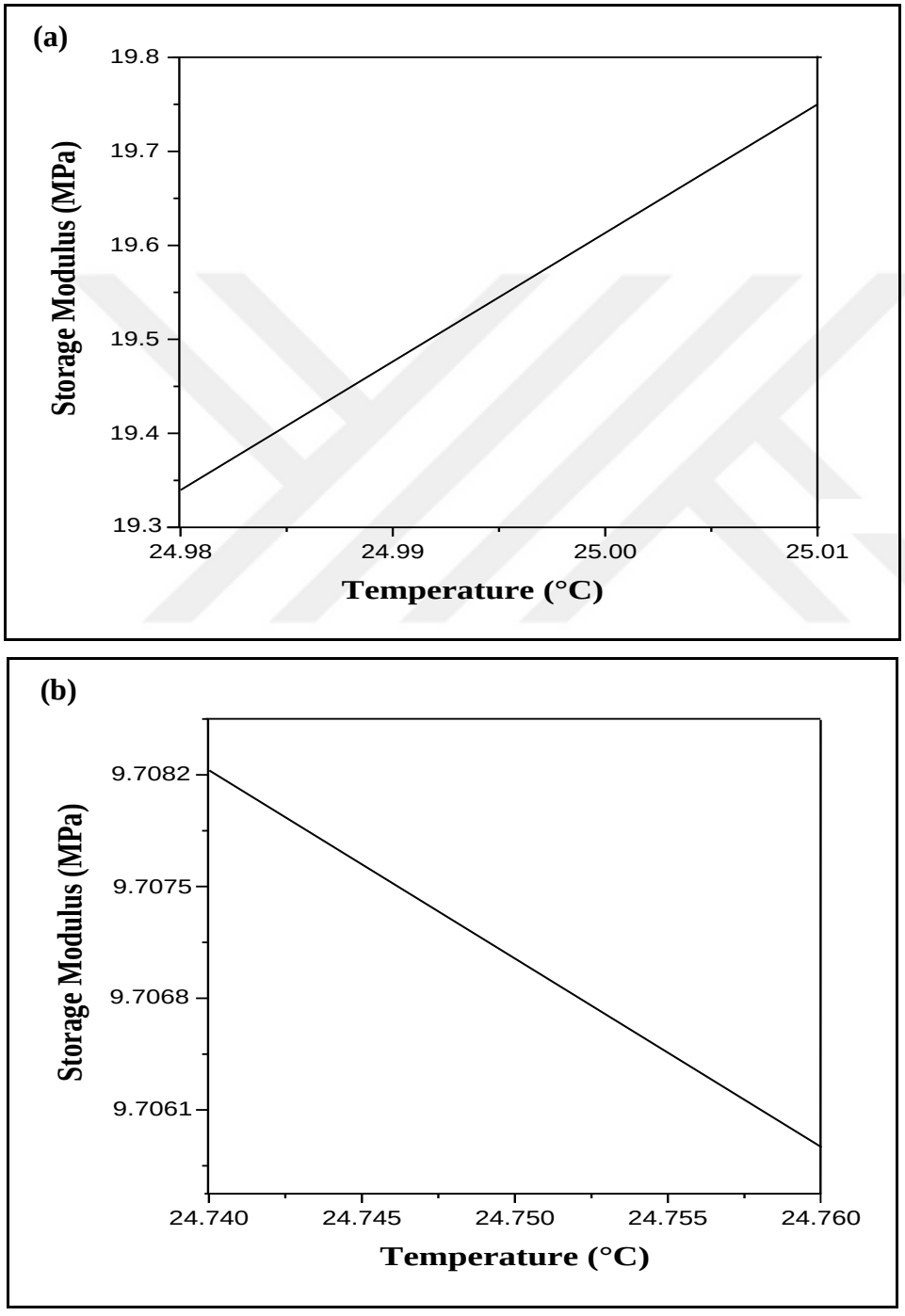

Figure 4.13 Plots of storage modulus versus temperature for (a) 40 and (b) 60 vol.% of 2-EHA doped TTEGDA substrates.

After the addition of 20 vol.% of 2-EHA as an additive into the system, this range decreased to around 345.7-347 MPa (Figure 4.12b). When the 2-EHA content was increased up to 40 and 60 vol.% the storage modulus was lowered to approximately 19.35-19.75 MPa and 9.7 MPa, respectively (Figures 4.13a and 4.13b). Moreover, the general trend of the storage modulus curve for 60 vol.% 2-EHA containing substrates (see in Figure 4.13b) showed a decreasing trend with respect to the time.

It can be said that increasing the amount of 2-EHA contents in the substrate provided a considerable decrease in the storage modulus. This means that the elasticity of the acrylate-based substrates was increased. Due to the lack of limitation related to the characterization instruments, the substrate including 80 and 95 vol.% of 2-EHA in the TTEGDA composition were not able to be analyzed by DMA. According to the trends followed by other samples, the softness of the substrates was decreased by increasing the 2-EHA content. It was assumed that they have smaller storage modulus than 9.7 MPa which was the measured value for 60 vol.% of 2-EHA added substrate.

4.5.2 DSC results for substrates

Thermal behavior of the substrates was investigated by performing DSC curves measured in the temperature range of -60 to 120 °C. This characterization provides the better understanding of the softness of the substrates by detecting the glass transition temperature (Tg) of the materials. As a general acceptance, at glass transition temperature, there emerge sudden alterations in specific heat owing to the structural flexibility although sample stays in its glassy state. Therefore, an endothermic peak is observed in at glass transition. This is not a special temperature, yet a certain range of temperature at which such structural alterations occur in the materials.

In the literature, the Tg of TTEGDA was measured around 40 °C, meaning that the material is not soft at room temperature. According to the DSC results, for the TTEGDA substrates including 20, 40, 60 and 80 vol.% of 2-EHA, the Tg was found between -50 and -40 °C. The maximum peak observed for all samples

indicated the same thermal distributions (Figures 4.14a-b and 4.15a-b). Hence, it can be said that adding 2-EHA into the formulation of TTEGDA substrates decreased the value of Tg. This means that these substrates can be accepted as soft material at room temperature.

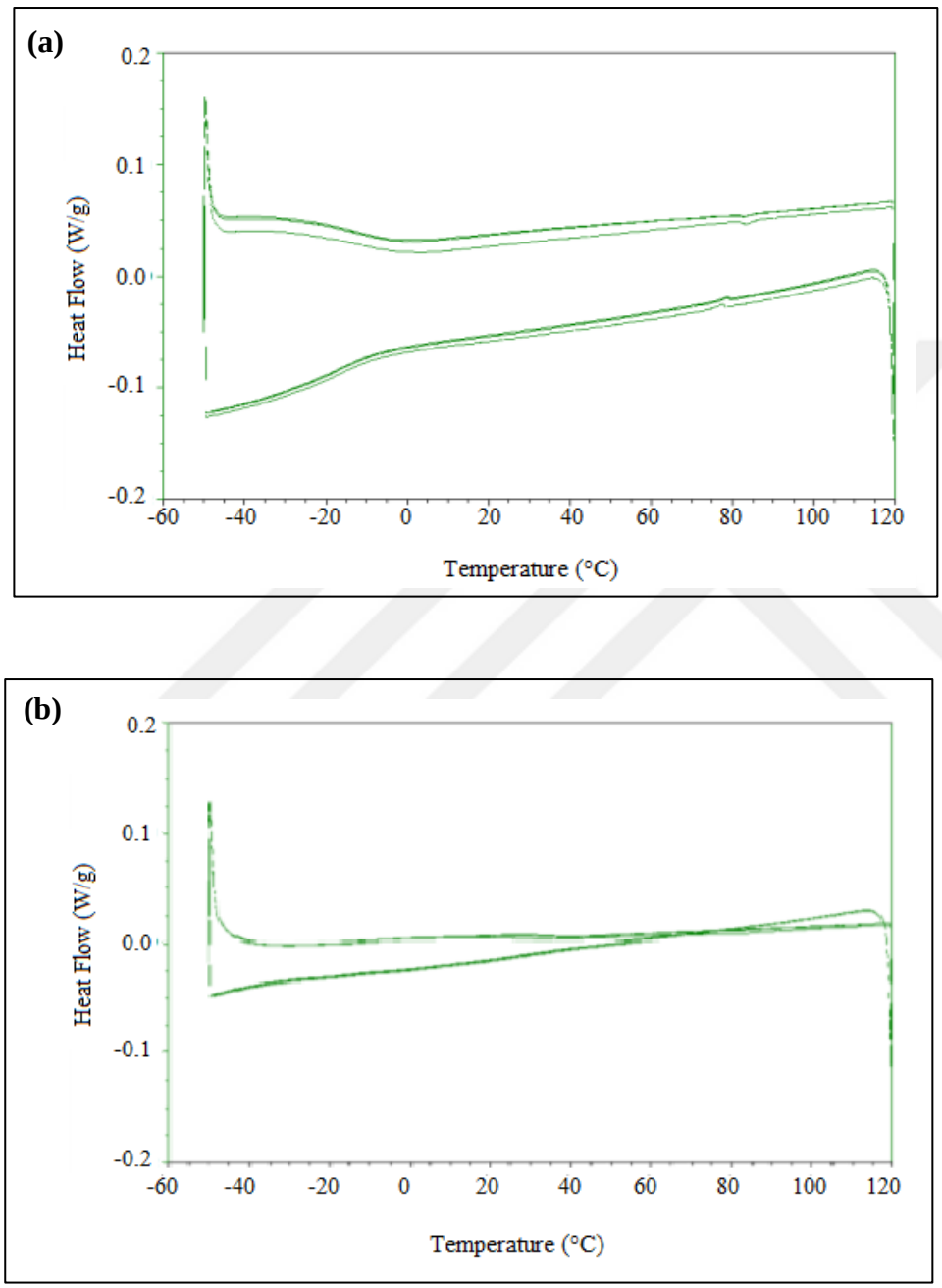

Figure 4.14 DSC measurement exhibiting heat flow as a function of temperature for (a) 20 and (b) 40 vol.% of 2-EHA containing substrates.

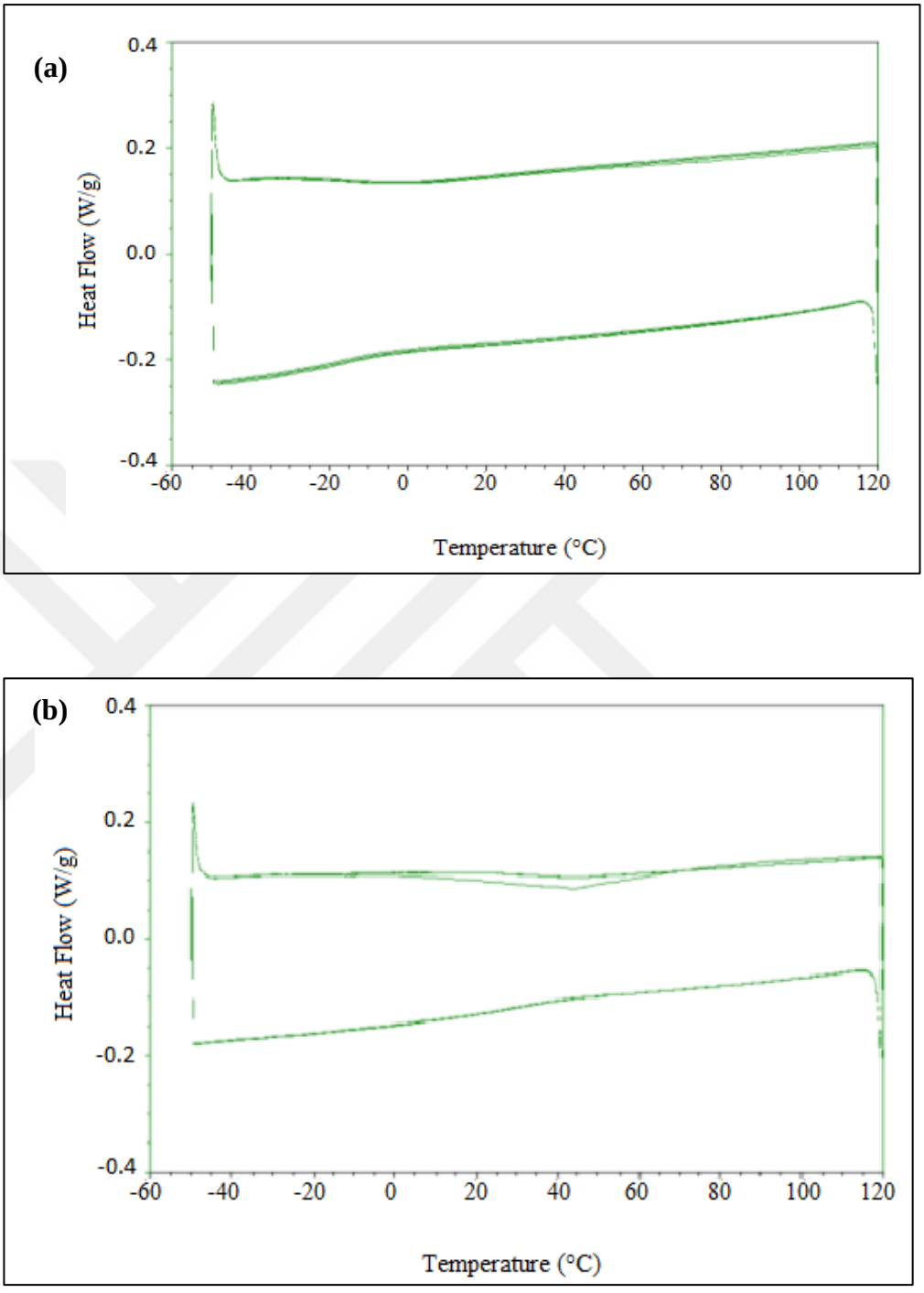

Figure 4.15 DSC measurement exhibiting heat flow as a function of temperature for (a) 60 and (b) 80 vol.% of 2-EHA containing substrates.

4.5.3 Uniaxial planar layered system

In this subsection, the optical anisotropy and polarized light actuated oscillation behavior of UA_T100, UA_T80E20, UA_T60E40, UA_T40E60, UA_T20E80_UA_T5E95 samples were examined as a parametric study on uniaxial aligned layered systems.

4.5.3.1 Alignment results

Figure 4.16 represents the cell viewing of those samples between crossed polarizers (at the angles of 0° and 45°). While turning the rubbing directions of the samples with respect to one of the polarizers, a noticeable color change was observed on the cells. Hence, it can be said that highly anisotropic optical responses were achieved on the samples. This result supports the previous result obtained for UA_T100 sample (see in Figure 4.9). Moreover, due to the availability of directly curing methods, using additive 2-EHA did not have an impressive effect on the quality of birefringence. Because there was no chemical interaction between the LCs and the substrates.

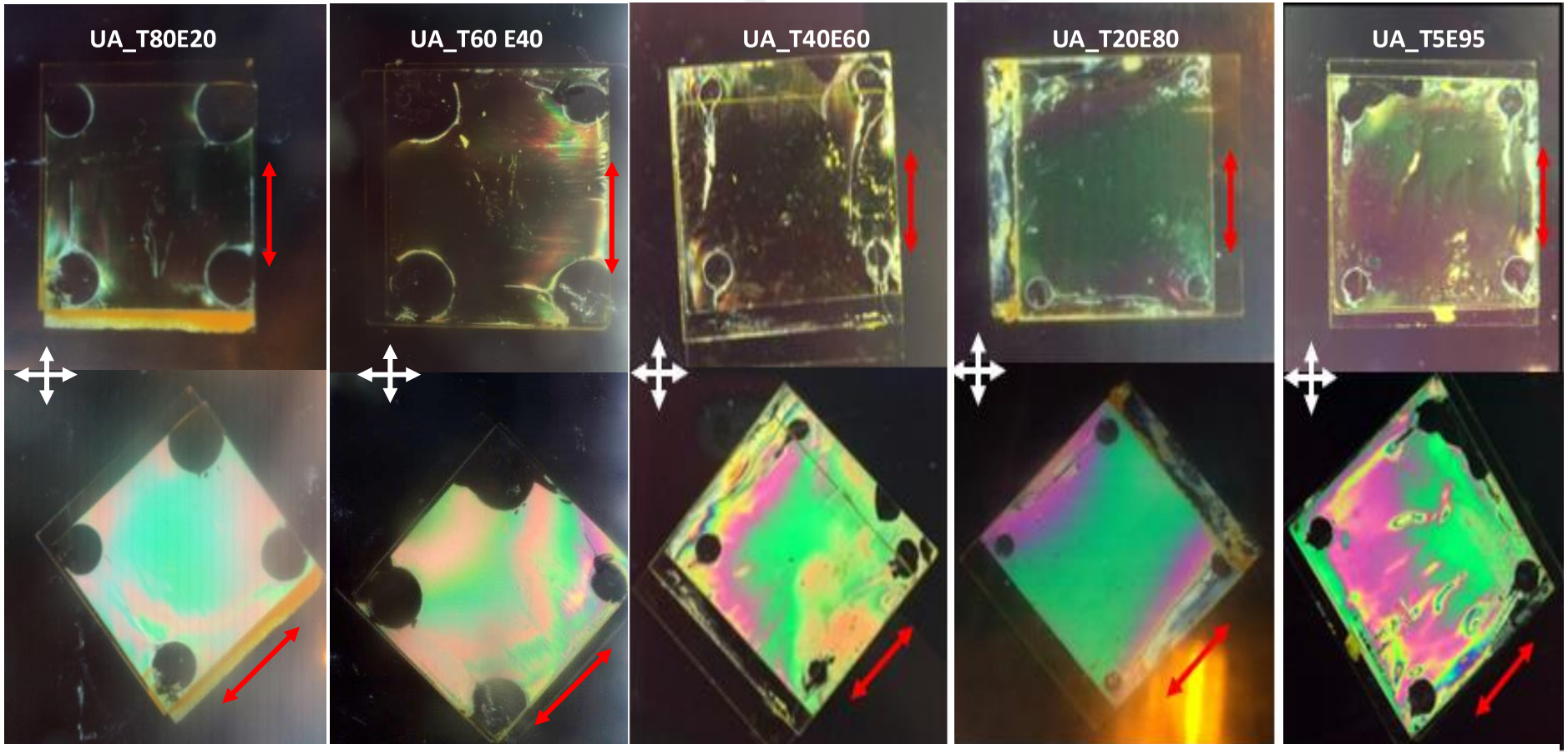

Figure 4.16 Macroscopic images of 20, 40, 60, 80 and 95 vol.% of 2-EHA containing samples between crossed polarizers. The captured dark image corresponds to rubbing direction location at 0˚ with respect to one of the polarizers while the bright image is taken after rotating the cell at 45˚.

4.5.3.2 Polarized light actuation results

The dynamic oscillation behavior of planar azo-LCPN coated substrates including different concentrations of 2-EHA were characterized under the combination of polarized UV light (365 nm, 200 mW cm^{-2}) and unpolarized blue light (455 nm, 200 mW cm^{-2}). The direction of the polarized light was changed continuously to observe oscillation behavior during the light interaction. The expected dynamic movements on the surfaces are schematically illustrated in Figure 4.17.

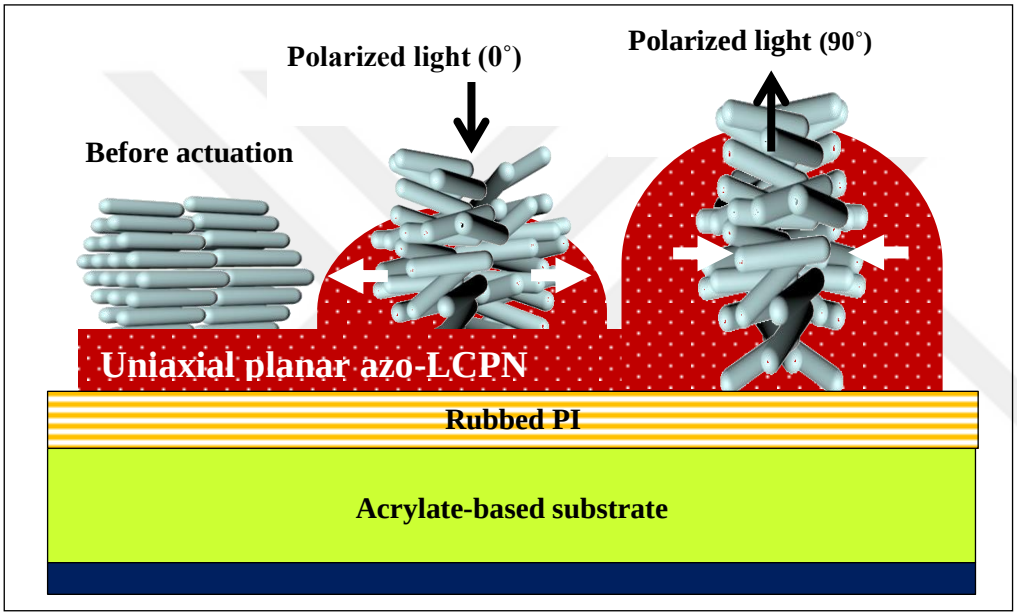

Figure 4.17 General mechanism of dynamic surface topographies on uniaxial aligned systems.

Figure 4.18 presents the graph of height changes in the samples during the polarized light actuation for 600 sec. The measured maximum height changes for UA_T00, UA_T80E20, UA_T60E40, UA_T40E60, UA_T20E80 and UA_T5E95 samples were 8.3, 15.5, 29, 38, 44.9 and 102.8 nm, respectively.

On the other hand, the amplitude of oscillation values (Δh) for in UA_T00, UA_T80E20, UA_T60E40, UA_T40E60, UA_T20E80 and UA_T5E95 samples were measured as 4.2,6, 6.2, 8.2, 14.7 and 18.8, respectively.

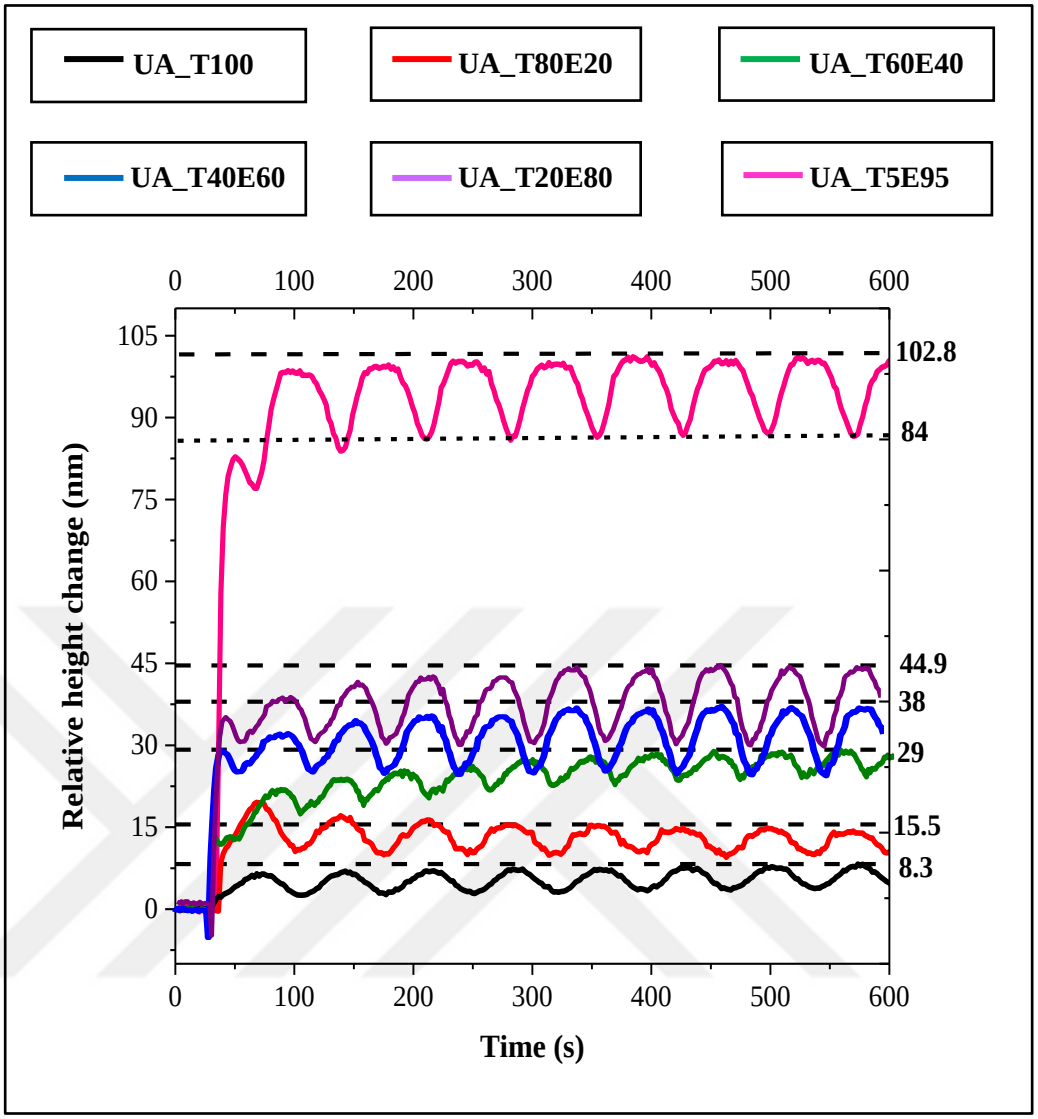

Figure 4.18 Relative height changes in UA_T00, UA_T80E20, UA_T60E40, UA_T40E60, UA_T20E80 and UA_T5E95 with respect to time.

One of the aims of this study was improving surface deformation on the smart layered systems by increasing the softness of the bottom layer. It was previously reported in the Subsection 4.4.1 that increasing the 2-EHA in the substrate contents increases the elasticity of the substrates by lowering the storage modulus. Taken together, the results from Figure 4.18 verify that increasing the content of 2-EHA in the acrylate substrates a good selection for enhancing the total height changes and the amplitude of oscillation in the smart coatings. There achieved an apparent improvement in the ability of processing of the system.

4.5.3.3 Temperature effect

For more detailed examination of the sensitivity against to light, the conducted experiments on UA_T100 sample were repeated at different temperatures (50 °C, 70 °C and 120 °C) for 1400 sec. Figure 4.19 represents the phase and intensity profiles of the substrates.

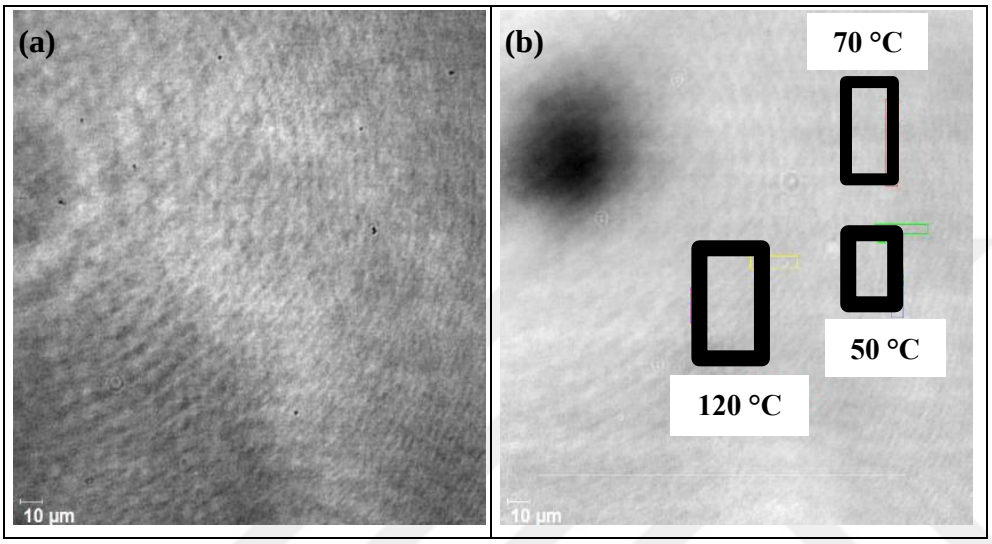

Figure 4.19 (a) Intensity and (b) phase profile of UA_T100 with selected zones.

As shown in Figure 4.20a, the surfaces came back to their initial state after switching off the polarized light system. The finishing values of all measurement for 50 °C, 70 °C and 120 °C reached its initial values, meaning that UA_T100 sample exhibits switchable behavior when exposed to light. The highest total height change was found at 50 °C. Raising the temperature from 70 °C to 120 °C also caused the decrease in this value. However, the exact value for total height changes was not being measured due to the unstable behavior of the zones.

There were significant fluctuations in the oscillating curves. The reason may be the hole deposited on the coating as indicated in Figure 4.19b. Moreover, Figure 4.20b-c shows the visualization of 3D images of the surfaces during the light actuation. The images also clearly induce the defect and hole emerged on the surface.

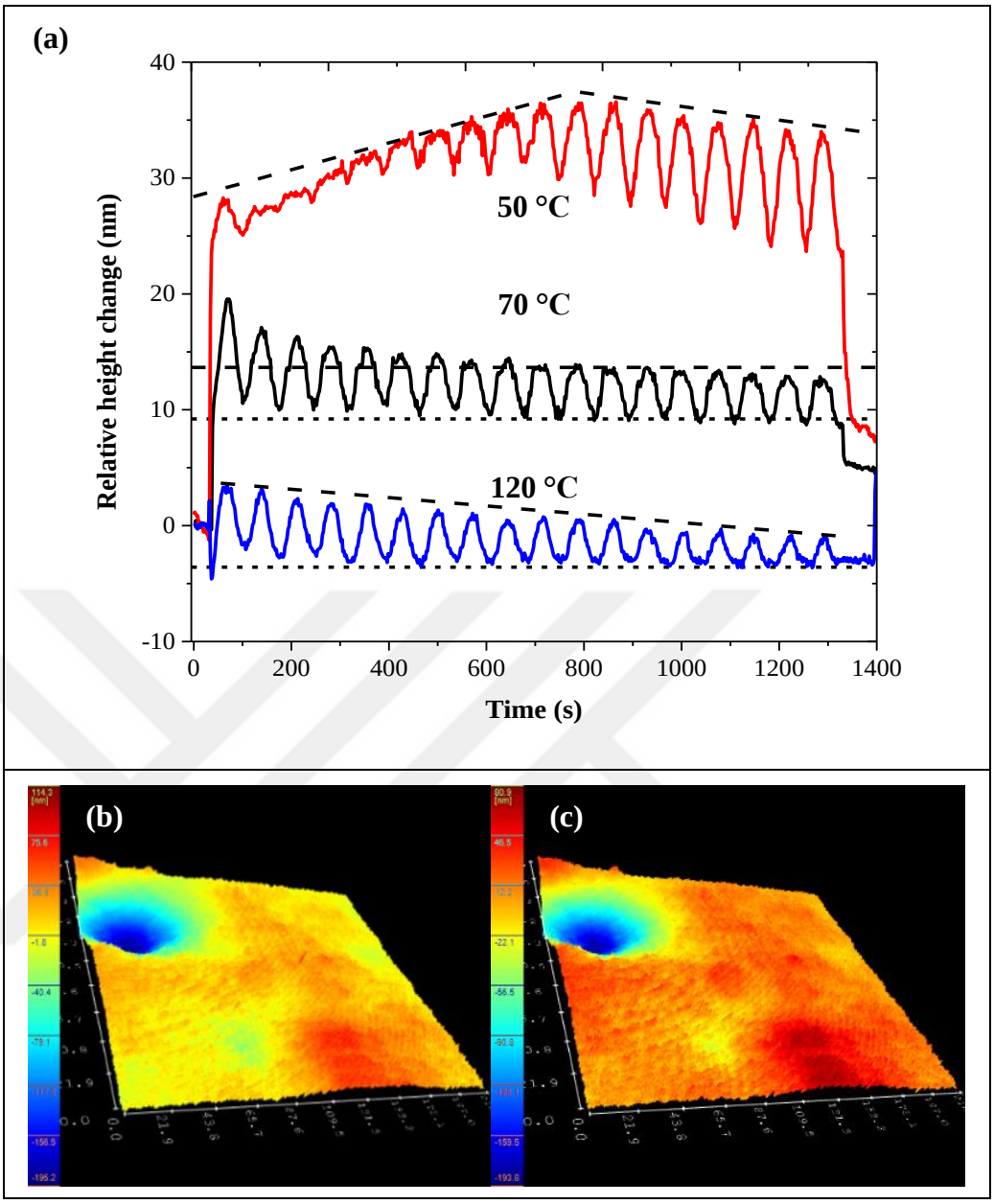

Figure 4.20 (a) Relative height change of UA_T100 at 50 °C, 70 °C and 120 °C with respect to time. 3D views of the surface (b) before and (c) during polarized light actuation.

4.5.3.4 Substrate thickness

To examine whether the substrate thickness used is an efficient parameter on the surface deformation, uniaxial coatings were fabricated on two substrates with different acrylate thicknesses. The substrate doped with 95 vol.% concentrations of 2-EHA was selected to combine with azo-LCN coating and were prepared with both 70 μm and 1000 μm thickness (notations of the samples:

UA_T5E95_70 µm and UA_T5E95_1000 µm). As shown in Figure 4.21, both samples exhibited high optic anisotropy.

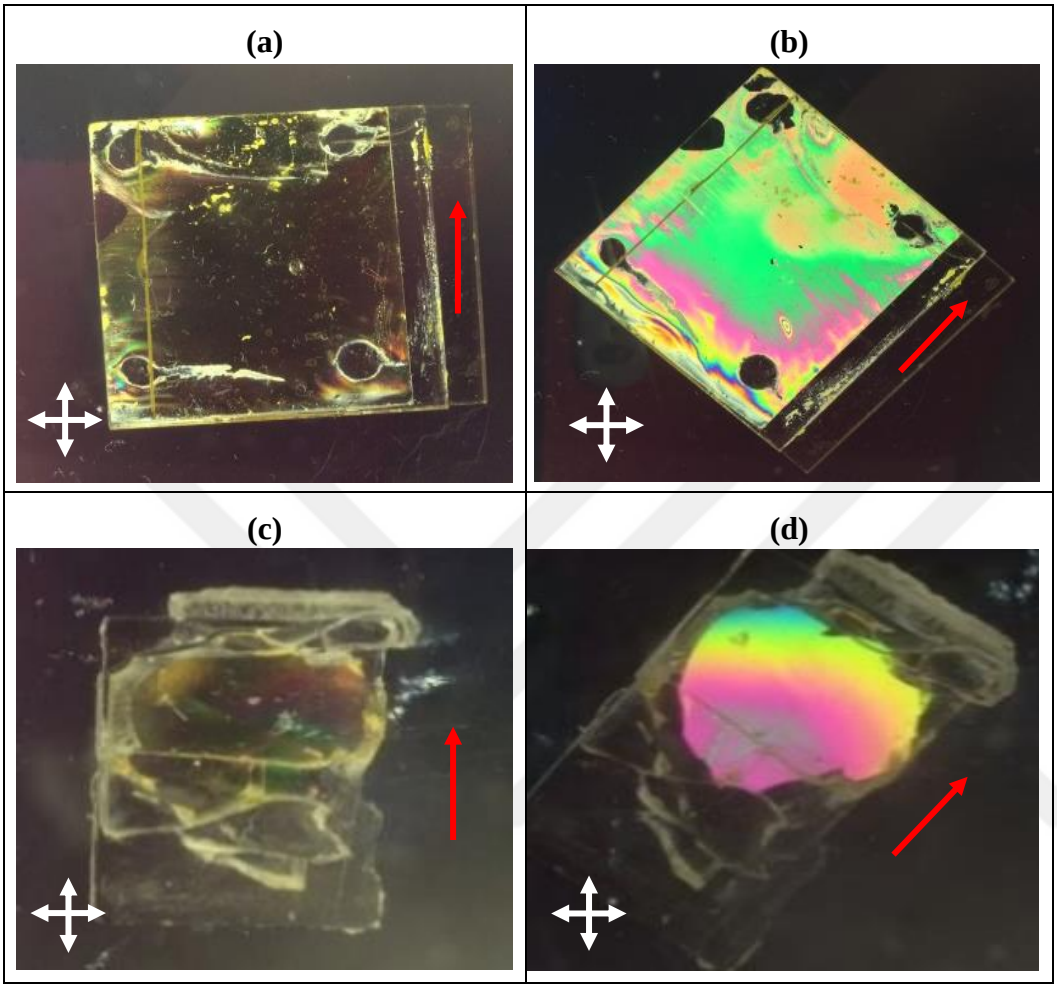

Figure 4.21 Macroscopic images of UA_T5E95_70 µm with (a) 0˚ and (b) 45˚ position. UA_T5E95_1000 µm with (c) 0˚ and (d) 45˚ position between crossed polarizers. Rubbing directions are shown by red arrows.

Figure 4.22 shows the detailed insights about the dynamic surface deformation behavior of the mentioned samples. By increasing the substrate thickness from 70 to 1000 µm, the height differences between light on and off state reached from 102.8 to 132 nm. Moreover, the amplitude of oscillation was also enhanced when altered the thickness of the substrates. UA_T5E95_70 µm sample has 18.8 nm under the continuous polarized light system while UA_T5E95_1000 µm sample has approximately 71 nm amplitude height. The enhancement of the surface deformation by increasing the thickness can be related to the mechanical forces provided by the light effect. A thicker soft substrate

provided these mechanical forces because the area which could be deformed throughout the thickness was higher.

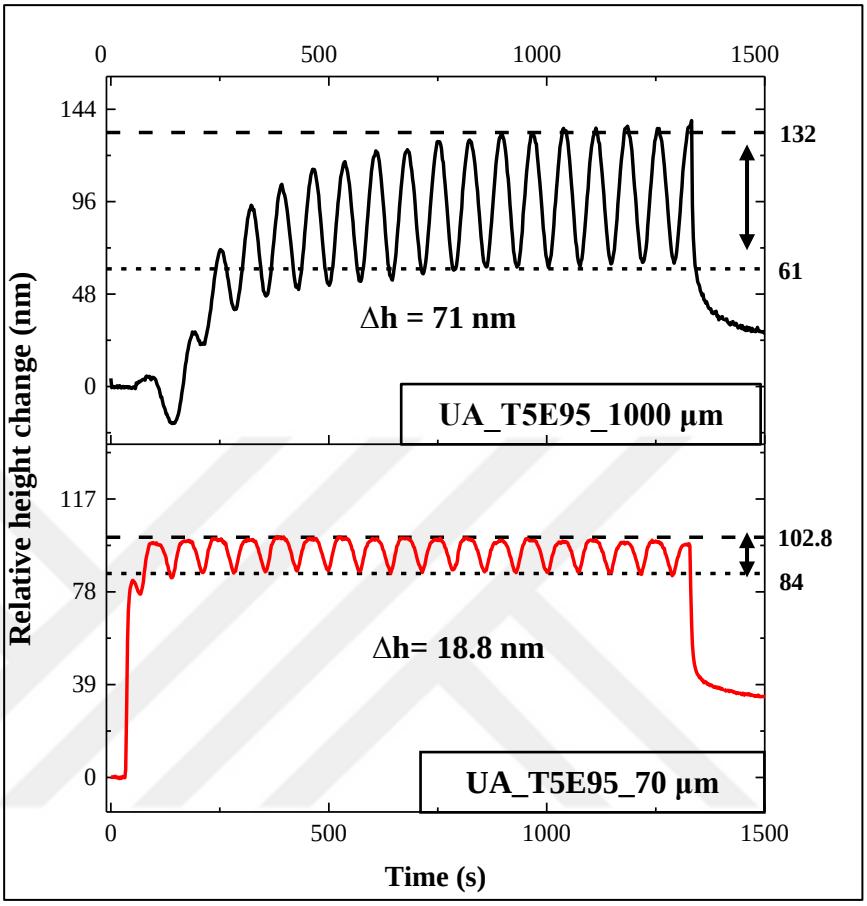

Figure 4.22 Relative height changes of UA_T5E95_1000 µm and UA_T5E95_70 µm sample.

Another important point was the time to reach a stable oscillation movement. For UA_T5E95_1000 µm sample, the stable oscillation trend was reached about 850 seconds. On the other hand, UA_T5E95_70 µm sample showed the stable oscillation amplitudes after the light exposure of 30 sec. As the thickness of the substrate increases, a certain amount of time was passed to allow the UV light to be absorbed on the substrate, which delayed the time for reaching the stability. Hence, it can be said that UA_T5E95_70 µm sample was selected as the best sample according to its surface deformation behavior.

4.5.4 Photo-aligned layered system

Photoalignment which is a contact-free method provides the complex alignment of LCs by implementing linearly polarized light. In this subsection, firstly the photo-induced optical anisotropy of patterned azo-LCN coatings was investigated to detect the required exposure time. Secondly, the selected patterned samples were combined with TTEGDA/2-EHA substrates to examine the oscillation behavior under the polarized light systems.

4.5.4.1 Suitable exposure time on patterned cells

As mentioned in Method Section (Section 3.2), the photoalignment of the cells was carried out employed two steps which were masked (M) and flat (F) exposure, respectively. In the second step, the direction of polarized light used to exposure was rotated with 90˚ with respect to the initial step to ensure perpendicularly aligned domains in azo-LCPN coating. The final alignment of the patterned samples depends on the exposure time.

Here, the time spent for masked and flat exposures was investigated to enhance the optical anisotropy. As an example, PAT_6M7F means that first masked exposure applied for 6 min and then flat for 7 min were done. However, the optical property of the sample was needed to be enhanced since the unaligned domains were observed on sample PAT_6M7F (Figure 4.23a). While using 6 min for the masked exposure, decreasing the duration of flat exposure (from 7 to 2) enhanced the quality of optical anisotropy of the patterned cells (Figure 4.23b-f). Hence, it is can be said that the alignment quality of LCs was improved conducting smaller flat exposure time than the first masked exposure.

(a) PAT_6M7F	(b) PAT_6M6F	(c) PAT_6M5F
F: 7 min	F: 6 min	F: 5 min
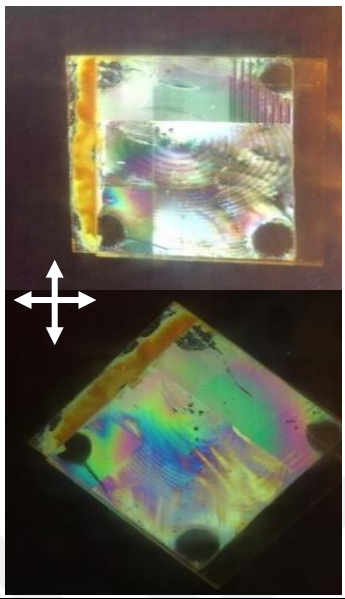	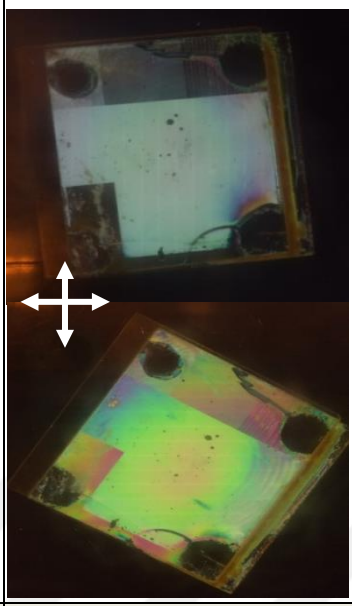	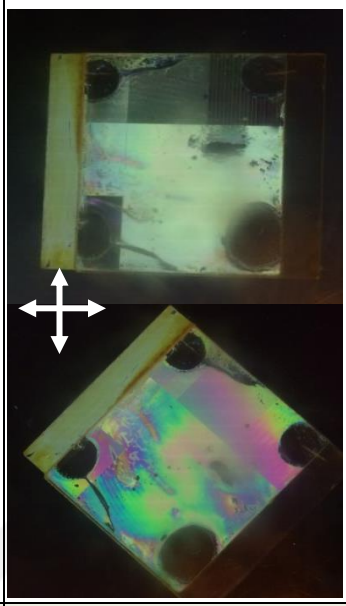
(d) PAT_6M4F	(e) PAT_6M3F	(f) PAT_6M2F
F: 4 min	F: 3 min	F: 2 min
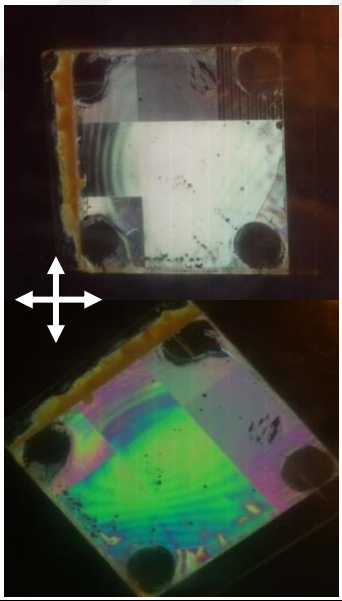	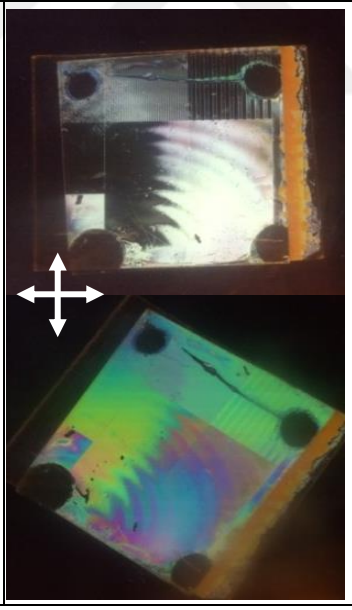	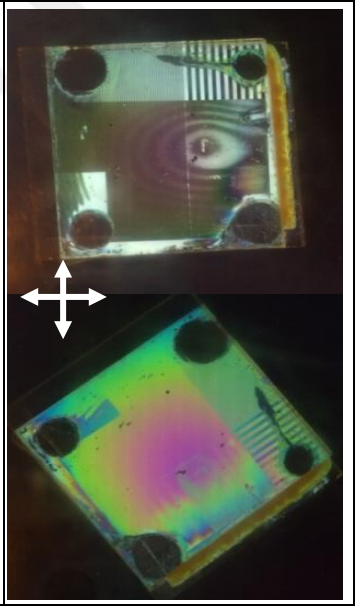

Figure 4.23 Macroscopic images of (a) PAT_6M7F, (b) PAT_6M6F, (c) PAT_6M5F, (d) PAT_6M4F, (e) PAT_6M3F, and (f) PAT_6M2F patterned cells between crossed polarizers.

The applicability of the findings was then tested with PAT_5M4F, PAT_5M3F and PAT_5M2F sample (Figure 4.24). Using 5 min for the first exposure provided better alignment quality than the results in Figure 4.23.

PAT_5M2F patterned cell was selected as the best combination because it exhibited excellent contrast between dark and bright states. Moreover, the perpendicularly aligned areas were changed their brightness while rotating the cells from the initial positions.

As a conclusion, the initial exposure can be accepted as a masking effect of all the bonds in the exposed regions. The second flat exposure having smaller treatment time than the masked exposure protected the alignment generated in the first exposure. In the following characterizations, the combinations of patterned PAT_5M2F coating and acrylate substrates will be used to enhance the functionality of the system.

(b) PAT_5M4F	(b) PAT_5M3F	(c) PAT_5M2F
F: 4 min	F: 3 min	F: 2 min
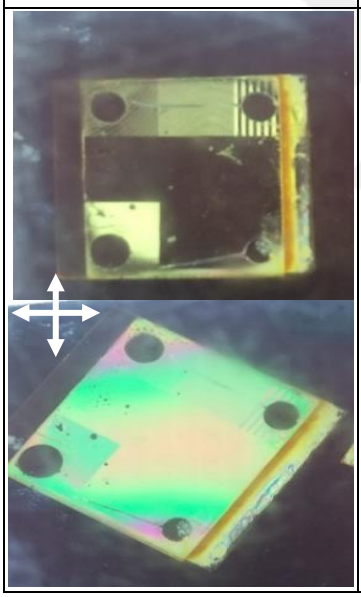	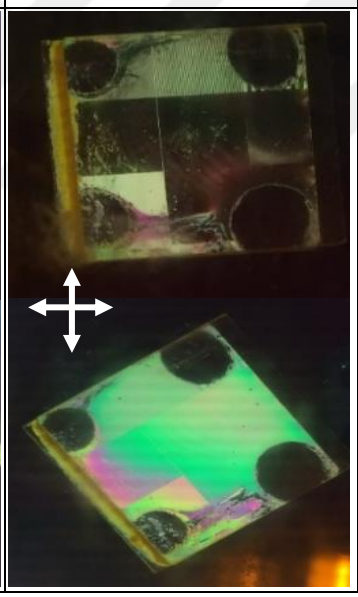	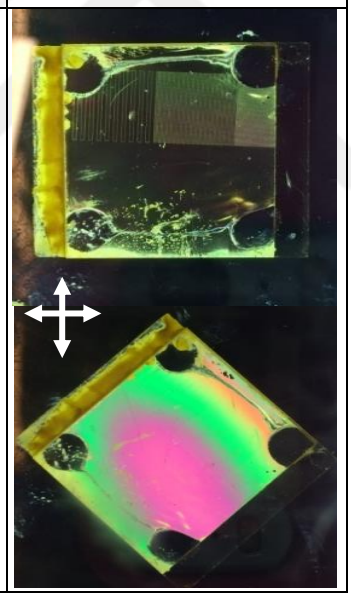

Figure 4.24 Macroscopic images of (a) PAT_5M4F, (b) PAT_5M3F and (c) PAT_5M2F patterned cells between crossed polarizers.

4.5.4.2 Alignment results

Figure 4.25a-f illustrates the optical response of PAT_5M2F coatings on T100, T80E20, T60E40, T40E60, T20E80 and T5E95 substrates, respectively between crossed polarizing films. It can be said that adding 2-EHA did not have

an impressive effect on the alignment quality since all samples show a uniform birefringence.

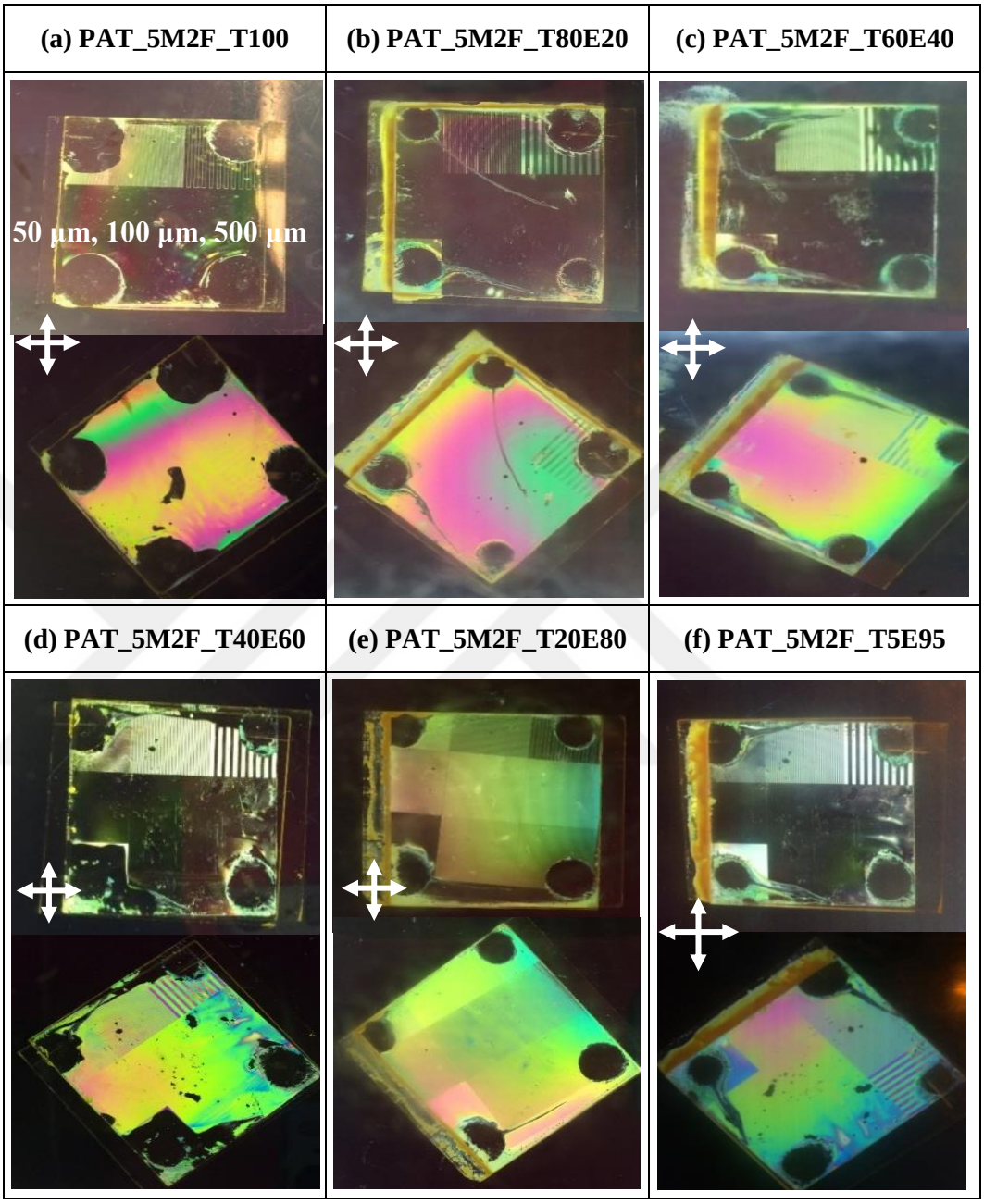

Figure 4.25 Macroscopic images of (a) PAT_5M2F_T100, (b) PAT_5M2F_T80E20, (c) PAT_5M2F_T60E40, (d) PAT_5M2F_T40E60, (e) PAT_5M2F_T20E80, (f) PAT_5M2F_T5E95 between crossed polarizers.

In general, the parts for the light experiments are the 500 µm domains of the layered samples. Areas with 50 and 100 µm areas have also been investigated when the detailed investigations were necessary. For gaining a better

understanding of the quality of the perpendicularly aligned domains, the patterned layered samples with 500 µm periodic lines were characterized using POM as shown in Table 4.1.

Table 4.1 POM results (x10 objective) patterned layered samples with 500 µm periodic lines

	0°	**45°**
PAT_5M2F_T100	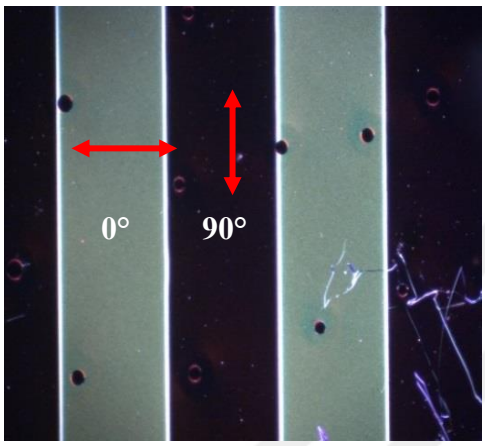	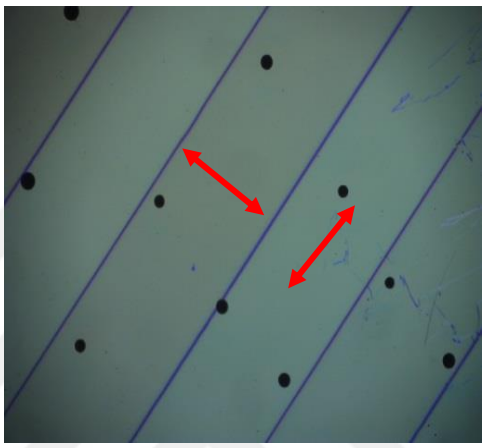
PAT_5M2F_T80E20	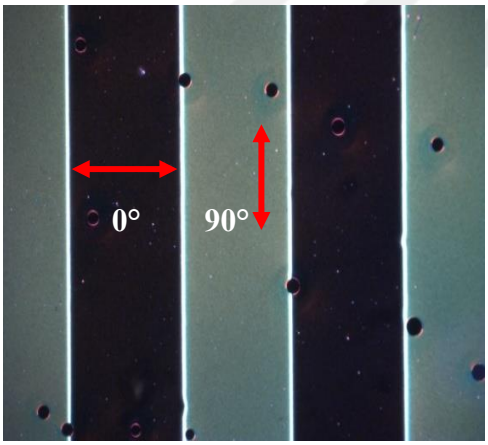	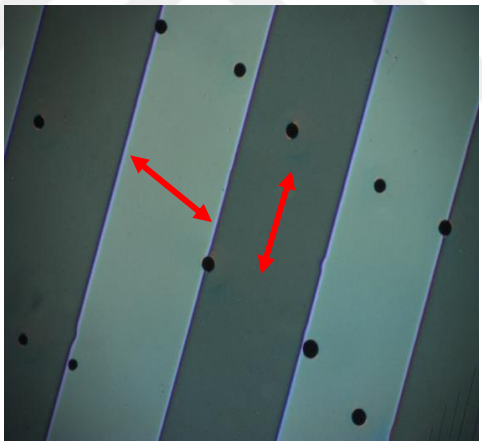
PAT_5M2F_T60E40	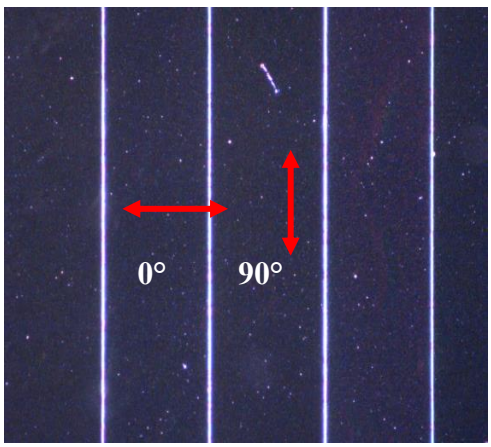	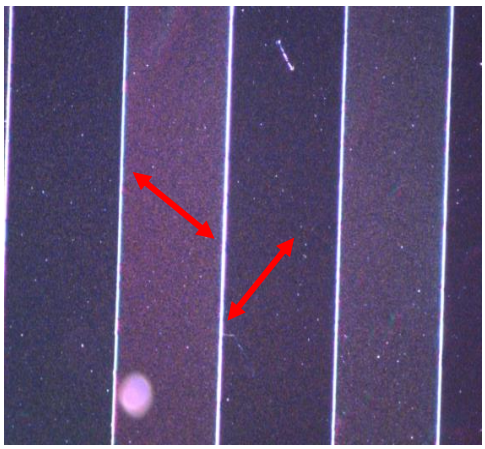

Table 4.1 POM results (x10 objective) patterned layered samples with 500 µm periodic lines (continued).

	0°	45°
PAT_5M2F_T40E60	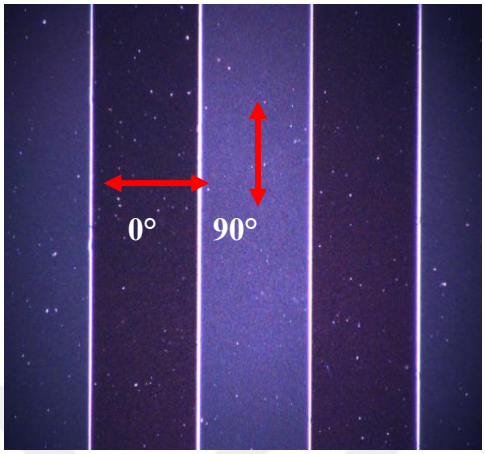	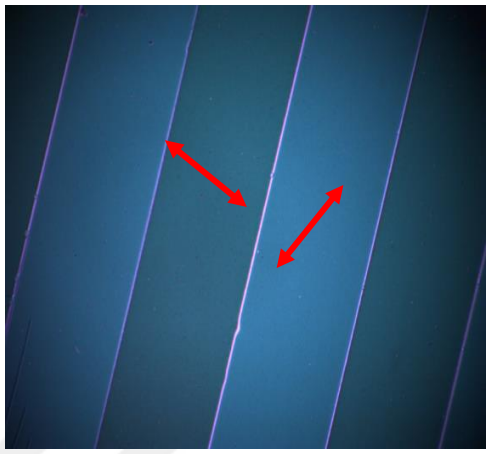
PAT_5M2F_T20E80	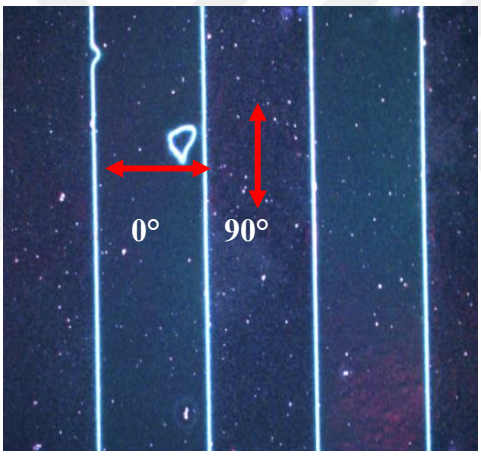	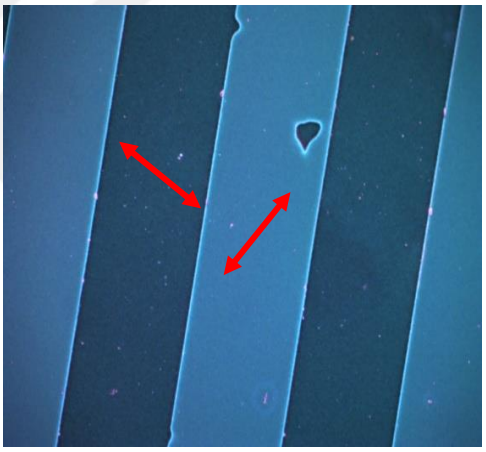
PAT_5M2F_T5E95	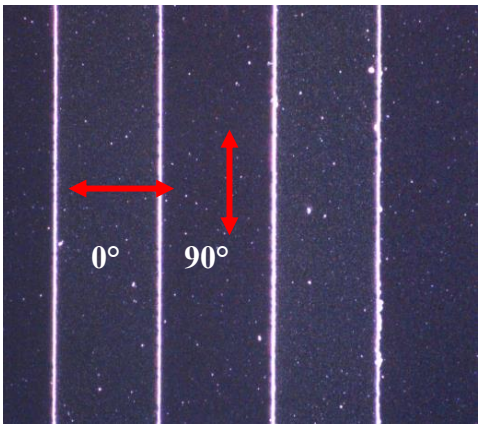	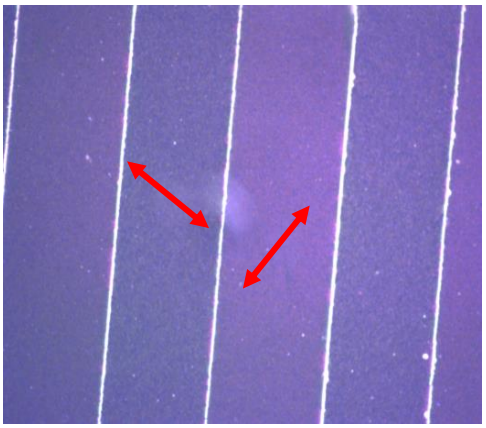

It can be said that the orthogonally aligned areas (0° / 90°) with respect to topological defect lines (masks line between two areas) in the coating show color

changes while rotating the sample. It means that the light actuation can be achieved for those samples without any doubts.

4.5.4.3 Polarized light actuation result

The light actuation experiments were carried out by DHM equipped with polarized UV (365 nm, 200 mW/cm^2) and blue (455 nm, 20 mW/cm^2) light. Figure 4.26a represents polarized light actuated oscillation principle in PAT_5M2F on acrylate soft substrates. For each characterization, two different zones (A and B) were selected as matching domains, meaning that all pairs are located at the same distance from the topological defect line. Also, each zone in those pairs existed in orthogonally aligned areas with respect to each other. Thus, it was assumed that they have different oscillation directions with the same magnitude. For all calculations in this thesis, the differences between the upwards and downwards part of the matched selected zones were defined as "total height change". On the other hand, the stable amplitude of the oscillations was given by using Δh as stated before. The schematic illustration of how it can be calculated on the graph is shown in Figure 4.26b.

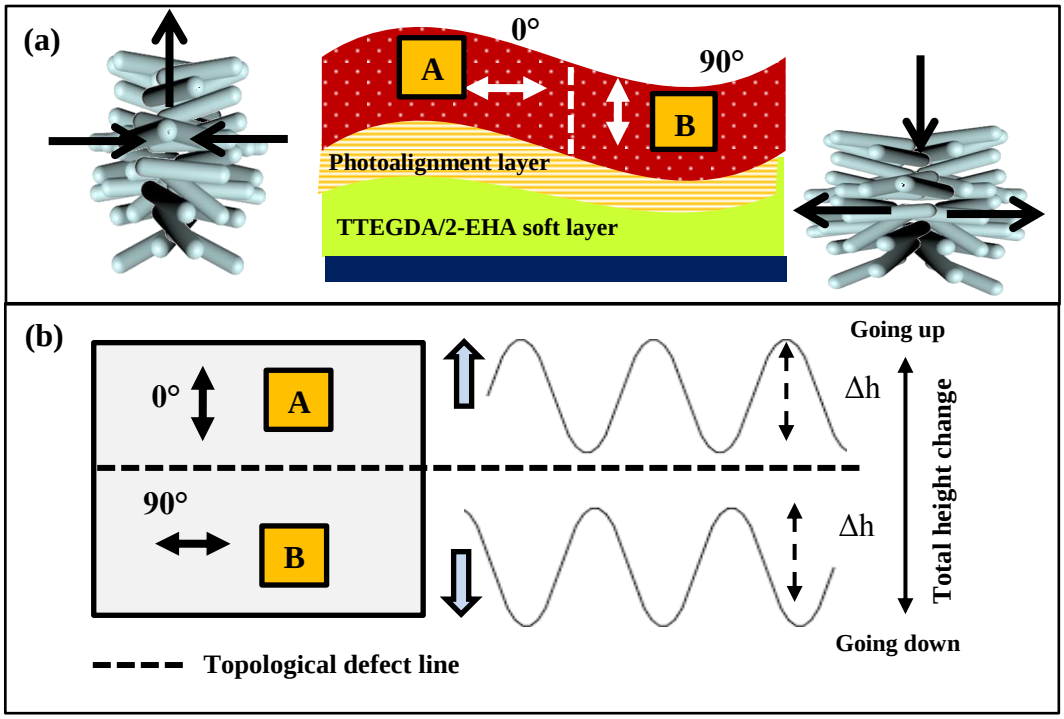

Figure 4.26 (a) Schematic illustrations of oscillation behavior in perpendicularly aligned areas. (b) Principle for calculating the total height changes in the matched zones.

Firstly, the polarized light actuated PAT_5M2F_T100 (0 vol.% 2-EHA) was investigated. The phase pattern and relative height change graphs depicted from DHM are shown in Figure 4.27. Zone 1-2 and zone 3-4 were chosen as matching domains to see whether the oscillation principle was working or not. Zone 1 and 3 started increasing while zone 4 decreased after light exposure. This means that zones 1, 3 and 4 immediately exhibit a growing self-oscillating behavior. However, the oscillation trend was not stable for zone 2. This can be due to the existence of some defects around the topographical defect line (Figure 4.27b).

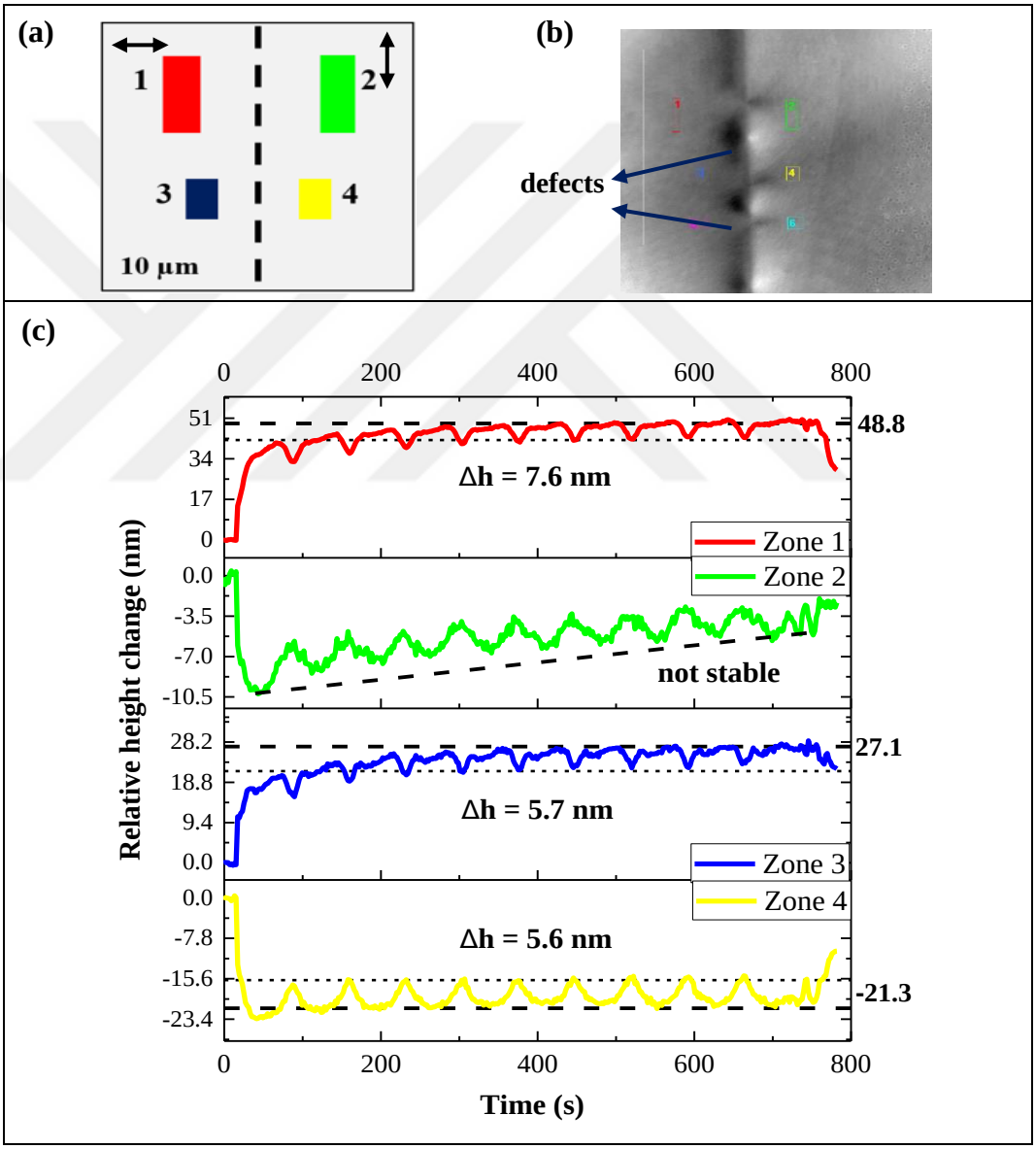

Figure 4.27 DHM results for PAT_5M2F_T100 with 500 µm periodic lines. (a) Schematic illustration of the selected zones (1-4) in the coating. (b) Phase profile. (c) Relative height change with respect to time.

For PAT_5M2F_T100 coating, the maximum total height change is approximately 48.4 nm for the stable zones 3 and 4 which were selected at the same distance from the defect line. On the other hand, the stable amplitude of the oscillation (Δh) for zone 3 and 4 reaches 5.7 and 5.6 nm, respectively.

Afterwards, the substrates PAT_5M2F_T80E20 having both TTEGDA and 2-EHA (80 vol.% and 20 vol.%, respectively) were used as a proof for the effect of the mechanical properties of the substrates on the light-sensitivity (Figure 4.28).

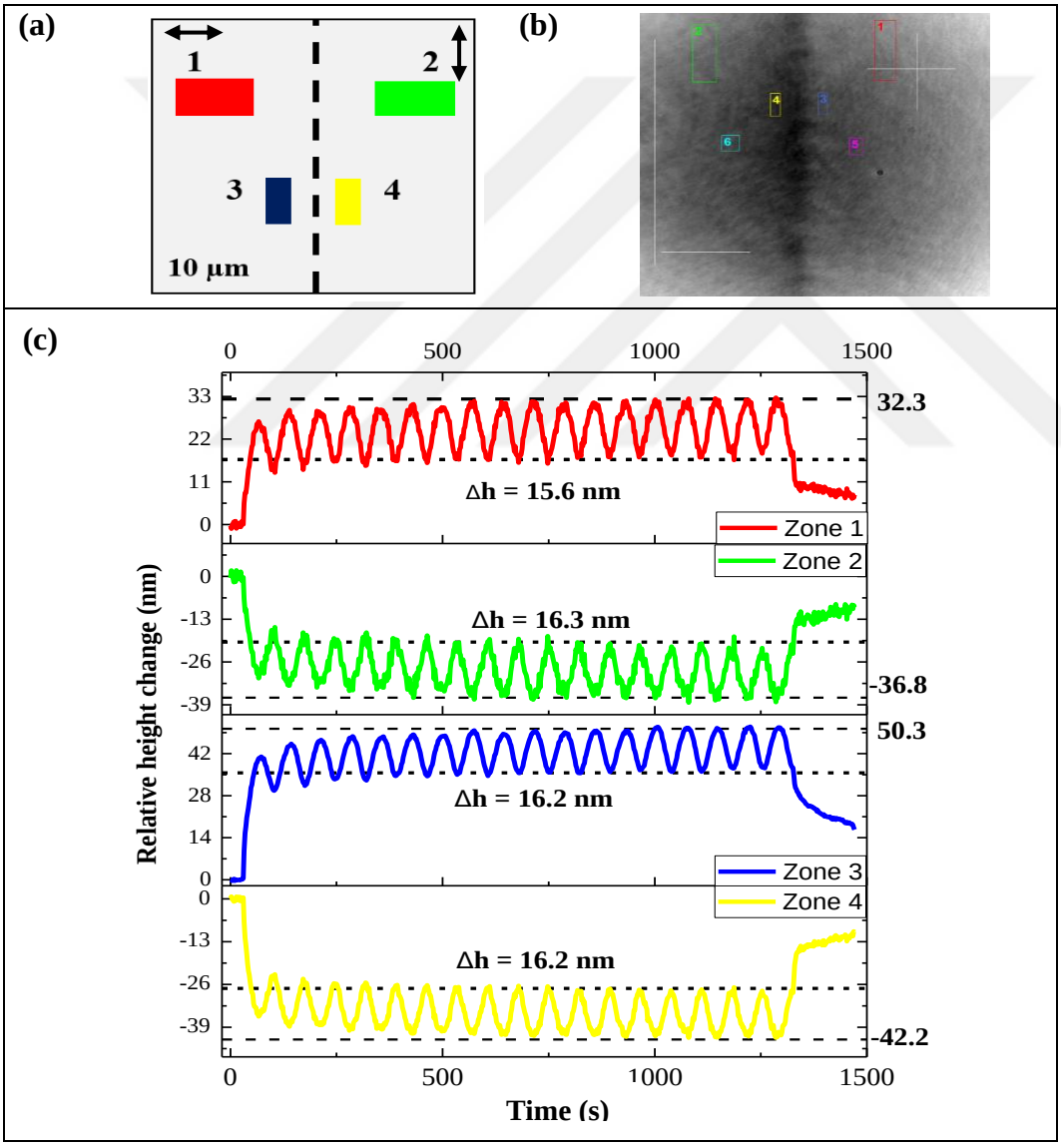

Figure 4.28 DHM results for PAT_5M2F_T80E20 with 500 µm periodic lines. Schematic illustration of the selected zones (1-4) in the coating. (b) Phase profile. (c) Relative height change with respect to time.

The total height changes for the matched zones 1-2 and 3-4 are 69.1 and 92.5 nm, respectively. Although a slight deviation was observed in zone 1, the amplitude of the oscillation is measured as 16 nm based on the averages of all Δh values for zone 1-4 (Figure 4.28c).

When compared the surface deformation in PAT_5M2F_T100 and PAT_5M2F_T80E20, it can be said that the maximum height change was increased from 48.4 to 92.5 nm, and the measured values of Δh had nearly tripled by adding 20 vol.% of 2-EHA. This could mean that the substrate having 2-EHA provided a higher deformation effect owing to providing lower storage modulus.

For further examinations, the patterned coating was combined with the acrylate substrate including 40 vol.% of 2-EHA. The schematic illustration and phase pattern of the coating with selected zones (1-4) are given in Figure 4.29a-b. According to the trends of the zones (4.29c), the stable total height changes for both matching regions (zone 1-2) were about 93.3 nm. When focusing on zones 1-2-4, a steady oscillation movement was provided from the beginning to the end of the polarized UV light interaction (1300 sec). However, this stability is corrupted in zone 3 and the unbalanced oscillation movement that was constantly increasing until 41.7 nm was observed (indicated by blue curves in Figure 4.29c). It was speculated that this might be due to the location of the zone 3. This domain was located close to the topological defect line. The unbalanced tensions might have arisen between the two orthogonal areas. However, this effect was not observed in zone 4. From this standpoint, the trend of the zones cannot be generalized.

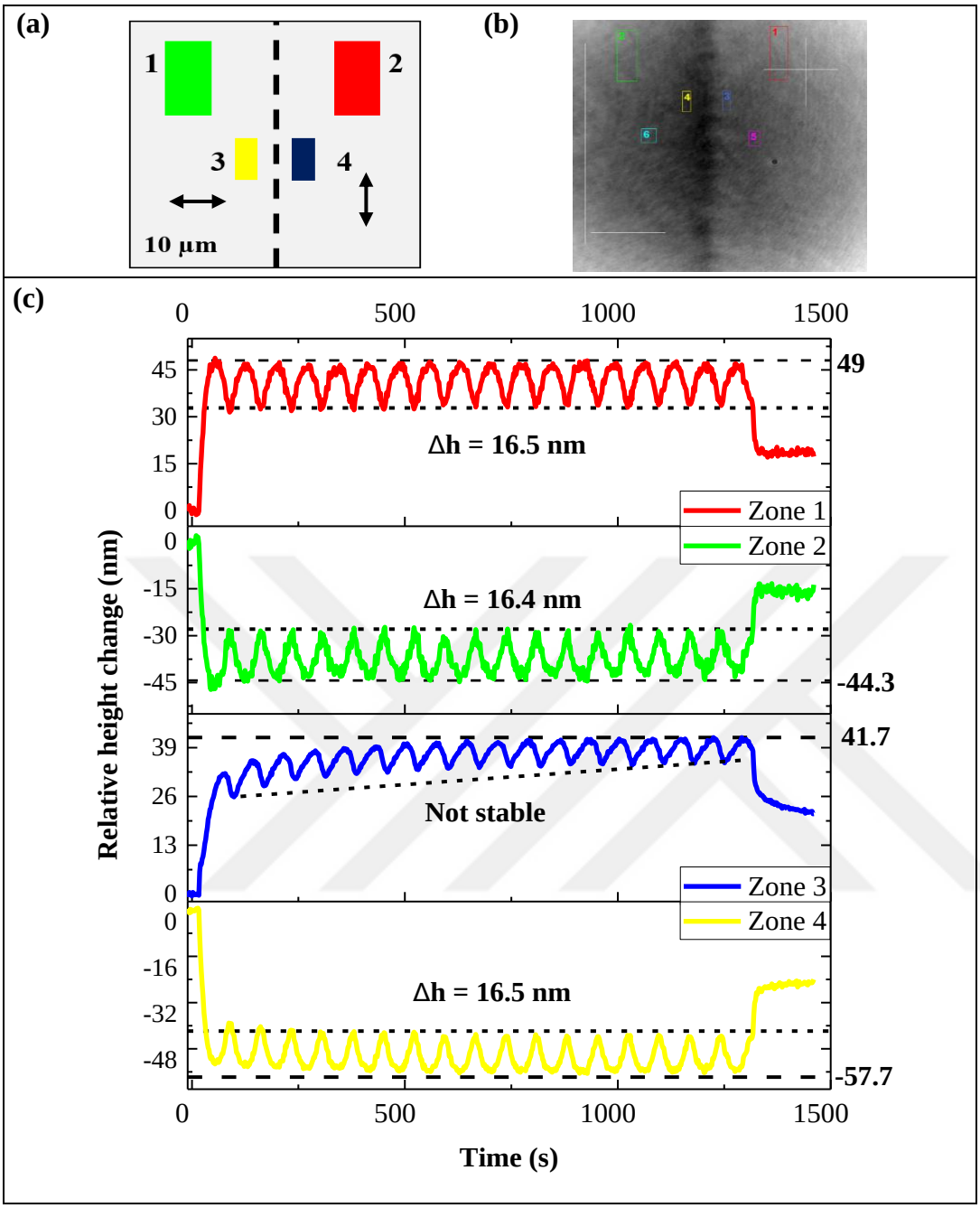

Figure 4.29 DHM results for PAT_5M2F_T60E40 with 500 µm periodic lines. Schematic illustration of the selected zones (1-4) in the coating. (b) Phase profile. (c) Relative height change with respect to time.

The results of coatings with 500 µm pitches are compared until 40 vol.% of 2-EHA, PAT_5M2F_T60E40 showed the highest total height change (93.3 nm), followed by PAT_5M2F_T80E20 (92.5 nm) and PAT_5M2F_T100 (48.4 nm). Furthermore, PAT_5M2F_T80E20 and PAT_5M2F_T60E40 presented significantly higher values (16.2, 16.5 nm, respectively) for the amplitude of the

oscillation than those of PAT_5M2F_T100 (maximum 7.6 nm). It can be said that the addition of 2-EHA monomer into the TTEGDA substrate was a good selection for increasing the surface deformation. Because T80E20 (345.7-347 MPa) and T60E40 (19.35-19.75 MPa) had lower storage modulus value than that was measured for T100 substrate (1120-1125 MPa), the substrates became softer. As expected, this softness enhanced the surface movement. Interestingly, the height variation obtained near the topological defect line was higher despite of some deviations from the stability (zone 3 in Figure 4.29c). For instance, if these values are sorted 48.8 nm for zone 1 in PAT_5M2F_T100 coating, 50.3 nm for zone 3 in PAT_5M2F_T80E20 and 57.7 nm for zone 4 in PAT_5M2F_T60E40 coating. (Figure 4.27c, 4.28c and 4.29c, respectively). However, the height changes and Δh values of the samples with 20 to 40 vol.% 2-EHA were really close to each other even though there measured a significant difference between the storage modulus of the substrates.

For detailed information, the conducted experiments with PAT_5M2F_T80E20 and PAT_5M2F_T60E40 were repeated using the areas having 50 μm lines which mean orthogonally aligned areas were close to each other. Table 4.2 represents the observations of the coatings captured by POM. The microscopic images were taken between crossed polarizer (x10 objective magnification).

While rotating both samples, entirely aligned textures were observed. It means that orthogonally aligned molecules provide high optical anisotropy. Hence, PAT_5M2F_T80E20 and PAT_5M2F_T60E40 layered systems with 50 μm periodic lines were found suitable to actuate with the polarized light system.

Table 4.2 POM results for PAT_5M2F_T80E20 and PAT_5M2F_T60E40 (50 µm periodic lines)

	0°	45°
PAT_5M2F_T80E20	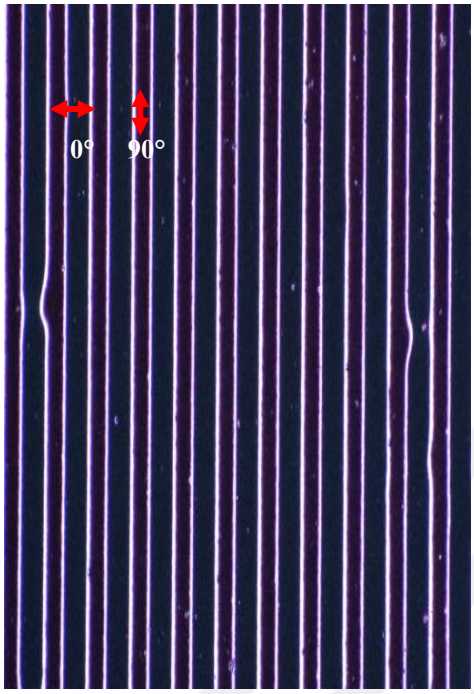	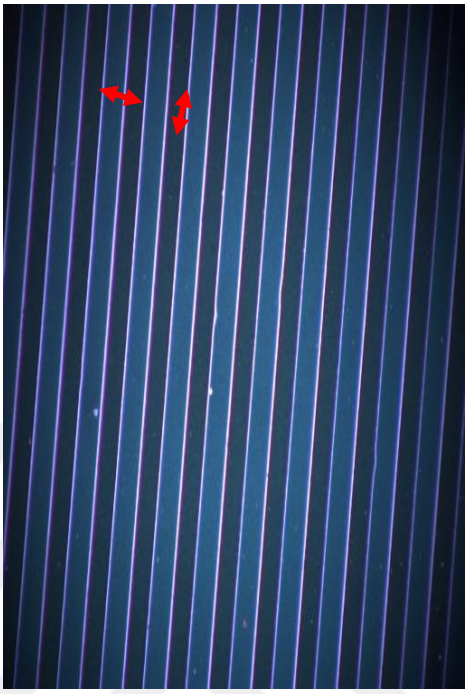
PAT_5M2F_T60E40	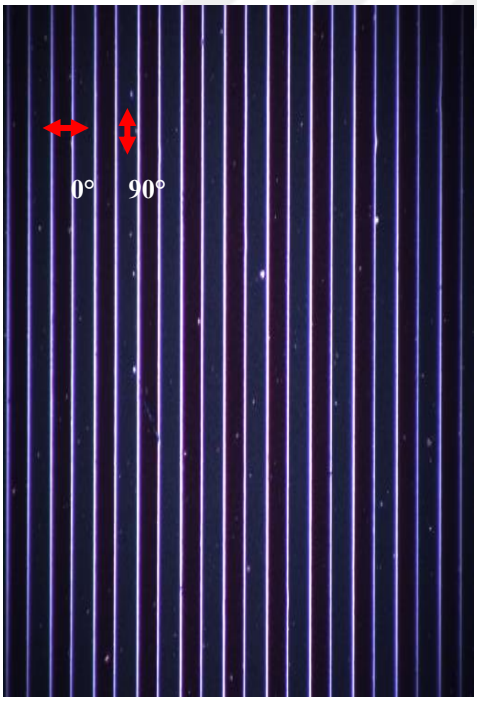	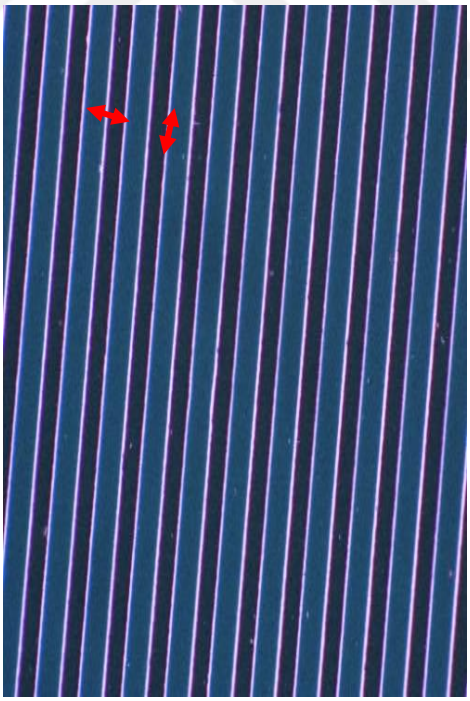

Figure 4.30a-b shows the phase profiles of both coatings characterized by DHM. As can be seen, there was no contaminations and defects which would

reduce surface movements. Polarized light actuated smart layered systems based on 20 and 40 vol.% 2-EHA containing acrylates are shown in Figure 4.30c.

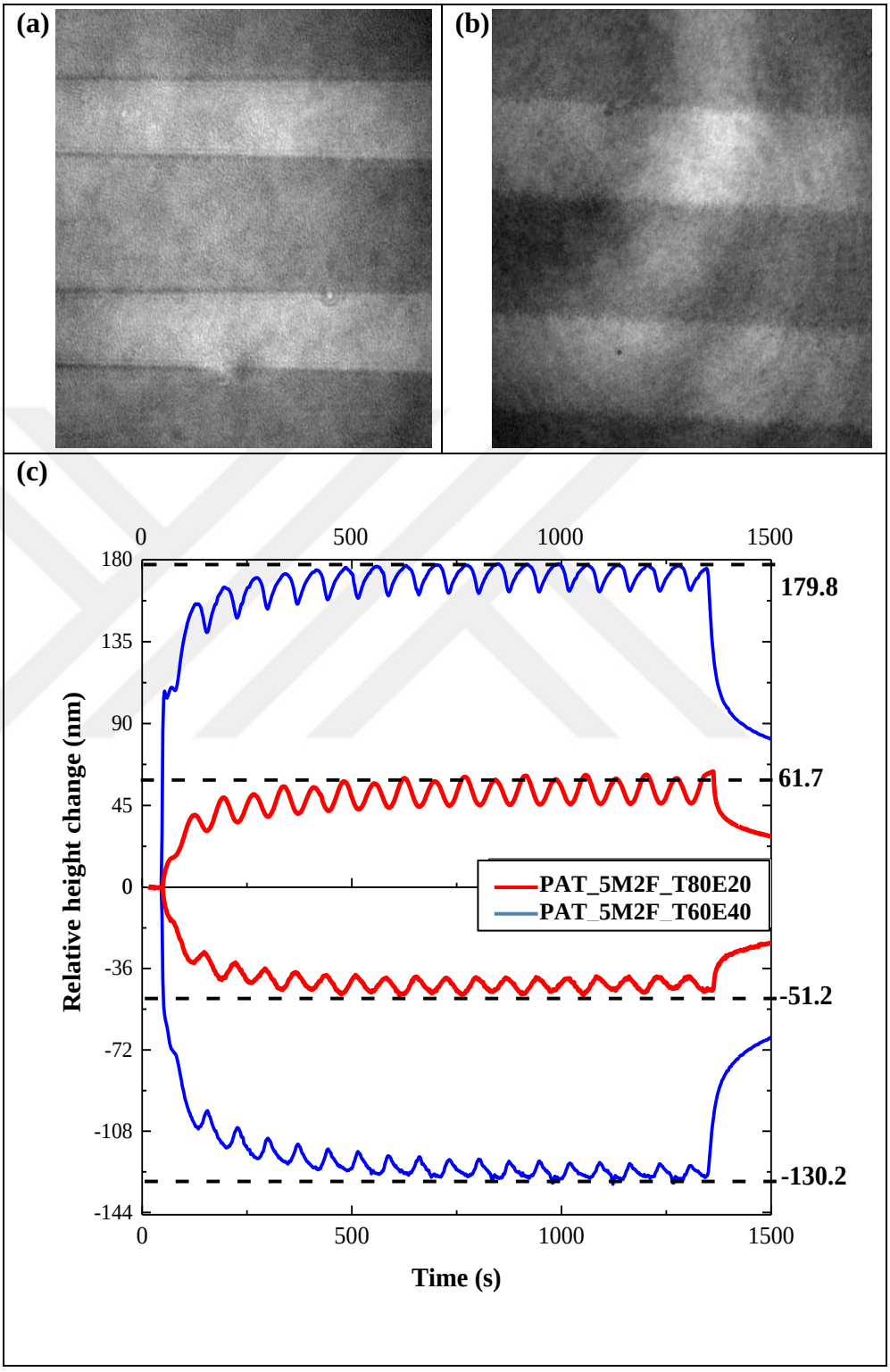

Figure 4.30 Phase profiles of (a) PAT_5M2F_T80E20 (b) PAT_5M2F_T60E40 with 50 µm pitches depicted from DHM. (c) Relative height change of both coatings with respect to time.

Both coatings (with 50 µm pitches) showed stability in the oscillation motion until closing the light. The maximum total height changes were measured as 113 and 310 nm for PAT_5M2F_T80E20 and PAT_5M2F_T60E40, respectively. These values meet the target expectation in that much larger surface deformation was found with 40 vol.% 2-EHA content. Decreasing elastic modulus from 347 to 19.75 MPa contributed to higher surface deformation behavior during light activation. On the other hand, when comparing 50 and 500 µm results, using perpendicularly aligned areas close to each other (spacing of 50 µm) increased the total height variations in both coatings, primarily PAT_5M2F_T60E40.

The oscillation trends were stable between 500 and 1000 sec for both coatings and a more detailed comparison is given in Figure 4.31. Measured Δh values were 17.3 and 19.5 nm for 20 and 40 vol.% of 2-EHA containing acrylate substrates, respectively.

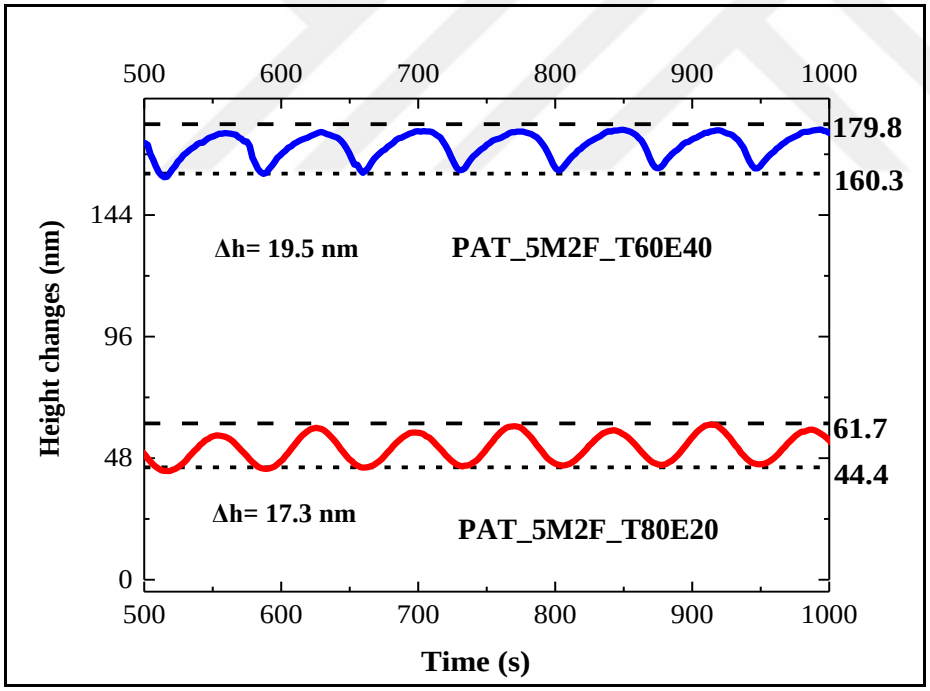

Figure 4.31 Oscillations of height change for PAT_5M2F_T80E20 and PAT_5M2F_T60E40 with 50 µm domains between 500 and 1000 sec.

As supported by the 3D visualizations which are shown in Figure 4.32, an asymmetrical movement is observed for both coatings. One area increases and the vertically aligned area with respect to this area decreases in height.

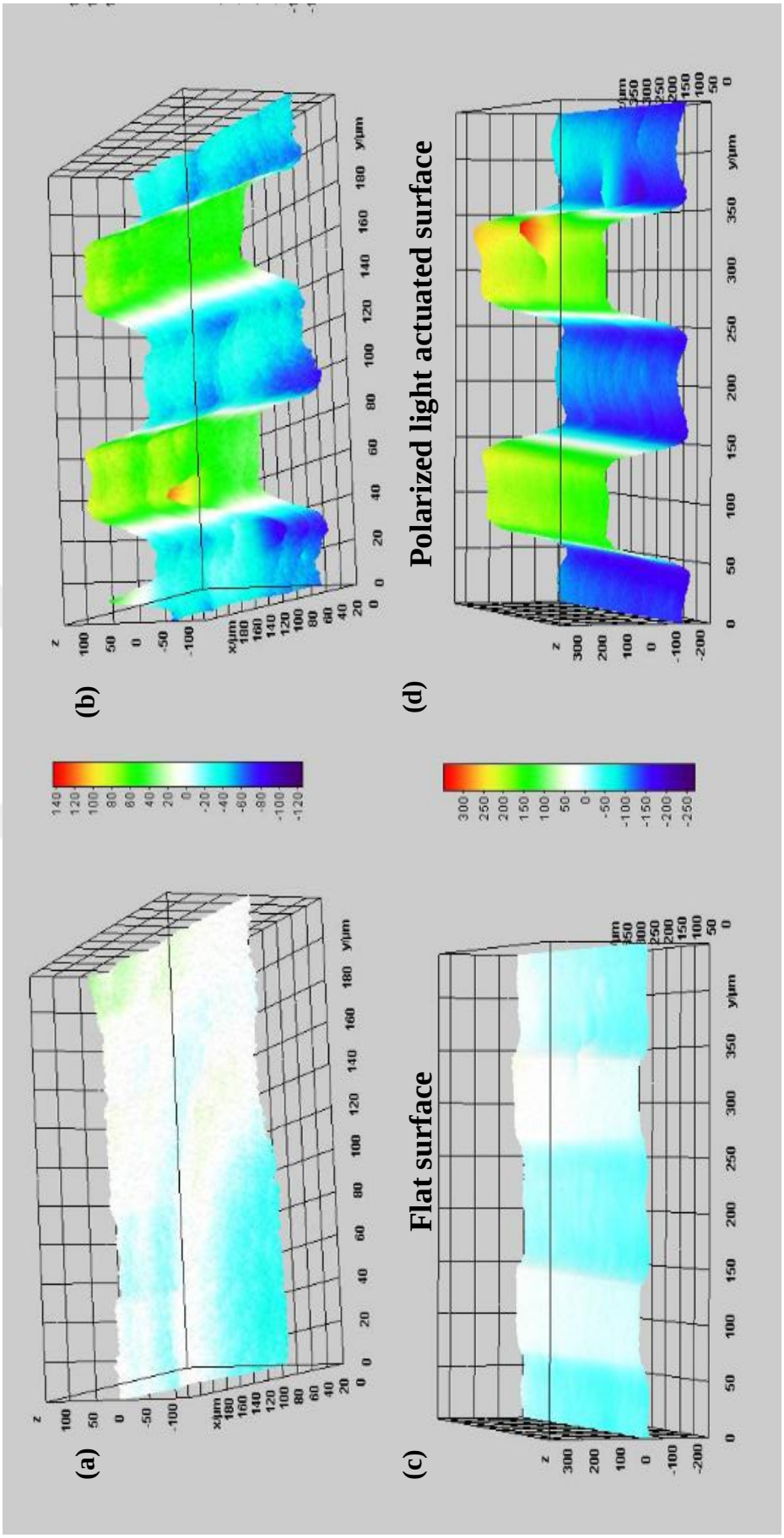

Figure 4.32 3D visualizations of (a, b) PAT_5M2F_T80E20 and (c, d) PAT_5M2F_T60E40 with a line of 50 µm pitch

Next characterization was continued with a line of 500 µm pitch. The light sensitivity of selected domains 1-4 in the patterned coating (Figure 4.33a-b) on 60 vol.% of 2-EHA containing acrylate was investigated to determine the deformation trend on the matched zones which were placed in both close and distant locations from the topological defect line (Figure 4.33). The total height change reached nearly 106 nm for depicted matched zones 1-2 (Figure 4.33c).

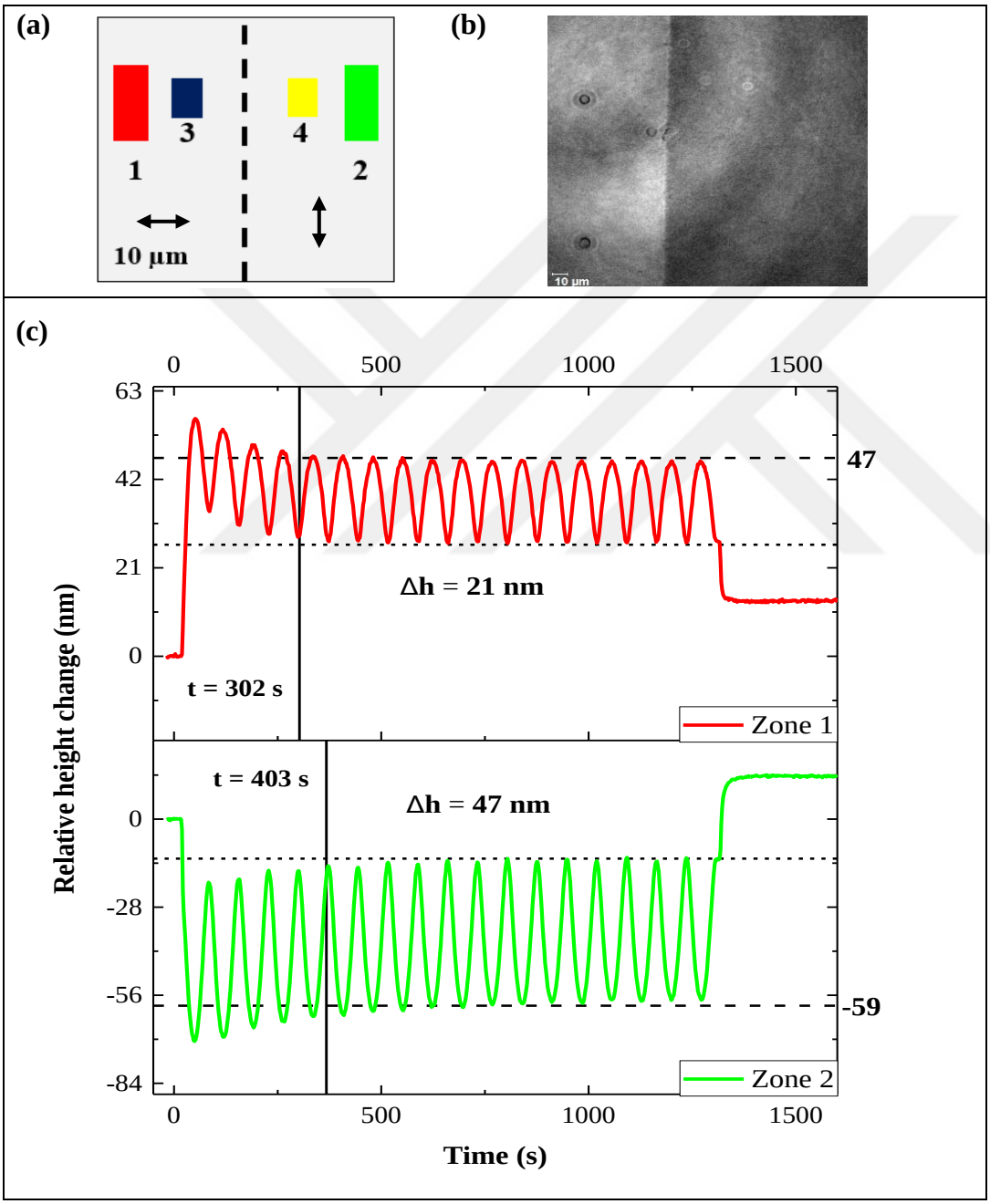

Figure 4.33 DHM results for PAT_5M2F_T40E60 coating with 500 µm pitches. (a) Schematic illustration of the selected zones (1-4). (b) Phase profile of the coating. (c) Relative height change for the matched zones 1-2.

For the matched zones 3-4, the total height change was measured as nearly 86 nm from the graph in Figure 4.34.

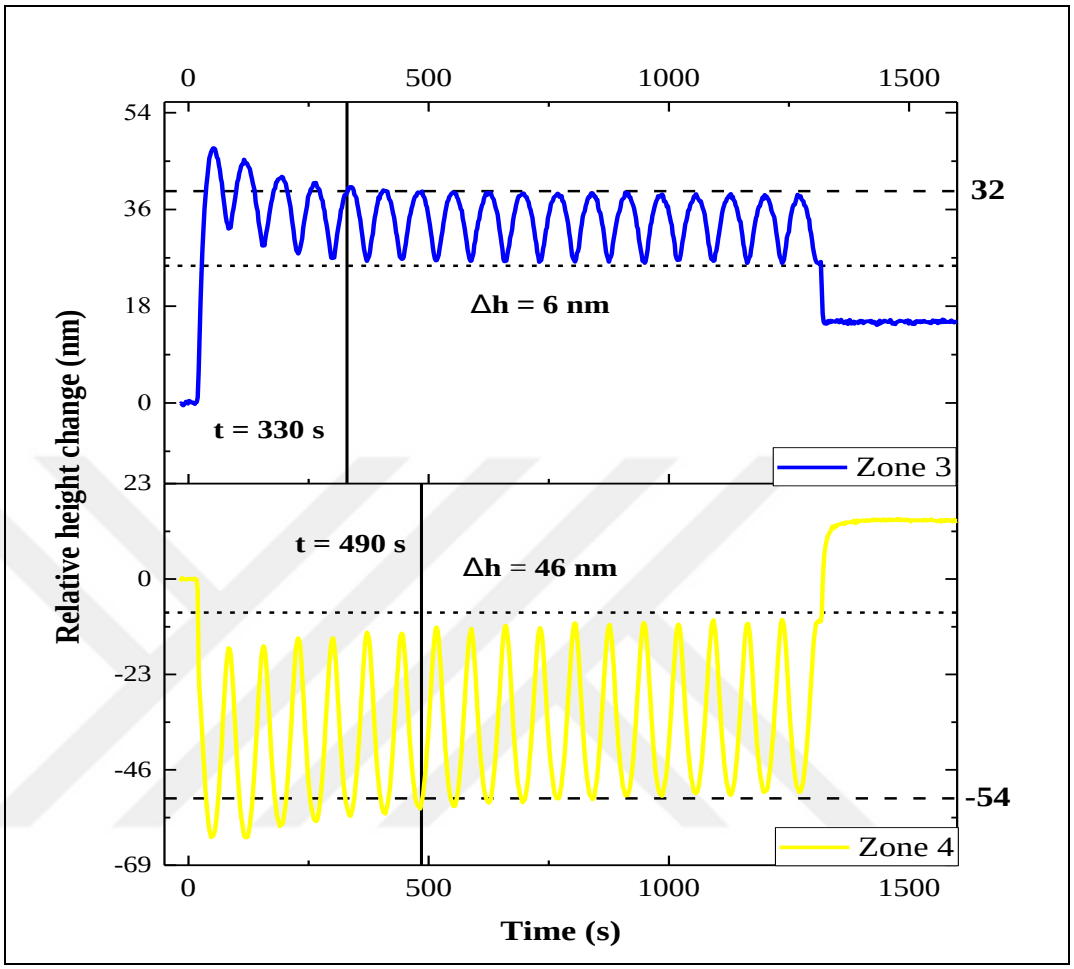

Figure 4.34 Relative height changes of the matched zones (3-4) in PAT_5M2F_T40E60 coating with 500 μm pitches.

It can be said that a relatively higher deformation was achieved for all matched zones compared to PAT_5M2F_T60E40 coating with 500 μm domains (93.3 nm). However, the same trend was not seen for the amplitude of the oscillation for each zone and the oscillation motion cannot be considered stable. A term t (stability time) value indicates the minimum time for the stable oscillation height can be measured. Stability times were 302, 403, 330 and 490 sec for zones 1, 2, 3 and 4, respectively. It means each matched zone came into balance at different times.

The obtained Δh values were 21 and 47 nm for zone 1-2 (Figure 4.30c). On the other hand, zone 3 and 4 also showed unexpected results. Whereas zone 3 has 6 nm, zone 4 had 46 nm (Figure 4.34). Overall, the oscillation trend of the matched domains is surprisingly different although they were all existed at the same distance from the defect line. One possible reason for the lack of stability might be counterbalance forces. As can be seen in the phase profile of the sample (Figure 4.33b), there were some flaws near the zones selected. These imperfections turned into two holes that also actively formed on the top layer during the light interaction. This might affect the surface deformations but the general mechanism that disrupts the system could not be fully understood. Figure 4.35 represents 3D images of the system that can support this idea about counterbalances forces (holes are indicated by black circles).

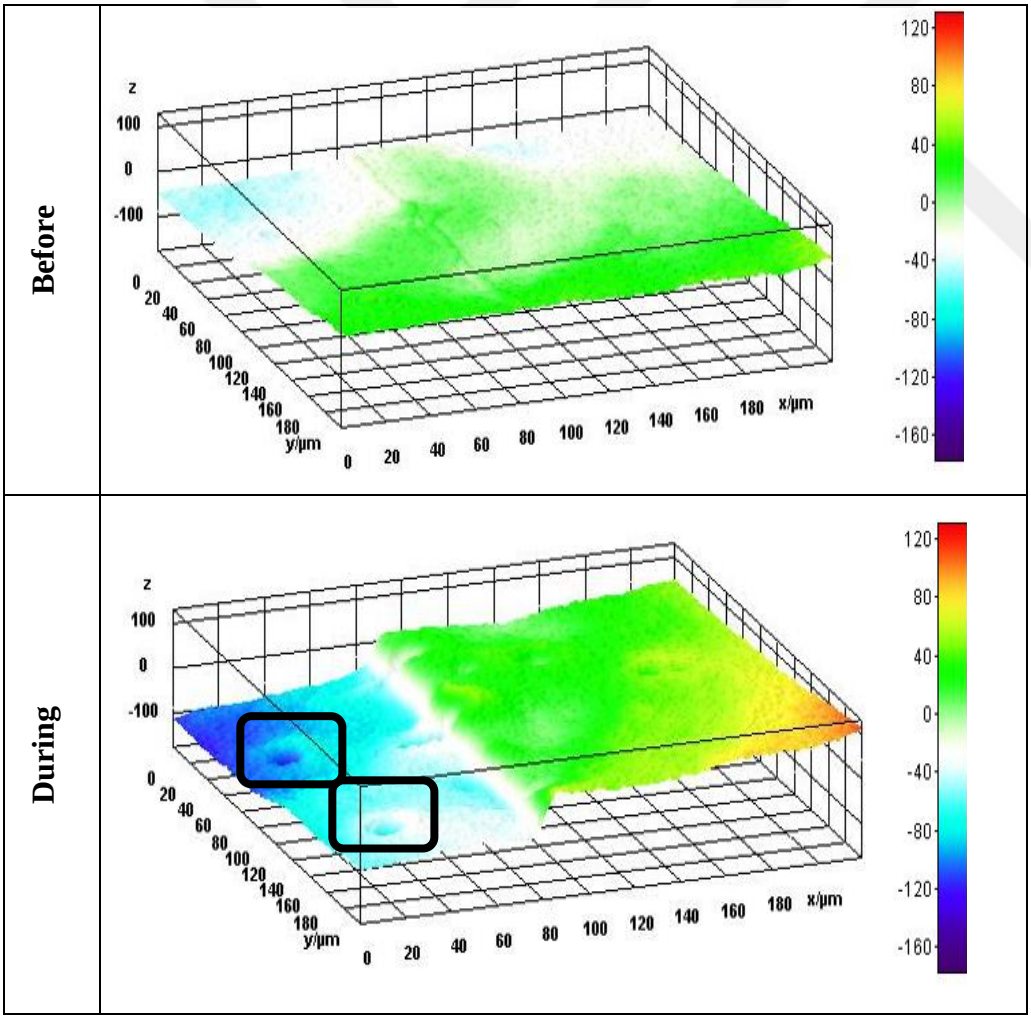

Figure 4.35 3D images of polarized light actuated PAT_5M2F_T60E40 with 500 µm pitches.

Figure 4.36 represents the selected zones and microscopic image of PAT_5M2F_T20E80 with 500 µm pitches. All matched zones were located nearly at the same distances from the defect lines to ensure the stability.

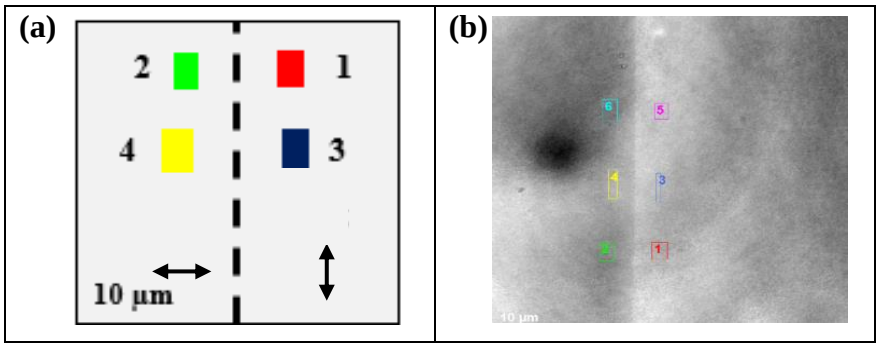

Figure 4.36 DHM results for PAT_5M2F_T20E80 coating with 500 µm pitches. (a) Schematic illustration of the selected zones (1-4) in the coating. (b) Phase profile of the coating.

As measured from the graph in Figures 4.37a-b, the sample showed a value of total height change is 173.2 and 169 nm for the matched zone combinations (1-2) and (3-4), respectively. This was much larger compared to the value calculated for PAT_5M2F_T40E60 coating with 500 µm pitches (106 nm was found, see in Figure 4.33c). It can be said that further increasing the 2-EHA content to 80 vol.% leads to a qualitative change in the surface deformation while light actuation.

The stability time (t) for each matched zone was observed at approximately 400 sec after exposing with the polarized light system. These trends are clearly shown in the related graphs in Figures 4.37a and 4.37b. Moreover, there was an apparent increase of the height for the zones 1, 3 and a decrease in the zones 2, 4. The increase and decrease were related to the average and Δh value is calculated roughly 18-20 nm in each direction. The maximum one was measure as 21 nm for zone 2 (Figure 4.37a).

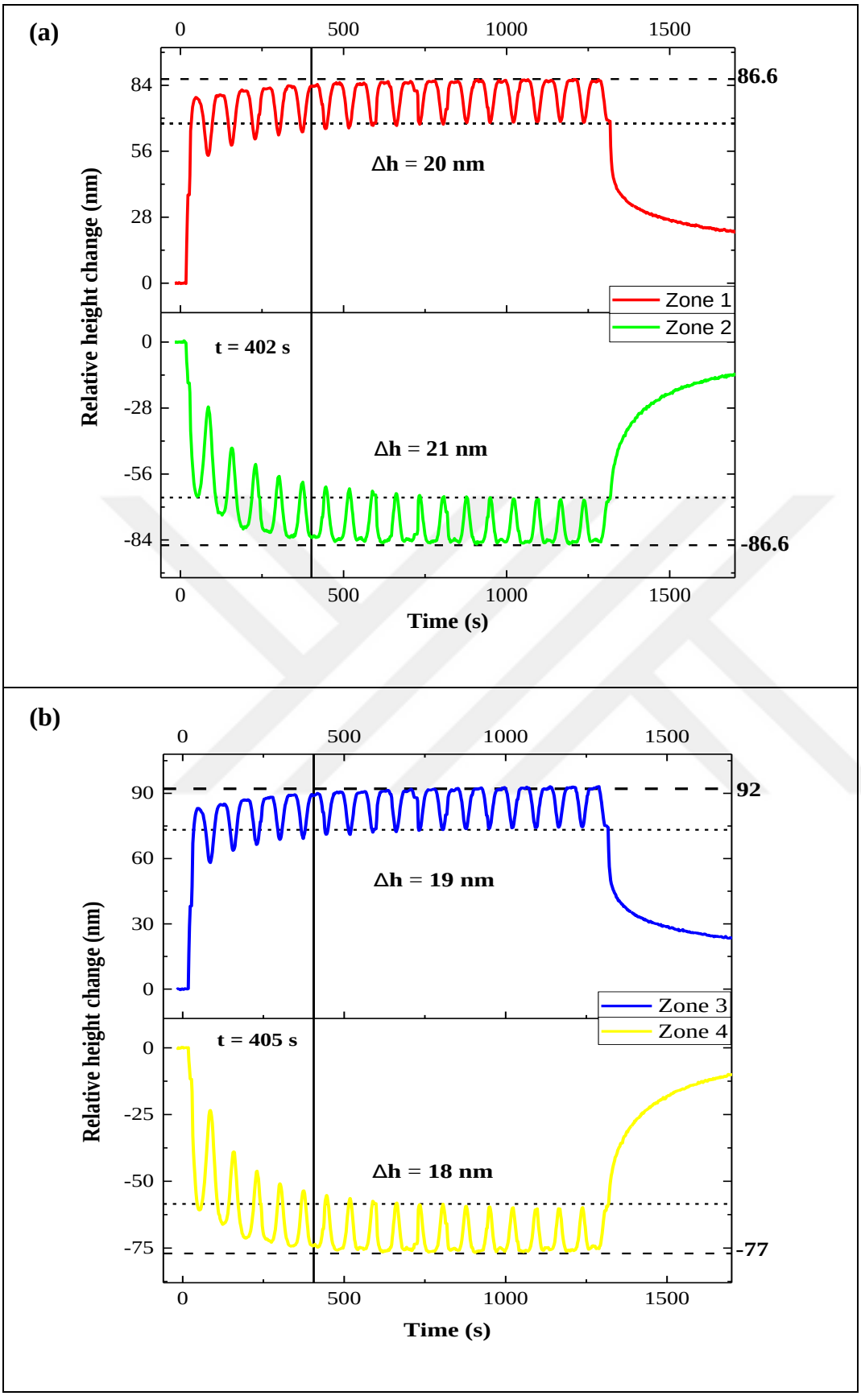

Figure 4.37 Relative height changes of the matched zones (a) 1-2 and (b) 3-4 in PAT_5M2F_T20E80 with 500 μm pitches.

For a detailed examination of the balanced oscillation motion, 3D images of PAT_5M2F_T20E80 were considered (Figure 4.38). As can be clearly seen that one domain started rising and matched one started falling.

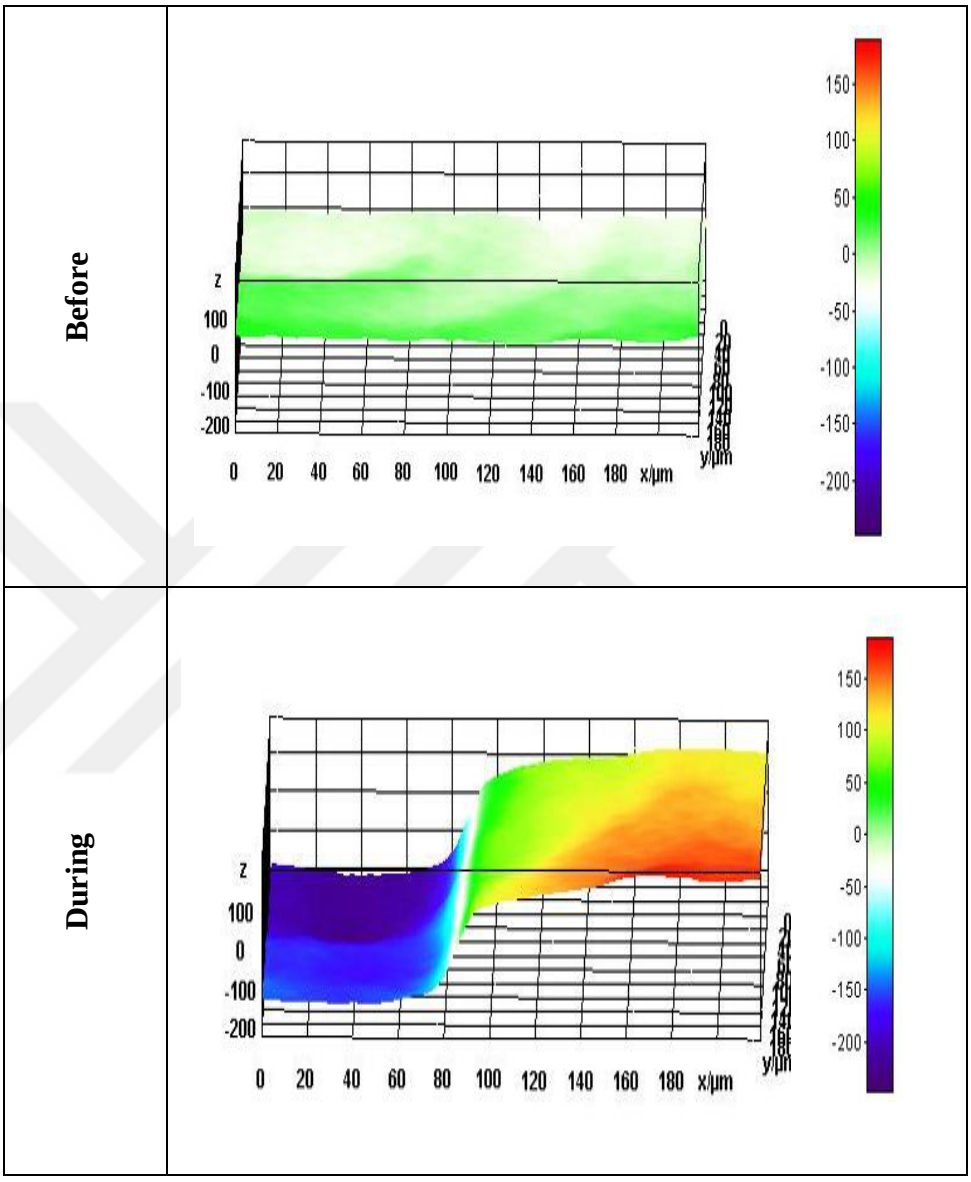

Figure 4.38 3D images of PAT_5M2F_T20E80 with 500 µm pitches during the light actuation.

Next, the last investigations were performed on the coating which has 500 µm pitches. PAT_5M2F_T5E95 coating was actuated under the polarized light to compare with the previous results. Figure 4.39a-b shows the selected zones (1-4) on the coating and phase profile during light actuation.

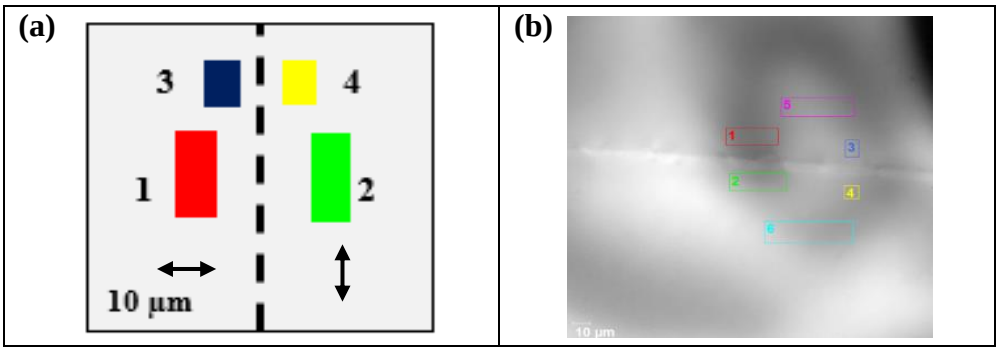

Figure 4.39 DHM results for PAT_5M2F_T5E95 coating with 500 µm pitches. (a) Schematic illustration of the selected zones (1-4) in the coating. (b) Phase profile of the coating.

From the graphs in Figure 4.40a-b, the largest deformation was found as 360 and 352 nm for the matched zones 1-2 and 3-4, respectively. These values correspond to the highest magnitude of the height change found for the samples studied with 500 µm pitches. The calculated Δh values were 86, 62, 81 and 72 nm for the zones 1, 2, 3 and 4.

It can be said that PAT_5M2F_T5E95 coating has the highest surface deformation and Δh values when compared to other calculated samples with 500 µm pitches. Moreover, this sample follows a stable motion from the beginning to the end of the light interaction. There is no need to mention about the stability time. The results show that using the softer combination as a substrate significantly increased the absolute height changes.

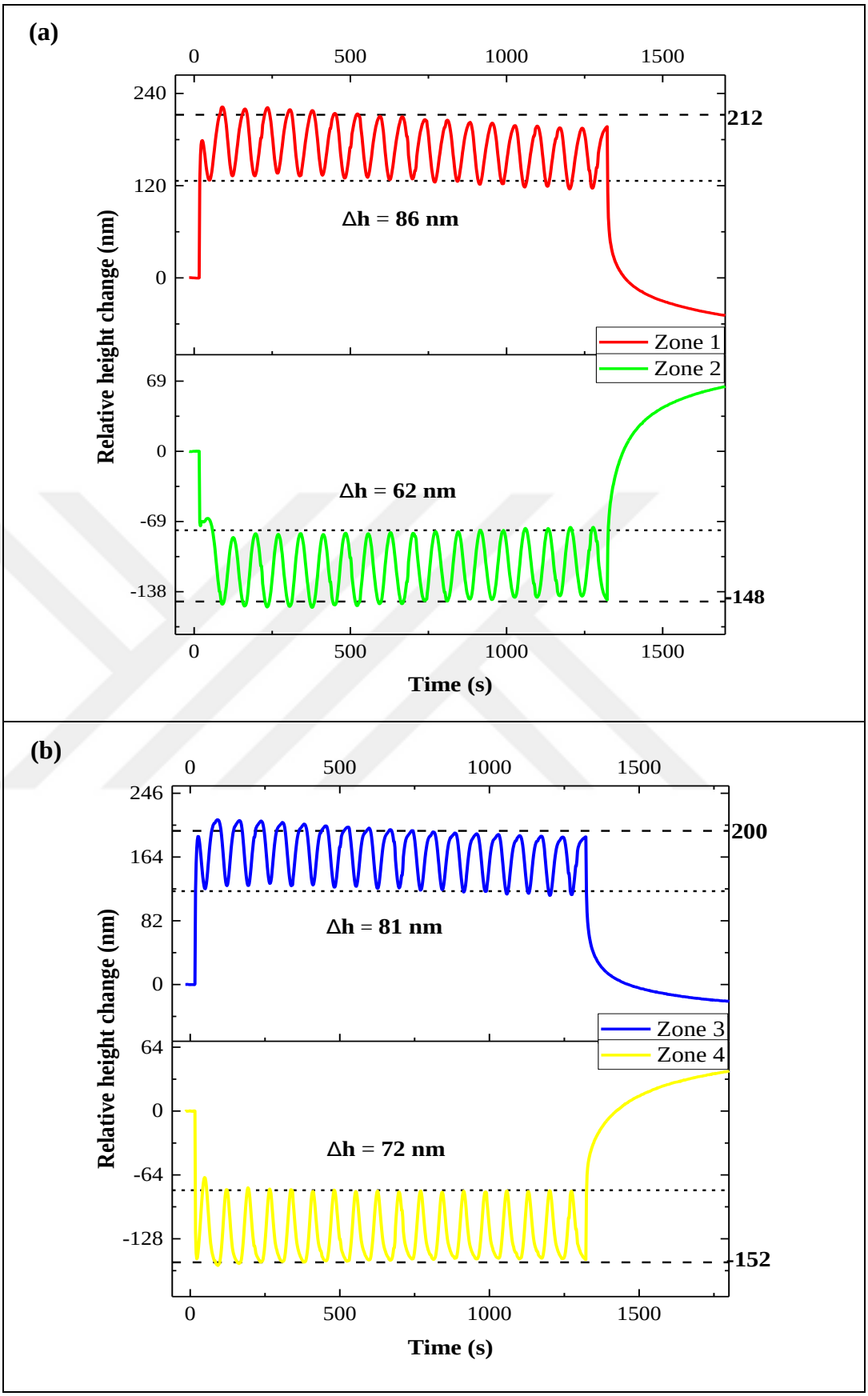

Figure 4.40 Relative height changes of the matched zones (a) 1-2 and (b) 3-4 in PAT_5M2F_T5E95 coating 500 µm pitches.

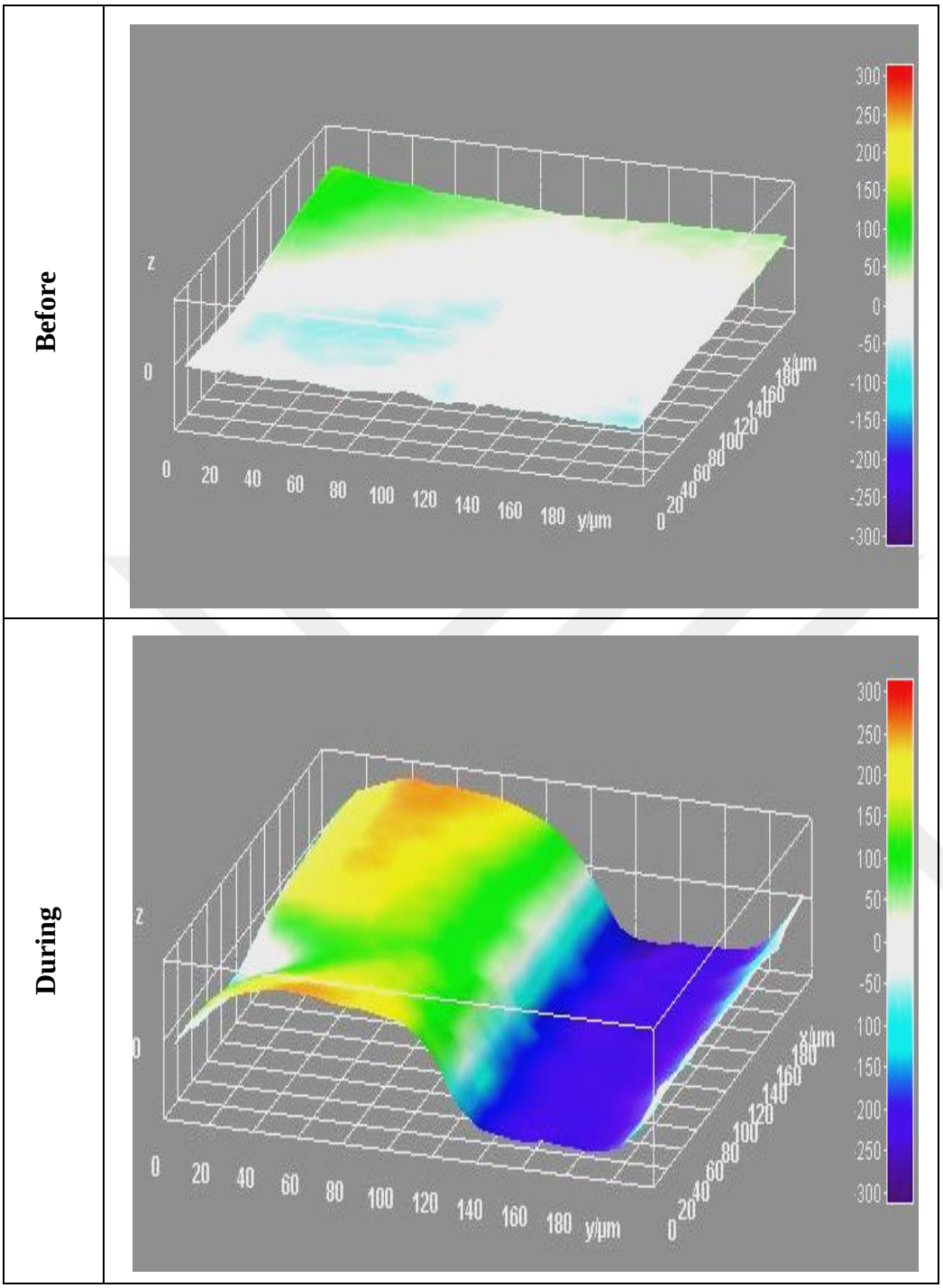

Figure 4.41 3D images of PAT_5M2F_T5E95 with 500 µm pitches (a) before and (b) during the polarized light actuation.

Another comparative study was employed using 100 µm periodic lines on PAT_5M2F_T100 and PAT_5M2F_T5E95 samples. The alignment quality of the selected samples was analyzed by POM (shown in Table 4.3). As can be seen, each domain showed color change while rotating the sample from 0˚ to 45˚ position.

Table 4.3 POM observation of patterned layered systems with 100 µm lines (x10 objective)

	0°	45°
PAT_5M2F_T100	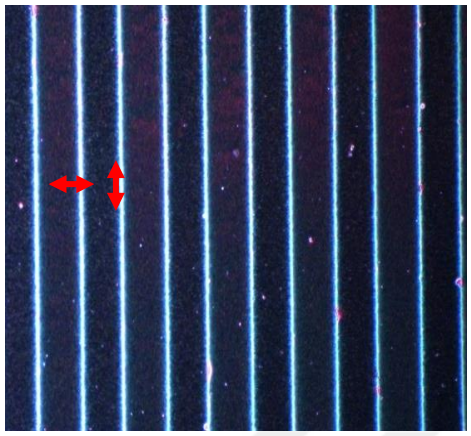	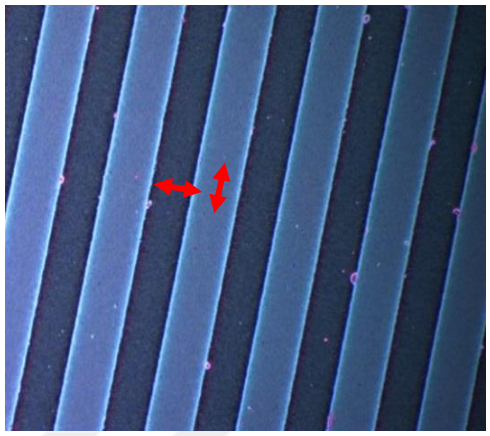
PAT_5M2F_T5E95	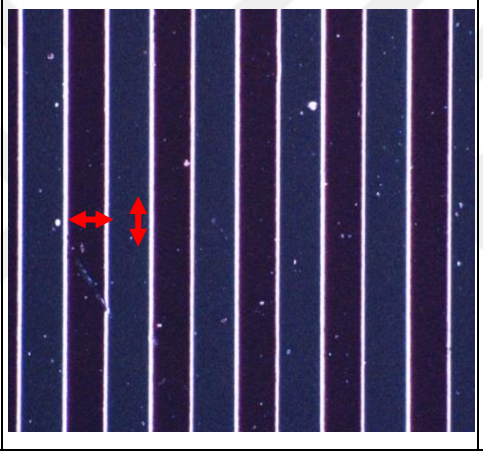	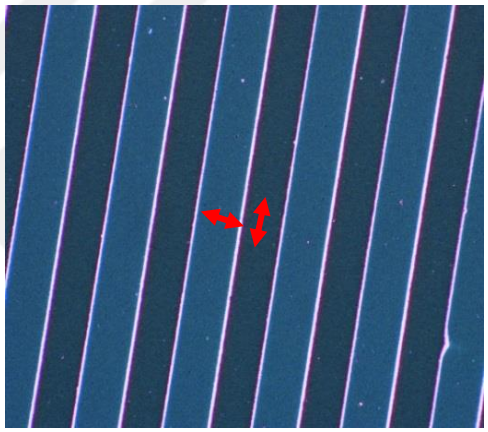

DHM measurements of the samples are given in Figure 4.42. The maximum amplitude of the oscillation and height change was obtained on the soft layer without using 2-EHA, correspond to 80.6 and 15.6 nm, respectively. When compared to the results for 500 um (maximum height change and amplitude were 48.4 and 7.6, respectively), it can be said that using smaller lines for the pattern (closer topological defect lines) provided an increase in the surface deformation for PAT_5M2F_T100 sample. Interestingly, PAT_5M2F_T5E95 sample reduced the amplitude of the oscillation to 52 nm but the total height change was 460 nm which was higher than the measured value for 500 µm pitches (see in Figure 4.40). On the other hand, the stability of the oscillation motion was not good for PAT_5M2F_T5E95 sample when compared to the results for 500 µm pitches. The reason can be explained by the undesired interaction of the topological defect lines when the domains were close to each other (100 µm pitches).

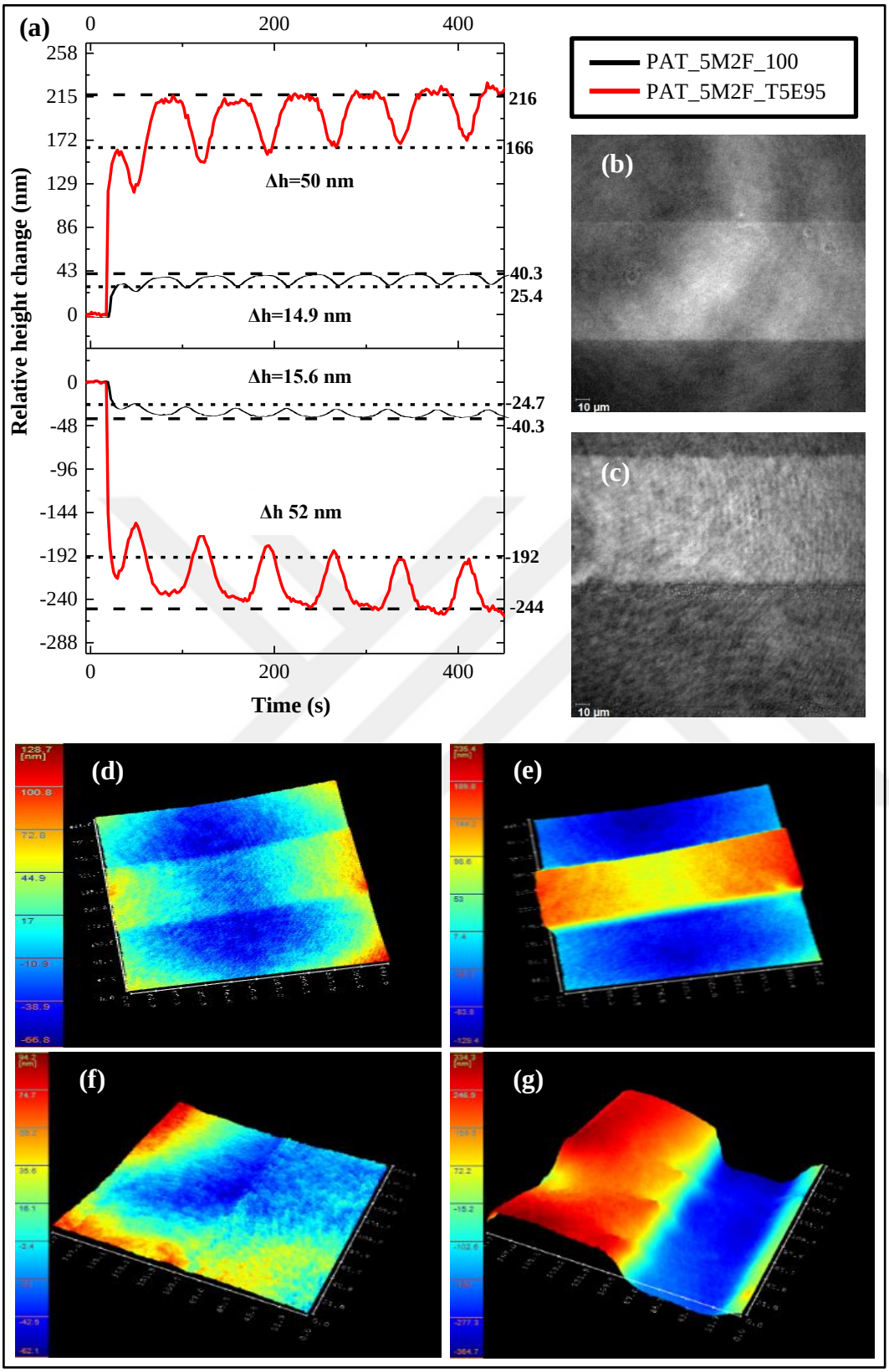

Figure 4.42 (a) Relative height changes. Phase patterns of (b) PAT_5M2F_T100 and (c) PAT_5M2F_T5E95. 3D images of (d, f) before and (e, g) during light actuation for PAT_5M2F_T100 and PAT_5M2F_T5E95, respectively.

Table 4.4 represents the summary of the alignment and unpolarized light actuation results for all obtained mechanically aligned azo-LCPN coated substrates.

Table 4.4 Summary of the alignment and unpolarized light actuation results of uniaxial planar smart layered systems on different substrates

Sample code		Treatment time (sec)	Alignment result	Total height change (nm)
O2 Plasma time for PDMS	UA_PDMS_0	0	Poor wettability, no alignment	No unpolarized light actuation
	UA_PDMS15	15	Increasing wettability, no alignment	
	UA_PDMS_30	30	Increasing wettability, no alignment	
	UA_PDMS_45	45	Poor alignment, good wettability	
	UA_PDMS_60	60	Poor alignment, good wettability	
	UA_PDMS_75	75	Poor wettability and alignment	
UV light curing time for precured TTEGDA	PCUA_15	0	No alignment	No unpolarized light actuation
	PCUA_30	15	No alignment	
	PCUA_45	30	No alignment	
	PCUA_60	45	No alignment	
	PCUA_75	75	No alignment	
	PCUA_90	90	No alignment	
	PCUA_120	120	Crack and wrinkling	
	PCUA_150	150	Crack and wrinkling	
	PCUA_180	180	Crack and wrinkling	
	PCUA_210	210	Crack and wrinkling	
	PCUA_240	240	Crack and wrinkling	
	PCUA_270	270	Poor alignment	
	PCUA_300	300	Good alignment	3.4
Directly cured TTEGDA	UA_T100	-	Good alignment	36

The summary of polarized light actuation results of mechanically- and photo-aligned azo-LCPN on different acrylate substrates can be seen in Table 4.5.

Table 4.5 Summary of the polarized light actuation results

Sample code		2-EHA concentration (vol.%)	Maximum total height change (nm)	Δh (nm)
Mechanically aligned	UA_T100	0	8.3	4.2
	UA_T80E20	20	15.5	6
	UA_T60E40	40	29	6.2
	UA_T40E60	60	38	8.2
	UA_T20E80	80	44.9	14.7
	UA_T5E95	95	102.8	18.8
500 µm	PAT_5M2F_T100	0	48.4	7.6
	PAT_5M2F_T80E20	20	92.5	16.2
	PAT_5M2F_T60E40	40	93.3	16.5
	PAT_5M2F_T40E60	60	106	47 (not stable)
	PAT_5M2F_T20E80	80	173.2	21
	PAT_5M2F_T5E95	95	360	86
100 µm	PAT_5M2F_T100	0	80.6	15.6
	PAT_5M2F_T5E95	95	460	52
50 µm	PAT_5M2F_T80E20	20	113	17.3
	PAT_5M2F_T60E40	40	310	19.5

5.0 CONCLUSION

The purpose of this study was to design and characterize light responsive smart layered systems which were made by combining three layers. From top to bottom, the used layers were functional azo-LCPN coating, alignment layer and soft polymeric layer, respectively. The azo-LCPN coating was fabricated on alignment layers (mechanically rubbed or photoalignment layer) by photopolymerization of LC monomer blend for each sample. Then, the smart coatings were combined with the substrates such as oxygen plasma treated PDMS, acrylate-based substrates (pre-cured TTEGDA, directly cured TTEGDA and TTEGDA/2-EHA) to detect the optimal process conditions to design layered system. Optical anisotropy of all samples was checked to provide alignment quality. Selected samples were exposed to unpolarized/polarized UV (365 nm) light and blue (455 nm) light combination to ensure their light sensitivity such as static/dynamic height changes and oscillation trend.

- PDMS substrates were treated with oxygen plasma for different times (0, 15, 30, 45, 60 and 75 sec) to detect a suitable modification time for covering with LCs. Optimal time spent for the treatment was selected as 30-45 sec according to the wettability properties of PDMS substrates. However, the optical anisotropy was not being obtained due to the high energy particles of the plasma atmosphere. For this reason, the characterization of light-sensitivity on PDMS based layered systems was not performed.

- Pre-curing of TTEGDA substrates under the low-intensity UV light prior to combining with azo-LCPN showed better optical anisotropy and wettability when the pre-treatment time was selected as 300 sec. On the other hand, unpolarized light triggered height change was measured as 3.4 nm. In contrast to the obtained findings from relevant literature (Zhou, 2016), the switchable surface topography could not be achieved between on and off states of the light. The reason could be explained by the liquid-liquid interaction between the LC monomers and incomplete cured acrylate monomers.

- Directly cured TTEGDA substrate / azo-LCPN layered systems based on independently preparing the azo-LCPN coating followed by assembling with the acrylate substrates showed 36 nm height changes compared to the initial surface after unpolarized UV light actuation. Different from the previous pre-curing approach, the surface came back to its initial position after turning off the light. The result has indicated that conducting present approach related to design azo-LCPN on TTEGDA, the surface deformation on this smart layered system could be switchable by means of unpolarized light. On the other hand, the alignment study evidenced that the optical quality was better for acrylate based substrates than PDMS based systems due to the good interaction between LCs and the substrate surface without damaging the orientation of LCs. Hence, next experiments were performed using directly curing approach to design oscillating layered system using polarized light.

- It was found that increasing the content of 2-EHA in the substrates enhanced the softness of the material by lowering the storage modulus. By taking advantages of these findings, it was aimed to enhance dynamic surface topographies by increasing the softness of the substrates. Directly-cured TTEGDA/2-EHA substrates were characterized illuminating with the polarized light to observe the impact of 2-EHA concentration in the formulation on height change and oscillation behavior. For preparation, both mechanically rubbed and photo-aligned azo-LCPN coatings were combined with the substrates consisting different volume concentrations of 2-EHA (0, 20, 40, 60, 80, 95 vol.%). When compared the results of this examination, it can be said that using concentration of 95 vol.% 2-EHA enhance dynamic surface height changes and amplitude of the oscillation for both alignment techniques.

- For uniaxial planar aligned (mechanically rubbed) azo-LCPN, the maximum height change was increased from 8.3 to 102.8 nm and the oscillation amplitude was enhanced from 4.2 to 18.8 nm by adding 95 vol.% of 2-EHA. For perpendicularly aligned (photo-aligned) azo-LCPN, the maximum total height change was increased from 48.4 to 360 nm and the

oscillation amplitude was enhanced from 7.6 to 86 nm by adding 95 vol.% of 2-EHA.

- For each concentration of the 2-EHA, patterned samples showed higher amplitude and height changes than the measured values for mechanically aligned substrates. These findings emphasize the importance of photoalignment method, which is an untouched approach, in enhancing the surface deformation.

Recent studies in the field of azo-LCPN have only concentrated on designing static surface deformation on glass plates by switching on and off the unpolarized light. In the literature, there were no studies related to design smart layered systems exhibiting oscillation behavior. This is the first study presenting advantages of using polarized light to ensure oscillation motion on the azo-LCPN coated soft layers. The obtained findings ensure a new understanding for designing and characterizing oscillating coating. Moreover, this study revealed that azo-LCPN supported acrylate-based polymer (TTEGDA/2-EHA) was a promising material for achieving polarized light responses.

6.0 RECOMMENDATION AND FUTURE WORK

In this study, the main limitation related to PDMS is that the material shows a hydrophobic character, and thus the surfaces have to be modified for converting the surfaces from hydrophobic to hydrophilic. The modification could be carried out performing different techniques or temperatures in order to prevent the damages on the azo-LCPN coating which were caused by the oxygen plasma effect. On the other hand, contact angle measurements of uncoated/coated PDMS could be performed to figure out the interaction with LCs.

Detailed investigation on acrylate based systems could be tested with different intensities of UV and blue light. Moreover, different soft polymeric substrates which have lower storage modulus than the materials used in this study could be assessed to achieve both optical anisotropy and higher surface deformations on the azo-LCPN coating. Fourier transform infrared spectroscopic analysis could be done to provide information about the chemical bonding of the system.

Future research should therefore focus on enhancing dynamic surface topographies and oscillation trend in azo-LCPN. If this smart layered system could be improved, it would be interesting to use such systems in designing self-cleaning surfaces for solar panels, haptic screens that giving a feedback to the users and actuators.

REFERENCES

Bisoyi, H. K. and Kumar, S., 2011, Liquid-crystal nanoscience: an emerging avenue of soft self-assembly, Chemical Society Reviews, 40(1):306-319 pp.

Bisoyi, H. K. and Li, Q., 2016, Light-driven liquid crystalline materials: from photo-induced phase transitions and property modulations to applications, Chemical reviews, 116(24):15089-15166 pp.

Bodas, D. and Khan-Malek, C., 2007, Hydrophilization and hydrophobic recovery of PDMS by oxygen plasma and chemical treatment—An SEM investigation. Sensors and Actuators B: Chemical, 123(1):368-373 pp.

Broer, D. J., Boven, J., Mol, G. N. and Challa, G., 1989, In- situ photopolymerization of oriented liquid- crystalline acrylates, 3. Oriented polymer networks from a mesogenic diacrylate. Die Makromolekulare Chemie: Macromolecular Chemistry and Physics, 190(9):2255-2268 pp.

Chiou, D. R., Chen, L. J. and Lee, C. D., 2006, Pretilt angle of liquid crystals and liquid-crystal alignment on microgrooved polyimide surfaces fabricated by soft embossing method, Langmuir, 22(22):9403-9408 pp.

Emoto, A., Uchida, E. and Fukuda, T., 2012, Optical and physical applications of photocontrollable materials: Azobenzene-containing and liquid crystalline polymers. Polymers, 4(1):150-186 pp.

Fujikake, H., Kuboki, M., Murashige, T., Sato, H., Kikuchi, H. and Kurita, T., 2003, Alignment mechanism of liquid crystal in a stretched porous polymer film, Journal of Applied Physics, 94(5):2864-2867 pp.

Geelhaar, T., Griesar, K. And Reckmann, B., 2013, 125 years of liquid crystals—a scientific revolution in the home, Angewandte Chemie International Edition, 52(34):8798-8809 pp.

Hale, P. S., Shapter, J. G., Voelcker, N. H., Ford, M. J. and Waclawik, E. R., 2004, Liquid-crystal displays: Fabrication and measurement of a twisted nematic liquid-crystal cell, Journal of Chemical Education, 81(6):854 p.

Harris, K. D., Cuypers, R., Scheibe, P., van Oosten, C. L., Bastiaansen, C. W., Lub, J. and Broer, D. J., 2005, Large amplitude light-induced motion in high elastic modulus polymer actuators, Journal of Materials Chemistry, 15(47):5043-5048 pp.

REFERENCES (continued)

Hendrikx, M., Schenning, A. P. H. J, Debije, M. G. and Broer, D. J., 2017a, Light-triggered formation of surface topographies in azo polymers, Crystals, 7(8), 231 p.

Hendrikx, M., Schenning, A. P. H. J., and Broer, D. J., 2017b, Patterned oscillating topographical changes in photoresponsive polymer coatings, Soft matter, 13(24):4321-4327 pp.

Hikmet, R. A. M. and Broer, D. J., 1991, Dynamic mechanical properties of anisotropic networks formed by liquid crystalline acrylates. Polymer, 32(9):1627-1632 pp.

Holland, N. B., Hugel, T., Neuert, G., Cattani-Scholz, A., Renner, C., Oesterhelt, D., Moroder, L., Seitz, M. and Gaub, H. E., 2003, Single molecule force spectroscopy of azobenzene polymers: switching elasticity of single photochromic macromolecules, Macromolecules, 36(6):2015-2023 pp.

Hwang, J. Y. and Chien, L. C., 2009, Liquid crystal alignment on inkjet printed and air-buffed polyimide with nano-grove surface, Journal of Physics D: Applied Physics, 42(5).

Jin, Y., 2013, Photomechanical Effects in Ruthenium Sulfoxide Complexes, PhD Thesis, Ohio University.

Johnston, I. D., McCluskey, D. K., Tan, C. K. L. and Tracey, M. C., 2014, Mechanical characterization of bulk Sylgard 184 for microfluidics and microengineering. Journal of Micromechanics and Microengineering, 24(3): 7 p.

Kim, Y. J., Bae, J. W. and Song, K., 2014, P- 4: Effects of surface polarity on nematic liquid crystal alignment, In SID Symposium Digest of Technical Papers, 45(1):956-959 pp.

Kularatne, R. S., Kim, H., Boothby, J. M. and Ware, T. H., 2017, Liquid crystal elastomer actuators: synthesis, alignment, and applications, Journal of Polymer Science Part B: Polymer Physics, 55(5):395-411 pp.

Lee, K. M., Koerner, H., Vaia, R. A., Bunning, T. J. and White, T. J., 2010, Relationship between the photomechanical response and the thermomechanical properties of azobenzene liquid crystalline polymer networks, Macromolecules, 43(19):8185-8190 pp.

REFERENCES (continued)

Lee, K. M., Smith, M. L., Koerner, H., Tabiryan, N., Vaia, R. A., Bunning, T. J. and White, T. J., 2011, Photodriven, flexural–torsional oscillation of glassy azobenzene liquid crystal polymer networks, Advanced Functional Materials, 21(15):2913-2918 pp.

Liu, D., 2013, Responsive Surface Topographies: liquid crystal networks and polymer hydrogels forming micrometer sized surface structures triggered by light, heat or pH, PhD Thesis, Eindhoven University of Technology.

Liu, D., Bastiaansen, C. W., den Toonder, J. M. and Broer, D. J., 2012a, Photo- witchable surface topologies in chiral nematic coatings, Angewandte Chemie International Edition, 51(4):892-896 pp.

Liu, D., Bastiaansen, C. W., den Toonder, J. M., and Broer, D. J., 2012b, Light-induced formation of dynamic and permanent surface topologies in chiral–nematic polymer networks, Macromolecules, 45(19):8005-8012 pp.

Liu, D. and Broer, D. J., 2014a, Liquid crystal polymer networks: preparation, properties, and applications of films with patterned molecular alignment, Langmuir, 30(45):13499-13509 pp.

Liu, D., and Broer, D. J., 2014b, Self- assembled dynamic 3D fingerprints in liquid- crystal coatings towards controllable friction and adhesion, Angewandte Chemie International Edition, 53(18): 4542-4546 pp.

Liu, D. and Broer, D. J., 2015, New insights into photoactivated volume generation boost surface morphing in liquid crystal coatings, Nature communications, 6: 8334 p.

Liu, D., Liu, L., Onck, P. R. and Broer, D. J., 2015, Reverse switching of surface roughness in a self-organized polydomain liquid crystal coating, Proceedings of the National Academy of Sciences, 112(13):3880-3885 pp.

Liu, L. and Onck, P. R., 2018, Topographical changes in photo-responsive liquid crystal films: a computational analysis, Soft matter, 14(12):2411-2428 pp.

Lötters, J. C., Olthuis, W., Veltink, P. H. and Bergveld, P., 1997, The mechanical properties of the rubber elastic polymer polydimethylsiloxane for sensor applications, Journal of Micromechanics and Microengineering, 7(3):145 p.

Luckhurst, G. R., 1993, What creates liquid crystal phases?, Liquid Crystals Today, 3(1):3-5 pp.

REFERENCES (continued)

Nemoto, F., Nishiyama, I., Takanishi, Y. and Yamamoto, J., 2012, Anchoring and alignment in a liquid crystal cell: self-alignment of homogeneous nematic, Soft Matter, 8(45):11526-11530 pp.

Ohzono, T., Monobe, H., Yamaguchi, R., Shimizu, Y. and Yokoyama, H., 2009, Dynamics of surface memory effect in liquid crystal alignment on reconfigurable microwrinkles, Applied Physics Letters, 95(1).

Palffy-Muhoray, P., 2007, The diverse world of liquid crystals, Physics Today, 60 (9):54-59 pp.

Park, M. K. and Advincula, R. C., 2002, In-plane photoalignment of liquid crystals by azobenzene− polyelectrolyte layer-by-layer ultrathin films, Langmuir, 18(11):4532-4535 pp.

Pavlin, J., Vaupotič, N. and Čepič, M., 2013, Direction dependence of the extraordinary refraction index in uniaxial nematic liquid crystals, European Journal of Physics, 34(2):331 p.

Qaddoura, M. A. and Belfield, K. D., 2009, Synthesis, characterization and texture observations of calamitic liquid crystalline compounds, International journal of molecular sciences, 10(11):4772-4788 pp.

Rey, A. D. and Herrera- Valencia, E. E., 2012, Liquid crystal models of biological materials and silk spinning, Biopolymers, 97(6):374-396 pp.

Sahu, N., Parija, B. and Panigrahi, S., 2009, Fundamental understanding and modeling of spin coating process: A review, Indian Journal of Physics, 83(4):493-502 pp.

Sasaki, A., Aoshima, H., Nagano, S. and Seki, T., 2012, A versatile photochemical procedure to introduce a photoreactive molecular layer onto a polyimide film for liquid crystal alignment, Polymer Journal, 44(6):639 p.

Schadt, M., 1997, Liquid crystal materials and liquid crystal displays, Annual review of Materials Science, 27(1):305-379 pp.

Seki, T., Fukuda, R., -Tamaki, T. and Ichimura, K., 1994, Alignment photoregulation of liquid crystals on precisely area controlled azobenzene Langmuir-Blodgett monolayers, Thin Solid Films, 243:675–678 pp.

REFERENCES (continued)

Seki, T., Nagano, S. and Hara, M., 2013, Versatility of photoalignment techniques: From nematics to a wide range of functional materials, Polymer, 54(22), 6053-6072 pp.

Serak, S., Tabiryan, N., Vergara, R., White, T. J., Vaia, R. A. and Bunning, T. J., 2010, Liquid crystalline polymer cantilever oscillators fueled by light, Soft Matter, 6(4):779-783 pp.

Tan, S. H., Nguyen, N. T., Chua, Y. C. and Kang, T. G., 2010, Oxygen plasma treatment for reducing hydrophobicity of a sealed polydimethylsiloxane microchannel, Biomicrofluidics, 4(3), 032204.

Tang, S, 2015, Wettability in liquid crystal coatings based on switchable surface topographies, Master Thesis, Eindhoven University of Technology.

Tanigaki, N., Mochizuki, H., Mizokuro, T., Yoshida, Y. and Yase, K., 2006, Orientation patterning of liquid crystals by UV-irradiated polysilane oriented films, Molecular Crystals and Liquid Crystals, 445(1):119-409 pp.

Trantidou, T., Elani, Y., Parsons, E. and Ces, O., 2017, Hydrophilic surface modification of PDMS for droplet microfluidics using a simple, quick, and robust method via PVA deposition, Microsystems & Nanoengineering, 3: 16091 p.

Van Oosten, C. L., 2009, Responsive Liquid Crystal Networks, PhD Thesis, Eindhoven University of Technology.

Van Oosten, C. L., Corbett, D., Davies, D., Warner, M., Bastiaansen, C. W. and Broer, D. J., 2008, Bending dynamics and directionality reversal in liquid crystal network photoactuators, Macromolecules, 41(22):8592-8596 pp.

Wei, M., Gao, Y., Li, X. and Serpe, M. J., 2017, Stimuli-responsive polymers and their applications, Polymer Chemistry, 8(1):127-143 pp.

White, T. J., 2018, Photomechanical effects in liquid crystalline polymer networks and elastomers, Journal of Polymer Science Part B: Polymer Physics, 56(9):695-705 pp.

White, T. J. and Broer, D. J., 2015, Programmable and adaptive mechanics with liquid crystal polymer networks and elastomers, Nature materials, 14(11):1087 p.

REFERENCES (continued)

White, T. J., Serak, S. V., Tabiryan, N. V., Vaia, R. A. and Bunning, T. J., 2009, Polarization-controlled, photodriven bending in monodomain liquid crystal elastomer cantilevers, Journal of Materials Chemistry, 19(8):1080-1085 pp.

White, T. J., Tabiryan, N. V., Serak, S. V., Hrozhyk, U. A., Tondiglia, V. P., Koerner, H., Vaia, R. A. and Bunning, T. J., 2008, A high frequency photodriven polymer oscillator, Soft Matter, 4(9):1796-1798 pp.

Yepes, I. S. and Gesualdi, M. R., 2017, Dynamic digital holography for recording and reconstruction of 3D images using optoelectronic devices, Journal of Microwaves, Optoelectronics and Electromagnetic Applications, 16(3):801-815 pp.

Yu, Y., Nakano, M. and Ikeda, T., 2003, Photomechanics: directed bending of a polymer film by light, Nature, 425(6954):145 p.

Zhou, Y., 2016, Formation of Surface Topograpies in Liquid Crystal Networks on Soft Substrates, MSc Thesis, Eindhoven University of Technology.

CURRICULUM VITAE

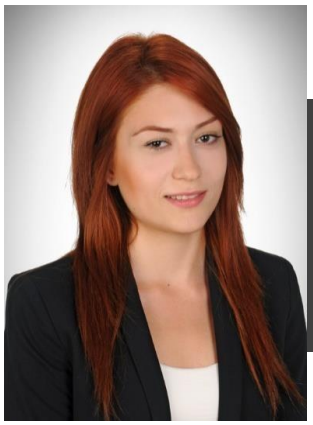

BURCU SIRMA

burcusrma@gmail.com

1665. sokak no:4/11, 35600 Karşıyaka/İzmir, Turkey

+90 545 746 81 09

PERSONAL INFORMATION

Marital Status: Single

Nationality: Turkish

Date of Birth and Place: 31/03/1991 Konak, Turkey

EDUCATIONAL BACKGROUND

2016-2017	**Eindhoven University of Technology** Master of Chemical Engineering and Chemistry (100% English)	**Research project**
2015-present	**Ege University** Master of Science in Chemical Engineering (100% English)	-
2010-2015	**Istanbul University** Bachelor of Science in Chemical Engineering (30% English)	**GPA: 92.3/100**
2006-2010	**Izmir Ataturk High School**	**GPA: 79/100**

PROJECT EXPERIENCES

Sept. 2016-Jul. 2017	**Master's Thesis Project: "Enhanced Surface Topographies in Liquid Crystal Polymer Networks"** Functional Organic Materials and Devices Group
Feb. 2016	**Poster Presentation: "Physicochemical, functional, antioxidant and antibacterial properties of chitosan extracted from shrimp wastes"** International Workshop on Special Topics on Polymeric Composites Ege University-Mechanical Engineering Department
March 2015	**Poster Presentation: "Chemical recycling of poly(ethylene terephthalate)"** 3rd National Students Congress of Chemical Engineering Istanbul University
Sept. 2014-Jul. 2015	**Bachelor's Thesis Project: "Recycling of poly(ethylene terephthalate)**" Istanbul University
Feb.-June 2014	**"Comparison of Solid-Liquid Equilibrium Data for the Adsorption of Propionic Acid from Aqueous Solution onto Amberlite XAD-16"** 11th National Chemical Engineering Congress Eskisehir Osmangazi University

CERTIFICATES

- Ege University: Mechanical Engineering Department – International Workshop on Special Topics on Polymeric Composites - Certificates of Attendance**.**
- Istanbul Business Institute: Production Management Certificate
- Istanbul Business Institute: TS EN ISO 9001 Quality Management System Certificate
- Istanbul University: Department of Foreign Language: Proficiency Basic French Language Certificate
- Istanbul University: Industrial and Quality Club - Traditional, Development, Enterprise Days Certificate
- Istanbul University: Industrial and Quality Club and Global CV – Business Solutions Certificate

LANGUAGE SKILLS

Turkish: Native Language

English: Professional working proficiency

COMPUTER SKILLS

Proficient with Ms Office Programs (Word, Excel, PowerPoint, Outlook, Access), Origin, Koala, Latex

Experienced with MATLAB, ANOVA, Minitab

Basic knowledge of CHEMCAD

WORK EXPERIENCE

May 2018-Present **Research Assistant at Izmir Institute of Technology**
Chemical Engineering Department

INTERNSHIP EXPERIENCES

Jul. – Sept. 2014 **Esen Plastic San. Tic. A.Ş. -** Material and Production Planning Department

Jul. – Sept. 2013 **Kansai Altan Boya San. A.Ş. -** Process and Quality Control Laboratory

CURRENT STUDIES

Oral presentation: **"**Smart Layered Systems Based on Liquid Crystal Polymer Networks"

Accepted by KOMPEGE 2018, Presentation date: Sept. 6-8, 2018

Poster presentation: **"**Permanent Surface Deformations on Light-Responsive Liquid Crystal Polymer Network Droplets"

Accepted by KOMPEGE 2018, Presentation date: Sept. 6-8, 2018